LBL-9047 c.2

Lawrence Berkeley Laboratory
UNIVERSITY OF CALIFORNIA

Materials & Molecular Research Division

MECHANICAL PROPERTIES AND MICROSTRUCTURES OF DUAL PHASE STEELS CONTAINING SILICON, ALUMINUM AND MOLYBDENUM

RECEIVED
LAWRENCE
BERKELEY LABORATORY

JAN 14 1980

LIBRARY AND
DOCUMENTS SECTION

Thomas John O'Neill
(M.S. thesis)

March 1979

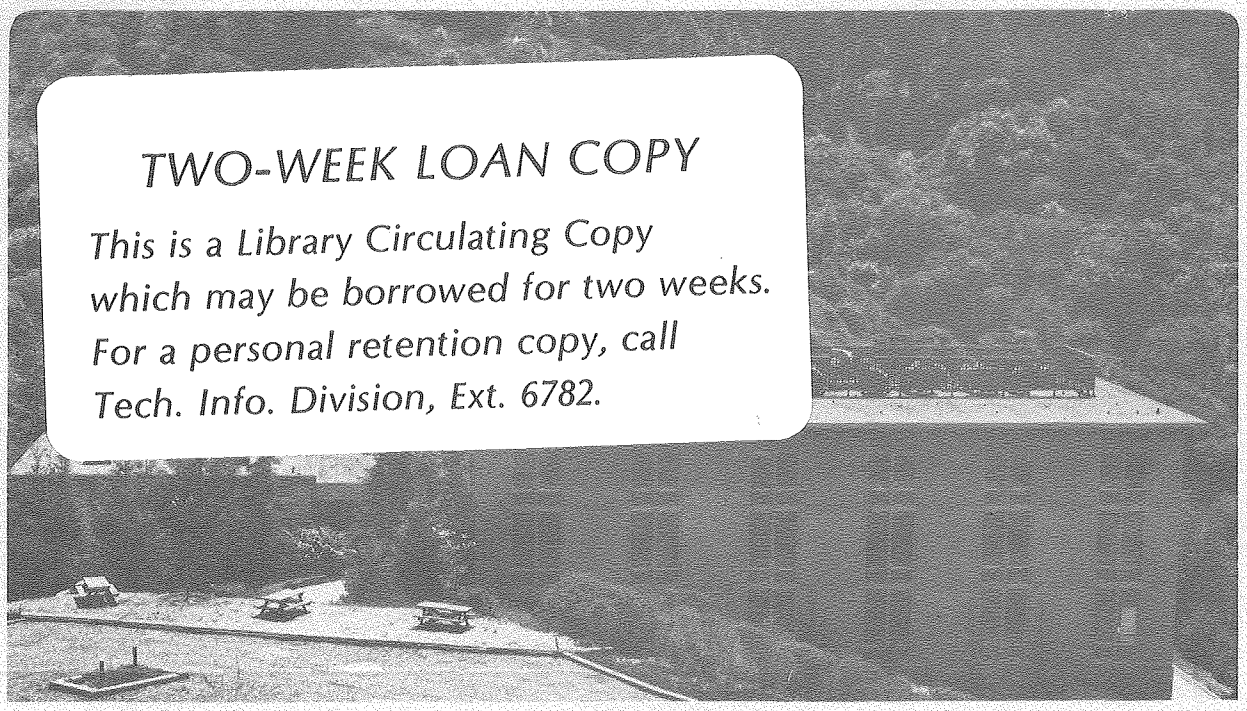

TWO-WEEK LOAN COPY

This is a Library Circulating Copy which may be borrowed for two weeks. For a personal retention copy, call Tech. Info. Division, Ext. 6782.

LBL-9047 c.2

Prepared for the U.S. Department of Energy under Contract W-7405-ENG-48

DISCLAIMER

This document was prepared as an account of work sponsored by the United States Government. While this document is believed to contain correct information, neither the United States Government nor any agency thereof, nor the Regents of the University of California, nor any of their employees, makes any warranty, express or implied, or assumes any legal responsibility for the accuracy, completeness, or usefulness of any information, apparatus, product, or process disclosed, or represents that its use would not infringe privately owned rights. Reference herein to any specific commercial product, process, or service by its trade name, trademark, manufacturer, or otherwise, does not necessarily constitute or imply its endorsement, recommendation, or favoring by the United States Government or any agency thereof, or the Regents of the University of California. The views and opinions of authors expressed herein do not necessarily state or reflect those of the United States Government or any agency thereof or the Regents of the University of California.

TABLE OF CONTENTS

		Page
I.	Introduction	1
II.	Alloy Design Considerations	5
	A. Two Phase Mixture Rule	6
	B. Selection Principles	7
	C. Processing and Choice of Alloying Elements	10
III.	Experimental Procedure	13
	A. Material Preparation	13
	B. Heat Treatment	13
	C. Mechanical Testing	14
	D. Microscopy	15
IV.	Results and Discussion	17
	A. Morphology: General Considerations	17
	B. Characterization of DFM Microstructures	23
	C. Fractography	30
	D. Mechanical Properties	30
	E. Microstructure/Mechanical Property Correlations	35
	F. Comparisons to Previous Work	41
V.	Conclusions	43
Acknowledgements		46
References		47
Tables		49
Figure Captions		54
Figures		

Mechanical Properties and Microstructures of Dual Phase Steels Containing Silicon, Aluminum and Molybdenum

Thomas J. O'Neill, Jr.

Materials and Molecular Research Division
and
Materials Science and Engineering
Lawrence Berkeley Laboratory
University of California
Berkeley, California 94720

ABSTRACT

An investigation concerning the heat treatment of duplex ferritic-martensitic low carbon steels containing silicon, aluminum and molybdenum has been carried out. Tensile properties of intermediately quenched and directly annealed specimens have been characterized and microstructural correlations established. The two-phase mixture rule may be used as a fairly good approximation of the mechanical behavior of the duplex system, but it has been recognized that the properties of both the ferrite and martensite depend on the volume fraction of martensite produced in the final morphology.

Thus, although the volume fraction of martensite appears to be the most influential factor in controlling the behavior of the duplex steel, ferrite strengthening may occur by precipitation hardening, and the strength of martensite may increase due to carbon enrichment as its volume fraction is decreased. Utilization of both of these factors results in a composite whose properties do not depend upon the martensite volume fraction (up to about .4). This means greater leeway can be achieved in controlling the heat treatment temperatures of the alloy. Such a steel, a Fe/.06C/.93Al alloy, has been investigated in this study.

I. Introduction

The exigency of energy and resource conservation has triggered intensive alloy development programs, resulting in new steel compositions and processing techniques. Higher strength steels with good formability are needed in the transportation industry to achieve weight and fuel savings and to conserve energy and resources. High strength, low alloy (HSLA) steels have satisfied many design goals, although formability appears to be a problem with such steels. Also, the alloying and processing of HSLA steels are not always economically justifiable by their strength-to-weight increase.[1] Hence, recent emphasis[2-8] has been placed on duplex, low carbon steels as a viable alternative in meeting the present demands of industry.

Duplex ferritic-martensitic (DFM) steels are a new class of HSLA steels whose approach to strengthening markedly contrasts with the micro-alloyed HSLA steels in chemistry as well as in processing technique. A fine dispersion of carbide forming elements is the principle strengthening mechanism in HSLA steels. In contrast, the major source of strengthening in duplex structures arises from the incorporation of inherently strong martensite as the load-carrying constituent in a relatively soft ferrite matrix which supplies the essential element of ductility.

Practical interest in DFM steels has arisen for several reasons. First, duplex microstructures can be produced by simple heat treatment,

without resorting to mechanical or thermomechanical processes. Second, a wide range of strength and ductility combinations can be achieved by simply altering the temperatures of the heat treatment. Also, since DFM alloys generally do not depend on carbide forming elements for their strength, such elements, which are usually relatively expensive, may be omitted, facilitating lower production costs.

The production of duplex aggregates has been more than just a novel idea. An early program aimed at developing laminates and composites through combinations of mechanical work and heat treatment was instituted by Cairns and Charles.[9] However, the mechanical properties produced by these treatments were no better than those which could be obtained from heat treated alloy steels. Grange[10] later utilized the phase transformation occurring in the two phase ($\alpha+\gamma$) region of the Fe-C system to obtain fibrous mixtures of martensite and ferrite by thermomechanical treatments. Again, only limited success was achieved in improving mechanical properties.

Koo,[5,6] Koo and Thomas,[3] and Young[25] modified the thermal process originated by Grange[10] to include two-phase annealing. This significantly increased the strength of commercial 1010 steel and several experimental alloys while maintaining good ductility. The capability of optimizing the conflicting property requirements of strength and ductility, contingent upon a favorable choice of alloying elements and processing, is the most attractive aspect of DFM structures.

The recent work by Koo,[5,6] Koo and Thomas,[3,4] and Young[25] has produced a fundamental understanding of the origin and the characteristic mechanical behavior of several DFM steel alloys. Coherent microstructure-property correlations have been obtained for several duplex steels whose properties meet or exceed commercial specifications. In particular, a Fe/2%Si/0.1%C alloy consisting of about 40% martensite has shown quite attractive mechanical properties, e.g. yield strength ~70Ksi, tensile strength ~112Ksi, uniform elongation ~15%, and total elongation ~25%. Intricate interactions between parameters such as size, shape, distribution and volume fraction of martensite particles have also been investigated in this 2% Si steel. While DFM Fe/Si/C alloys have also been studied by Nakaoka et al.,[11,12] their work neglects to take into account the role of microstructural morphology in influencing mechanical behavior.

The industrial application of the Fe/Si/C alloys may be hindered by difficulties in galvanizing silicon steels. The presence of silicon in these steels creates a surface oxide layer onto which the galvanizing zinc is deposited. This zinc-oxide skin can easily be sheared or scraped away to expose new, ungalvanized metal which quickly oxidizes.

The objective of this research is to establish and characterize the mechanical properties and microstructures of selected dual-phase steels in which the amount of silicon is reduced or eliminated. Correlations between microstructure and mechanical properties are to be

ascertained. It should be emphasized that while this investigation is of technological interest, the primary reason for this research is not to find a replacement for the Fe/2%Si/0.1%C steel, but rather to investigate the properties and microstructures of similar alloys, thus adding to the present understanding of duplex steels.

Alloying elements to be used in this study are aluminum, molybdenum and silicon. The rationale behind this selection of alloying elements is to be discussed presently.

II. Alloy Design Considerations

Many materials of engineering and technological importance are aggregates of two or more phases. In physical metallurgy, these composites can be divided into two categories in terms of the strengthening mechanisms involved and the associated processing techniques. One is fibre reinforced composites and the other is dispersion hardened materials. Both of these composites contain a second phase which is harder than the matrix.

In the case of fibre composites, two physically separable materials, particle or fibres and a metal matrix are compounded into an aggregate. The strengthening mechanism involved is principally described by the well established, fibre-loading concept.[13] In dispersion-hardened alloys, the second phase particles and matrix are, in most cases, of the same component system, and the Orowan mechanism[14] for yielding is applicable when the particle size is less than several microns. However, when the size of the second phase is of the order of 1μ-50μ, which corresponds to the transition between fibre reinforced strengthening and dispersion hardening, there exists no simple model for strengthening in the alloy. Nevertheless, it can be expected that the strengthening mechanism in a particular dual phase alloy is determined by the amount and morphology of the second phase. While favorable mechanical properties of strong second phase particles are exploited in duplex morphologies, some of their less desirable features,

such as brittleness, are simultaneously mitigated by the presence of a ductile matrix which binds the particles together.

It is important to emphasize that the strengthening mechanisms involved in a composite, and the mechanical properties associated with such an alloy depend on the specific system under consideration. In what follows, the two phase mixture "rule" and the selection guidelines for a two phase system with particular references to DFM steels will be considered.

A. Two Phase Mixture Rule

The current understanding of the mechanical behavior of randomly oriented coarse two phase structures is far from complete.[15] Much of the empirical evidence accumulated to date suggests that, in spite of an exact theoretical explanation, the strengthening of duplex alloys can be predicted with reasonable accuracy by the mixture rule[4,6,13,15]

$$\sigma_c = \sigma_m V_m + \sigma_\alpha (1 - V_m) \qquad (1)$$

where the subscripts c, α, m refer to composite, ferrite and martensite, V_m is the martensite volume fraction, σ_α is the ultimate tensile strength of the ferrite and σ_m is the ultimate tensile strength of the martensite. In a strict sense, equation (1) describes the mechanical behavior of unidirectionally aligned, continuous fibre composites where the fibres and the matrix are well bonded and the fibre strain, matrix strain and composite strain are all equal.

B. Selection Principles

The morphology of duplex ferritic-martensitic steels is critical to the mechanical properties produced by these steels. Consideration of parameters such as size, shape and distribution of martensite particles and the morphologies of the individual phases have led to guidelines for developing desirable DFM structures.[6]

(1) Optimum Volume Fraction: The volume fraction of the martensite particles is a primary factor in the mechanical properties of DFM alloys. The amount of martensite present must exceed a lower limit in order to achieve a substantial contribution to strengthening. At the same time, there must not be so much martensite in the composite where a failure in the martensite particles would propagate throughout the structure and lead immediately to its failure. If the volume fraction of martensite is in the optimum range, the ferrite matrix can locally work harden upon failure of an adjacent martensite particle, and carry the transferred load.

(2) Size and Shape of Martensite Particles: If the size of the martensite particles is small (on the order of ~1μm or less), and if the particle spacing is such that a micro-mechanistic model instead of a fibre-loading concept applies, the properties of the alloy will be effected.[16-17] An increased yield stress of the ferrite matrix and an increased rate of work hardening of the material is to be expected.

The influence of martensite particle shape is important in the transferral of loads between the martensite and the ferrite. Since load transfer occurs by shear action along the particle/matrix interface[6], a fibrous morphology of martensite particles would be superior to a spherical shape. The increased ratio of interfacial area to particle volume in the case of an acicular particle would be the major reason for this. A high degree of coherency between the martensite and ferrite would also be a favorable influence in the transferral of load between the martensite particle and the ferrite matrix.

(3) Martensite Distribution: Through the simple heat treatments to be used in this study, it is more likely that a macroscopically randomly oriented DFM structure will be obtained rather than unidirectionally aligned martensite particles in a ferrite matrix. This will result in desirable isotropic mechanical properties. Should the martensite particles be connected throughout the ferrite matrix, the particle network would fail in the early stage of plastic deformation, and prevent the ferrite from contributing its full ductility. Superior mechanical properties is thus expected to be a result of discontinuous, randomly oriented martensite particles in a continuous ferrite matrix.

(4) Martensite Carbon Content: The inherently strong martensite in DFM structures is a diffusionless transformation product of carbon enriched austenite. Maintaining the carbon level below about

~0.3% in austenite will result in dislocated lath martensite. Carbon levels (above) ~0.3% in austenite will result in twinned plate martensite. Since higher carbon content can drastically reduce the toughness of the martensite,[18] the average carbon content of the initial alloy must be kept sufficiently low to maintain carbon levels at or below about 0.3% in austenite.

(5) Precipitation Reactions: The stress in the continuous ferrite matrix is transferred to the strong martensite particles by shear action at the ferrite/martensite interface. Hence, the nature of the interface is of critical importance. If carbide particles should precipitate along this interface, their brittle mechanical properties will greatly reduce the properties of the composite. Therefore, the precipitation of brittle phases at the ferrite/martensite interface is to be avoided.

Small precipitates within the ferrite matrix may serve as obstacles to dislocation motion. In this study, the dispersion hardening of the ferrite will be considered as a secondary strengthening mechanism, and will result in a lower ferrite ductility. Although investigation of the ferrite substructure is necessary, as the details contained therein may provide the information necessary to the understanding of the mechanical properties of the material.

(6) Grain Refinement: In any alloy grain refinement may serve as a strengthening mechanism. Thermal cycling may produce this refinement in grain size.[3] Since a non-standard thermal-cycling treatment is used in this study, the resulting grain refinement may be considered as an additional strengthening mechanism.

C. Processing and Choice of Alloying Elements

The above considerations suggest microstructural features which are desirable in a DFM steel which is both strong and ductile. Producing these mechanical properties at a sufficiently small cost premium is a critical challenge.

The production of a controlled amount of martensite in a ferrite matrix has been done using many different heat treatments,[6,19] all of which involve phase transformations in the two-phase ($\alpha+\gamma$) region. In this study, two types of heat treatments, viz., intermediate quench and direct anneal, will be used (see Fig. 1).

The intermediate quench heat treatment was devised so as to fully exploit the characteristics of an initial martensite structure prior to subsequent annealing in the ($\alpha+\gamma$) range. The initial martensitic structure provides sufficient heterogeneous nucleation sites for austenite during the two phase anneal, resulting in a more uniform distribution of martensite particles in the final morphology.

The direct anneal heat treatment produces a morphology which is dependent on the initial, as-received, microstructure of the alloy.

It has the advantage of reduced heat treatment which may result in lower production costs.

Since the microstructures produced by these heat treatments are dependent upon the morphologies present prior to two-phase annealing, it is expected that the mechanical properties produced will reflect these morphological differences.

In this study, silicon, aluminum and molybdenum have been chosen as alloying elements. The selection of these elements is based upon the following observations:

(1) Silicon,[20] aluminum[21] and molybdenum[22] all broaden the ($\alpha+\gamma$) field when added to the Fe-C system. This facilitates practical control of the volume fraction and composition of the martensite produced.

(2) Silicon and aluminum promote a fine distribution of martensite in the ferrite matrix.[23]

(3) Silicon and aluminum improve the ferrite/martensite interface by inhibiting the formation of coarse carbides there during the final quench.[6]

(4) Silicon and aluminum increase the activity of carbon in ferrite. This has the effect of increasing the amount of supersaturated carbon atoms in the ferrite matrix resulting in a very effective solid solution strengthening in the ferrite.[6]

(5) Molybdenum improves the hardenability of steel.[24]

(6) The deoxidizing action of aluminum results in grain refinement and subsequent strengthening.

As mentioned before, the amount of carbon to be used in these steels is to be about 0.1 wt. pct., so as to produce dislocated lath martensite in the martensite phase of the duplex structure.

III. Experimental Procedure

A. Materials Preparation

The compositions of the alloys used in this study are listed in Table 1. In addition to the listed elements, there are also traces of sulfur and phosphorous (less than .005 wt. pct.) in all steels. The steels were provided by the Republic Steel Company. The material was received in the form of plates which were air melted, cast, forged and hot rolled.

B. Heat Treatment

Several small cylindric test "pellets" were made for each steel (see Fig. 2). The dimensions of the test pellet were made similar to those of the test area of a tensile blank that would be used in testing (see Fig. 3).

For each steel, these test pellets were heat treated for twenty minutes in an argon atmosphere at various temperatures beginning at 740°C and increasing thereafter in steps of 30°C. All specimens were quenched in agitated ice brine at the end of the twenty minute anneal.

Cross sectional areas at the middle of each pellet were studied using an optical microscope. The amount of martensite was assessed from the optical micrographs. Annealing temperatures which result in ~20%, ~40% and ~100% martensite were selected for annealing and austenitizing temperatures, respectively. These temperatures are listed in Table 2.

Round tensile test blanks (Fig. 3) were made from each steel. Specimens were made for each of the following heat treatments; an intermediate quenched steel with ~20% martensite, an intermediate quenched steel with ~40% martensite, a directly annealed steel with ~20% martensite, and a directly annealed steel with ~40% martensite. Hence, with four steels and four heat treatments per steel, there were sixteen different tests made. Using one hundred and forty-four tensile test blanks (nine blanks per test) these heat treatments were carried out in a vertical tube furnace. Annealing and austenitization were done in an argon atmosphere, and subsequent quenching was done in agitated ice brine. TEM specimens were also heat treated in this manner. Annealing and austenitization temperatures were controlled within $\pm 5^{\circ}C$.

C. Mechanical Testing

Tensile properties were determined using 1 inch gage round tensile specimens, following ASTM specification (Fig. 3). Testing was done at room temperature in an Instron machine with a cross head speed of 0.05cm/min and a full scale load of 1000 kg. During testing, uniform elongation was continuously monitored by measuring the distance between gage marks using an optical magnifier. Measurements of each gage section before and after testing were accurately determined using an optical microscope with a vernier translating stage calibrated to 0.001 inch. The values of tensile properties reported are those from

tensile specimens whose deformation was confined to a 1 inch gage length.

Microhardness testing was done on a Leitz Wetzlar Mini-load hardness tester. Vickers hardness was done using a 50 gm load for a 25 sec. application. Values reported are averages from five measurements.

D. Microscopy

(i) Optical Metallography

Samples for optical metallography were cut from undeformed regions of tested tensile specimens. They were mounted in Bakelite and ground on successively finer paper from 120 to 600 grit, and then polished on a one micron diamond abrasive wheel lubricated with kerosene. A 2% nital etch was used to reveal duplex microstructural features. Samples were examined on a Zeiss Ultraphot II metallograph.

(ii) Transmission Electron Microscopy

The alloys used in this investigation have limited hardenability due to low carbon content. Consequently, samples of different thickness may result in different microstructures. In order to characterize the true microstructure in tensile test specimens, precaution was taken to insure that the samples for thin foils had the same thickness as round tensile specimens, and were subjected simultaneously to the same heat treatment.

Slices ~.02 in thick were cut from heat treated samples. Flood cooling was employed to minimize specimen heating during cutting. The specimens were then chemically thinned to about 5 mils in H_2O_2 containing 2% HF at room temperature. Specimen discs were spark cut and then ground to .0012 in. thickness. Final thinning was done in a twin jet-polishing apparatus using a chrome-acetic acid solution (75 gms CrO_3 + 400 ml CH_2 COOH + 21 ml H_2O). The resultant foils were examined in a Phillips 301 transmission electron microscope at an accelerating voltage of 100KV.

(iii) Scanning Electron Microscopy

Fracture surfaces of tensile specimens were examined using an AMR 1000 scanning electron microscope operating at 25 KV. Specimens were cut, ultrasonically cleaned and stored in dessicators until examination.

IV. Results and Discussion

A. Morphology: General Considerations

Heat treatment in the two-phase ($\alpha+\gamma$) field does not necessarily involve equilibrium conditions, and the temperatures, tie lines and compositions dictated by an equilibrium diagram are not necessarily applicable. The volume fractions of ferrite and austenite formed by annealing in the two-phase field will thus be difficult to predict. This difficulty is compounded by the general lack of information on equilibrium diagrams available in the literature for the alloys listed in Table 1. The amount of phase separation corresponding to twenty minutes at the holding temperature may be determined by experimentally finding the A_3 (γ solidus) and the α solidus lines for the exact compositions used.[25]

The amount of phase separation may be more directly determined by annealing test specimens of proper size at various temperatures in the two-phase region and observing the transformed products. Also, the transformation of austenite to martensite may be monitored by this method, thus checking the hardenability of the systems under study.

An important result of non-equilibrium conditions concerns the composition of the martensite in the duplex structure. The low atomic number of carbon has prevented its chemical detection by x-ray spectroscopy. Only through the use of lattice imaging techniques has the non-equilibrium carbon content of martensite been ascertained.[6]

Although the results are not reported here, an investigation is currently underway to determine, by the lattice imaging technique, the carbon content of martensite in the duplex steels studied in this report.

The expected formation of duplex ferritic-martensitic structures in the systems under study is highly dependent upon the microstructure present prior to two-phase annealing. In the case of the intermediate quench heat treatment, the initial microstructure is ~100% martensite, whereas the direct anneal treatment employs the as-received alloy as the initial microstructure. Optical micrographs of the as-received structures and of the ~100% martensitic structures are shown in Figures 4 and 5 respectively.

In the as-received alloys, ferrite and pearlite are common to all morphologies. In the Mo containing steels (Figures 4(a) and 4(b)) a coarse-grained structure of uniformly dispersed pearlite in ferrite is present. In the Al-containing steels (Figures 4(c) and 4(d)), a definite rolled texture is present. Also, these steels are somewhat finer grained than the Mo containing steels, presumably because of the deoxidizing action of the aluminum. Additionally, the pearlite colonies are smaller and more highly dispersed in the Al steels.

The initial martensitic microstructure used in the intermediate quench heat treatment has been shown to produce favorable mechanical properties.[3,5,6,25]

Figure 5 shows the martensitic structure of the alloys prior to two-phase annealing. The Mo containing steels (Figures 5(a) and 5(b)) show a finely grained lath martensite structure in which some large carbides are dispersed. The martensite morphology in the Al-containing steels is more complicated and will be discussed fully in what follows.

Figures 5(c) and 5(d) show dislocated lath martensite formed within prior austenite grains. Ferrite decorates the former austenite grain boundaries. Large carbides are dispersed throughout the structure. The presence of ferrite in the morphology shows that the quenching rate from the austenitizing temperature was not high enough to prevent the formation of proeutectoid ferrite. Also, the reduced γ range, due to alloying elements, creates difficulties in defining the austenitizing temperature. In these cases, the austenitizing temperature was selected so as to produce the smallest amount of ferrite possible. Lower austenitizing temperatures would result in the decomposition of the structure into ferrite and austenite, i.e. two-phase annealing would take place. Higher austenitizing temperatures would require a larger quench rate to avoid the formation of proeutectoid ferrite. Although alternative quenching media could have been used to prevent the formation of proeutectoid ferrite, the selection of agitated ice brine most closely reflects conditions present in industry. The effect of the transformed proeutectoid ferrite

in the martensitic structure will be seen in the final morphologies of the intermediate quench heat treatment.

The formation of duplex microstructures during the two-phase annealing takes place in different ways. In the direct anneal treatment, ferrite and martensite are formed from the as-received morphology whereas in the intermediate quench treatment, ferrite and martensite are products of the ~100% martensitic structure.

In the direct anneal process, the effect of a texture in the as-received alloy on the final morphology is pronounced. During the two-phase anneal, austenite nucleates in the carbon-rich pearlite colonies. The carbon content of the austenite is almost exclusively derived from the Fe_3C in the pearlite since the ferrite contains very little carbon. Carbon that is in excess of what is needed by the austenite may be dispersed throughout the microstructure, as the solubility of carbon is relatively large at the annealing temperature. The growth of austenite takes place at the expense of the pearlite and ferrite. Since the volume fraction of austenite dictated by the tie-line is greater than the amount of pearlite in the as-received structures, the growing austenite consumes the volume inhabited by the pearlite and advances into the surrounding ferrite. Thus, if the as-received microstructure has a texture, a similar texture of austenite in ferrite will appear at the annealing temperature. This scheme of austenite formation is consistent with theories found in the literature.[26,27]

Austenite formation proceeds in a different manner in the intermediate quench heat treatment. Reheating to the two-phase annealing temperature after quenching from the austenitizing temperature results in the nucleation of austenite at former austenite grain boundaries, martensite lath boundaries, and possibly other lattice defects. If retained austenite is present in the ~100% martensitic structure as thin films trapped between martensite laths, austenite formation will begin there. At former austenite grain boundaries in the Al-containing steels (see Figures 5(c) and 5(d) austenite formation is prohibited, due to the presence of proeutectoid ferrite.

It is expected that, for those steels containing retained austenite in the ~100% martensitic structure, the austenite formed during the two-phase annealing will be needle-like in shape. The growth of austenite from thin films of retained austenite suggests this. However, one must consider the effects of the alloying elements on austenite growth to correctly anticipate the final morphologies of the intermediate quench products.

Koo[6] has presented a theory of austenite growth from the ~100% martensitic structure during the two-phase anneal. He has postulated that for a silicon containing steel, a concentration "spike" of silicon at the interface between austenite and ferrite will act as a barrier to carbon diffusion because of the repellent interaction between carbon and silicon.[28] As a result, lateral thickening of the

austenite particles will be restricted at the martensite lath boundaries. However, austenite can grow more rapidly along the lath boundaries where the diffusion of carbon, and hence austenite growth, can occur. As a result, the austenite produced during two-phase annealing grows in an acicular manner along martensite lath boundaries.

Needle-like martensite morphologies are to be expected in the silicon-containing steels which undergo the intermediate quench heat treatment. Since aluminum, like silicon, also raises the activity of carbon in ferrite, an acicular martensite morphology is expected for the Al-containing steels undergoing the intermediate quench heat treatment. The alloying properties of molybdenum are not similar to those of Si and Al, since molybdenum is a carbide former. Therefore, the shape of the martensite produced by heat treating the steel containing only Mo as an alloying element is not easily predicted.

During the two-phase anneal of the intermediate quench heat treatment, ferrite nucleates at crystal imperfections, particularly at former austenite grain boundaries. At such imperfections, the surface energy barrier is reduced.[29] Moreover, in those steels containing Al, proeutectoid ferrite already decorates the former austenite grain boundaries as quenched from the austenitizing temperature (see Figures 5(c) and 5(d)). Growth of this existing ferrite is to be expected upon reheating to the ($\alpha+\gamma$) field.

Upon quenching from the two-phase holding temperature, the

ferrite will become heavily dislocated as a result of the accomodation of the martensite transformation strain. Depending on the holding temperature in the ($\alpha+\gamma$) field, precipitates may also appear in the ferrite matrix during the quench. At low temperatures in the ($\alpha+\gamma$) field, the solubility of carbon, or other solute elements in ferrite is many times greater than that at room temperature. Quenching from such a holding temperature creates a large supersaturation of the solute in the ferrite which may induce precipitation in the ferrite. In such a case, precipitation in the ferrite must play a role in the strengthening of the DFM structure.

B. Characterization of DFM Microstructures

The expected morphologies of the alloys under study have been explained in the preceding section. The specific details concerning the morphologies of each individual alloy will now be discussed.

Fe/.07C/.94Mo: Optical micrographs of the final morphologies of the directly annealed and intermediately quenched steels are shown in Figure 6. As is seen, the intermediate quench products are finer grained and have a better dispersion of martensite in ferrite than the directly annealed structures. Grain refinement in the intermediate quench products reflects the effects of thermal cycling. The more uniform dispersion of martensite is a result of the many heterogeneities present in the ~100% martensitic structure, which serve as nucleation sites for austenite growth during the two-phase

anneal. The banding of large martensite particles in the directly annealed structures gives them a higher connectivity than their intermediately quenched counterparts.

As experienced by previous authors,[30] the steels containing molybdenum only as an alloying element were difficult to electropolish. A composite transmission electron micrograph of a globular martensite particle is shown in Figure 7. This martensite particle is taken from a ~40% martensite, intermediately quenched steel (figure 6(c)) but is typical of all the martensite particles shown in the optical micrographs of Figure 6. The martensite is dislocated, indicating that its carbon content is less than about 0.35 wt. pct.

The ferrite surrounding the martensite particles is severely dislocated due to the martensite transformation strain, as shown in Figure 7. As illustrated in Figure 8, the ferrite in the Fe/C/Mo steels contains small precipitates which are presumed to be carbides. These spherical precipitates are found only by using two-beam illumination at bend contours of the foil specimen. There was no easily detected difference in particle density as the volume fraction of martensite increased. The martensite of the Fe/C/Mo steels is unique to this study insofar that it contains no retained austenite as evidenced by the micrographs of Figure 9. This finding substantiates those of Clark and Thomas.[3] The absence of retained austenite trapped between the laths of the ~100% martensitic structure

(Figure 5(a)) dictates that the martensite in the intermediate quench morphologies be globular in shape, as are the products of the direct anneal process.

The orientation of adjacent martensite laths in the Fe/C/Mo steels is investigated in Figure 10. The adjacent laths appear to be twinned across the $(\bar{2}1\bar{1})$ plane at the lath boundary. Since twinning results in a coherent interface at the twin plane, no retained austenite could be found at the lath boundaries.

Widmanstatten cementite (Fe_3C) is found within the martensite laths aligned in the <110> directions, as shown in Figure 9(b). Spherical carbides are found dispersed throughout the laths as is shown in Figure 11.

Fe/.07SC/.6Si/.94Mo: As seen in Figure 12, the optical morphology of these steels is dependent upon the heat treatment used. The directly annealed steels contain globular martensite particles, while the intermediately quenched steels show mixtures of globular and acicular martensite. Again, the intermediate quench products are finer grained and have a more even distribution of martensite in ferrite. In the directly annealed specimens (Figure 12(b) and (d)), large autotempered carbides are found, and from optical analysis the density of these large carbides is greater in the ~20% martensite, than in the ~40% martensite case.

The martensite of the Fe/C/Si/Mo steels is lath in nature, as

illustrated in the composite electron micrograph of Figure 13. Retained austenite is found as thin films trapped between the martensite laths. This austenite is imaged in the bright field/dark field mode in Figure 14 and 15, and is present in all these steels. In the intermediately quenched steels, the presence of retained austenite in the ~100% martensitic structure (Figure 5(b)) contributes to the needle-like shape of some of the martensite particles. The growth of these acicular particles during the two-phase anneal conforms to the theory presented by Koo.[6] Globular shaped martensite particles also appear. This is due to insufficient amounts of silicon appearing at the martensite/austenite interface during the two-phase anneal. This appearance of globular martensite particles appearing at former austenite grain boundaries is similar to that observed by Koo on chromium steels.[5]

Due to the austenite to martensite transformation strain, the ferrite is severely dislocated in the steels of Figure 12. Also, upon electron microscopy examination a large number of spherical particles are found distributed in the ferrite matrix, as shown in Figure 16. The density of these particles is much greater than the Fe/C/Mo steels, and there appears to be little variation in density from the differently heat treated Fe/C/Si/Mo steels. Again, these particles are assumed to be carbides as diffraction data was difficult to obtain since imaging of these particles was done in 2-beam

illumination at bend contours of the foil. The assumption that these particles are carbides concurs with Costello's opinion,[19] who investigated a similar alloy.

Fe/.06C/.93Al: Optical micrographs of these steels are shown in Figure 17. In the directly annealed products (Figure 17(b) and (d)), a banded structure of globular martensite particles in the ferrite results from the texture of the initial as-received microstructure (Figure 4(c)). Figure 18 illustrates that the martensite is lath in nature (carbon content below ~.35%) and that the ferrite surrounding the martensite particles is dislocated. Retained austenite is found within the martensite particles of both the intermediate quench and direct anneal products, as shown in Figure 19. The presence of retained austenite in the ~100% martensitic structures of the intermediate quench heat treatment (Figure 5(c)) along with the aluminum alloying element contributes to the acicular shape of the martensite particles in the intermediately quenched steels, as previously discussed. Also, fine Widmanstatten cementite (Fe_3C) is found lying on {110} planes within the martensite laths as shown in Figure 20.

The ferrite substructure in the Fe/.06C/93Al steels is interesting for two reasons. A mixture of spherical particles and rods are found within the matrix. This mixture is shown in Figure 21(a). The rod-shaped particles are shown in Figure 21(b) and (c) and again in Figure 22. The spherical particles are assumed to be carbides since they

are similar to the particles found in the other steels of this study. The rod-shaped particles are thought to be AlN precipitates for reasons discussed below. Both of these types of particles are seen under diffraction contrast in two-beam illumination only. Spectrographic microanalysis by Stem-X-ray methods was done from the martensite to the ferrite in a ~20% martensite, direct anneal Fe/C/Al steel.* The results are shown in Figure 23. As shown, the ferrite is enriched in Al, in fact the atomic concentration of Al in ferrite is twice that in martensite. Thus, precipitation of aluminum containing particles is to be expected. Nitrogen could easily be incorporated as an impurity during the air melting of the alloy. Thus, the rod-shaped particles are assumed to be AlN.

The densities of both the spherical and rod-shaped particles in the ferrite of the Fe/C/Al steels show little variation in the differently heat treated steels.

Fe/.065C/.42Si/.98Al: The optical morphologies of the Fe/.065C/.42Si/.98Al steels are shown in Figure 24. The directly annealed steels (Figure 24(b) and (d)), have a banded globular martensite particles in the ferrite due to the initial texture of the as-received alloy. The intermediately quenched steels (Figure 24(a) and (c)) are typified by composite martensite-ferrite "islands" in "rivers" of ferrite. Increased volume fractions of martensite involve primarily the thickening of the martensite fibres in the "islands" and also the

*Courtesy, Dr. M. Raghavan, Exxon, N. J.

appearance of new fibers within the "rivers". The reason for this banding in the intermediate quench product is that the presence of proeutectoid ferrite along former austenite grain boundaries in the ~100% martensitic structure (Figure 5(d)) nucleates the ferrite growth during the two-phase ($\alpha+\gamma$) anneal. The ferrite "rivers" in the morphology of the intermediate quench specimens is free from alloying element, while the composite "islands" are enriched, as seen in Figure 25.

Retained austenite is found as thin films between the martensitic laths in the Fe/C/Si/Al steels as shown in Figure 26. The presence of this retained austenite contributes to the acicular martensite shape in the intermediately quenched steels, as discussed earlier. A composite electron micrograph of a single martensite fiber in a ~20% martensite, intermediately quenched steel is shown in Figure 27. Small spherical particles are found in the dislocated ferrite which surrounds the lath martensite needle. An enlarged micrograph of a portion of the martensite fiber is shown in Figure 28. By tilting, some martensite laths are revealed to be internally twinned; also spherical particles in the ferrite are more evident.

The fine spherical particles in the ferrite phase of the Fe/C/Si/Al steels are again shown in Figures 29 and 30. These particles are seen only with two-beam illumination in the electron microscope. There is little variation in the density of these particles within the

Fe/C/Si/Al alloys heat treated. The density of the particles in the Fe/C/Si/Al steels is greater than their counterparts in the heat treated Fe/C/Al steels however.

C. Fractography

The fracture morphologies of all broken tensile specimens, as examined in a scanning electron microscope were remarkably similar. The appearance of the inner zone of the tensile fracture surfaces was randomly fibrous, which is indicative of stable, subcritical crack extension requiring relatively high energy. At higher magnifications, it is seen that microvoid coalesence led to crack propagation (see Figure 31). Thus, the dimpled rupture fracture surface is indicative of classic ductile failure.

Although the dimpled ruptured fracture surface was predominantly the only phenomenon observed in the SEM, particles of varying composition were occasionally found. A few of these particles are shown in Figures 32 and 33. The particle composition varied from non-metallic inclusions in Figure 31, to Al (or Al_2O_3) in Figure 33. These particles may be sites for microvoid growth and hence may accelerate failure in the specimen. However, the number of these particles is too few to significantly contribute to premature failure.

D. Mechanical Properties

As noted in Figure 3, tensile specimens were cut transverse to

the rolling direction of the plates. Since better mechanical properties, e.g., strength and ductility, usually result from test specimens cut along the rolling direction, the tensile properties reported in this study are conservative in nature. That is to say, better data would result from test pieces cut along the rolling direction.

The tensile properties found in this study are summarized in Table 3. The results listed in this table are presented graphically in Figures 34 through 41. In the discussion that follows, it is most convenient to refer to these graphs.

Difficulty was experienced in making microhardness measurements for several reasons. First, indentions made in the steels had to be limited to ~20μm, so as to obtain hardness values for only a single phase. Even with such small indentations, hardness measurements of the martensite could not be obtained because of the frequent small size of martensitic particles. Ferrite hardness measurements were also hampered by the impingement of martensite particles at the edge of the indentation. This was particularly the case in the ferrite measurements in the 40% martensite steels. Because of the finer dispersion of martensite particles in the intermediately quenched steels, ferrite hardnesses were unobtainable for the intermediate quench cases. Also the 50gm applied load was the lower limit upon making valid hardness measurements, and hence the values obtained may be somewhat in error.

The microhardness values and their associated strength values for the ferrite of the directly annealed specimens are listed in Table 4. The ferrite hardnesses and strengths in the 40% martensite cases are thought to be higher than is actually the case, due to the increasing impingement of martensite islands on the ferrite.

The above difficulties necessitate that the hardnesses and strengths listed in Table 4 be used only for argument, and are not to be taken as valid measurements. Nevertheless, the trends illustrated in Table 4 will be of some use in the discussion of the strengthening of the duplex structure.

Fe/.07C/.94Mo: The graphs of strength vs. uniform and total elongation for the Fe/.07C/.94Mo steels are presented in Figures 34 and 35. It can be seen from these figures that, as volume fraction martensite increases, the yield and ultimate tensile strengths increase and the elongations decrease. At a given volume fraction of martensite, the directly annealed and intermediately quenched products have very nearly the same strength values, but the elongations of the intermediate quench specimens are noticeably better.

Since the strengths of the directly annealed and intermediately quenched steels containing the same amount of martensite are about the same, we can, by the use of the two-phase mixture rule, find the strengths of the martensite and ferrite in the Fe/.07C/.94Mo steels. By doing this however, it is assumed that the strengths of the ferrite

and martensite are independent of the volume fraction of martensite. Substituting the ultimate tensile strengths of 96 Ksi and 103.5 Ksi into the two-phase mixture rule (Equation 1) at martensite volume fractions of 20 and 40 percent respectively, then $\sigma_m \sim 126$ Ksi and $\sigma_\alpha \sim 89$ Ksi.

From the hardness data of Table 4 it is seen that as the volume fraction of martensite increases, the strength of the ferrite decreases. Also, since there is a carbon content variation in the martensite with volume fraction martensite, the strength of the martensite will vary. Hence, the above analysis is not valid. A more detailed analysis of ferrite and martensite strengths will be developed later in this work.

Fe/.075C/.6Si/.94Mo: As reflected in Figures 36 and 37, the change in volume fraction martensite from 20 to 40 percent effects an increase of about 10 Ksi in strength in both the intermediately quenched and directly annealed products. However, a 1-4% loss in elongation accompanies the martensite volume fraction increase. Quite noticeably the intermediately quenched products have a ~7% better elongation values than their directly annealed counterparts, but this is accompanied by a ~10Ksi loss in yield and ultimate tensile strengths. The rationale behind these differences lies in the different morphologies of the steels and will be discussed later.

Again, as seen in Table 4, the strength of the ferrite decreases

with increasing volume fraction martensite. It can be expected that, due to carbon content variation, the strength of the martensite will vary with volume fraction martensite. This is also to be discussed later.

Fe/.06C/.93Al: Graphs illustrating the tensile behavior of the Fe/.06C/.93Al steels are shown in Figures 39 and 40. The intermediate quench specimens show properties superior to those of the direct anneal process (in both strength and elongation), but only slightly. The intermediate quench products provide better elongations than do their directly annealed counterparts, but only by about one percent. In a reversal of the previous trend, the intermediate quench products provide 3 to 5 Ksi higher strength values than their directly annealed equivalents.

Quite surprisingly, the ~20% martensite products have strengths and elongations equal to those of the ~40% martensite specimens. This, at first glance, creates an apparent exception to the two-phase mixture rule (equation 1). However, σ_α and σ_m can vary so that the same composite strength, σ_c, may result despite a change in the martensite volume fraction (see equation 1). Strengthening of the ferrite, as the volume fraction of martensite is lowered, may result in the same composite strength. Thus, this mechanical behavior would not create an exception to the two-phase mixture rule.

As seen in Table 4, the hardness and strength of the ferrite

increases with decreasing martensite volume fraction. The variation in ferrite strength from 20 to 40 percent martensite is the largest experienced by any of the steels studied. The reasoning behind this behavior will be more fully discussed later.

Fe/.065C/.42Si/.98Al: Graphs of strength vs uniform and total elongation for the Fe/.065C/.42Si/.98Al steels are shown in Figures 40 and 41. Again, it is seen that as the volume fraction of martensite increases, strengths increase and elongations decrease for both the directly annealed and intermediate quench products. The strengths and the uniform elongations of the directly annealed and intermediately quenched steels are about the same for the same fraction martensite, but the total elongation values of the intermediate quench specimens are about one percent better.

Hardness measurements indicate that the strength of the ferrite decreases slightly with increasing volume fraction martensite. This phenomenon will be discussed in what follows.

E. Microstructure/Mechanical Property Correlations

In this section, the microstructural features thought to affect the mechanical behavior of the steels under study are discussed. The rationale underlying the microstructural features which influence the properties will be explained.

Morphological differences have been noted between the products of the intermediate quench and direct anneal heat treatments used in

this study. The size, shape and distribution of the hard phase martensite affects variations in the tensile properties achieved by direct anneal and intermediate quench heat treatments. Previous authors[6,19,25] have described these same effects in relation to the connectivity of martensite. Large (~50μm diameter), globular, banded martensite textures have resulted from the direct anneal heat treatment. This morphology has generally led to higher strengths but poorer ductilities than the intermediate quenched steels containing the same volume fraction of martensite.

Due to thermal cycling in the austenite range, the intermediate quench products have a refined grain size. Moreover, the presence of retained austenite in the martensitic structure obtained after austenitization provides sites for the growth of randomly dispersed acicular austenite particles. These austenite particles grow in an acicular fashion if there is a concentration "spike" of alloying element at the moving austenite/ferrite interface which prevents the diffusion of carbon between phases. When quenched from the two-phase annealing temperature, the acicularly shaped austensite transforms to needle-like particles of martensite.

Thus, the products of the intermediate quench heat treatment have morphologies which are characterized by fine, randomly distributed martensite fibres. The exception to this is the Fe/C/Mo steel in which no retained austenite is found in the martensite. The tensile properties

of the intermediate quench steels generally have significantly better elongation values but slightly lower strengths than their directly annealed counterparts. Hence, it is seen that as the size of the martensite particles are reduced, the shape elongates and their distribution becomes more random, elongations increase at the cost of a slight loss in strength.

Aside from morphological factors caused by varying heat treatments, the tensile properties of the DFM steels of this study are affected by the volume fraction of martensite, the strength of the martensite and the strength of the ferrite. The two-phase mixture rule, $\sigma_c = \sigma_m V_m + \sigma_\alpha(1-V_m)$, easily depicts how these factors influence the strength of the composite.

Since $\sigma_m > \sigma_\alpha$, the strength of the composite, σ_c, will increase with increasing volume fraction martensite, V_m. A reciprocal argument shows, that since $\varepsilon_\alpha > \varepsilon_m$, the elongations of the composite will decrease with increasing amounts of martensite.

Variations in the strengths of the martensite and ferrite are achieved by increased carbon content and precipitation hardening respectively. The variation in martensite volume fraction by heat-treatment induces these changes in σ_m and σ_α (through carbon content; see Figure 42).

As illustrated by Figure 42, the carbon content of the austenite during the two-phase annealing varies as the volume fraction of austenite

changes. In the 20% austenite case, the carbon content of the austenite is about 0.3 wt. pct., whereas in the 40% austenite case, the carbon content is about half this value. Thus, as the volume fraction of austenite is increased, the carbon content of the austenite is decreased. The lowering of carbon content in martensite (quenched austenite) results in a decrease in σ_m. Hence, as the volume fraction of martensite in the composite is raised, the strength of the martensite is decreased. The difference in strength of the composite anticipated by raising the volume fraction of martensite is adjusted by a decreasing σ_m. The variation in martensite strengths agrees with the earlier findings of Young.[25]

Changes in the strength of ferrite may also occur with changing volume fractions of martensite, particularly if there is a ferrite stabilizer added to the Fe-C system. As shown in Figure 42, ferrite stabilizers broaden the α range, decrease the slope of the α-solvus line and increase the slope of the γ-solvus line. Silicon, molybdenum and aluminum are ferrite stabilizers and their effect on the Fe-C system is similar to that depicted in Figure 42.

By decreasing the slope of the α-solvus line, ferrite stabilizers may enhance changes in the equilibrium carbon concentration of ferrite. Thus, changes in the two-phase holding temperature (and hence, changes in the austenite volume fraction) affect changes in the carbon concentration in ferrite. The carbon concentration in ferrite at such

holding temperatures is, however, many times greater than that at room temperature. Upon quenching from the two-phase holding temperature, the supersaturated carbon must precipitate in the ferrite. Different carbon concentrations in ferrite, resulting from different holding temperatures, will thereby induce different amounts of carbon precipitation in the ferrite. The strength of the ferrite will, in turn, be enhanced by these precipitates. The amount of precipitation will decrease as the martensite (quenched austenite) volume fraction is increased. Thus, the strength of the ferrite is expected to decrease as the martensite volume fraction is increased.

It should be noted that, by this analysis, the difference in carbide precipitation between the ferrite of the 20 and 40 percent martensite volume fraction steels is important in identifying the relative ferrite strengthening. Yet, the variation in the precipitate density in the ferrite was observed to be negligible. However, the particle density in the ferrite of the steels studied is of the order of $\sim 10^{14}$ per cm^3. Detecting a change of about 2 in this number which would account for the change in σ_α would be impossible. Again, similar arguments concerning elongation properties apply.

A special case of precipitation occurs in the Fe/C/Al steels, in which rod-like particles are found in the ferrite. These particles, identified tentatively as AlN, are thought to result from the Fe-N system in which a ferrite precipitation situation, similar to the one

discussed above, occurs. This is wholly possible due to the similarities between the Fe-C and Fe-N equilibrium diagrams. Nitrogen could have been incorporated into the alloy by virtue of air melting.

It is informative to consider the amount of ferrite strengthening which can be predicted from the data which has been collected in the course of this investigation. In the analysis that follows, the ferrite strengths are not intended to have any validity in themselves: the strengths computed are used <u>only</u> in the identification of trends. Moreover, the assumptions made in this analysis are far from being justified; several of the values chosen are merely logical guesses.

Table 5 lists experimental data as well as computed values. The tensile stresses of the composite structure (σ_{uts}) are the same at those listed in Table 3. The strengths of martensite σ_m and ferrite, σ_α, are computed making several assumptions: 1) the carbon content of the martensite in the 40% martensite steels is about 0.15 wt. pct., the carbon content of the martensite in the 20% martensite steels is about 0.30 wt. pct.; 2) $\sigma_m = \beta(\%C)^{1/n}$ where β is a proportionality constant and the exponent n is either 1, 2 or 3, in accordance with several theories of martensite strengthening; 3) the proportionality constant, β, is derived from a 100% martensitic 0.07% C steel whose strength is $\sigma_{uts} = \sigma_m \simeq 150$ Ksi; 4) $\sigma_\alpha = \frac{1}{(1-V_m)}[\sigma_{uts} - \sigma_m V_m]$, in accordance with the two-phase mixture rule.

The computed values listed in Table 5 illustrate several points. First, the assumption that the strength of martensite is linearly proportional only to its carbon content appears to be erroneous. The term $\sigma_m V_m$ is greater than the measured strength and forces the ferrite strength to have a negative value which is, of course, impossible. Second, the strengths of the ferrite decrease with increasing martensite volume fraction, at least for the cases where $\sigma_m \propto (\%C)^{1/2}$ or where $\sigma_m \propto (\%C)^{1/3}$. Third, the assumption $\sigma_m \propto (\%C)^{1/3}$ most closely resembles the data derived from microhardness measurements, although both values are known to be erroneous. This last point, that $\sigma_m \propto (\%C)^{1/3}$, reaffirms the earlier results of Young.[25]

F. Comparisons to Previous Work

The intermediate quench heat treatment used in this study has been employed by earlier authors[5,6,19] in investigating the mechanical properties and microsturctures of DFM steels. The direct anneal heat treatment has not yet been extensively used by researchers in the DFM program at the University of California, and for this reason, comparison of the mechanical properties and microstructures is limited to the alloys undergoing the intermediate quench heat treatment.

Most of the mechanical data produced to date of intermediately quench alloys under study at the University of California are reflected in Figure 43. For each alloy listed, the different symbols represent the averaged value for tests done on a given volume fraction of martensite. As is seen by Figure 43, the duplex-ferritic martensitic

steels studied in this work easily exceed the specifications for commercial HSLA steels. Moreover, a wide range of mechanical properties are available among the listed alloys by varying the amount of martensite formed.

A comparison of the strengths vs. volume fraction martensite and elongations vs. volume fraction martensite for the intermediately quenched alloys represented in Figure 43 is shown in Figures 44 and 45, respectively. The banded regions of these figures indicate the usual trend experienced by the alloys listed in Figure 43. The alloys outlined are those which do not follow these trends. All three of these alloys experience precipitation strengthening in the ferrite. Of particular interest is the Fe/.06C/.93Al air melted alloy used in this study. For this steel there is almost no variation in the tensile properties produced despite the variation in volume fraction martensite. This result is of extremely important practical significance in that the reproducibility of properties can be sustained over a wide range of heat treatment. Annealing temperature in the two-phase region can be varied by as much as 65° C with reproducible results. Hence, this Fe/.06C/.93Al alloy appears to be especially attractive for commercial use.

V. Conclusions

Based upon the investigation and characterization of the duplex ferritic-martensitic steels used in this study, the following conclusions can be drawn:

1) The two-phase mixture rule, $\sigma_c = \sigma_m + \sigma_\alpha (1-V_m)$ may be used to empirically describe the tensile properties of these duplex alloys. It is necessary to consider <u>all</u> variables in this equation to understand the behavior of the composite structure.

2) The largest factor controlling the strength and ductility of the duplex steels under study is the volume fraction of martensite in the composite.

3) Ferrite strengthening, as a function of the amount of martensite formed, is important in controlling the properties produced in duplex steels. In particular, an air melted Fe/.06C/.93Al duplex steel has been found to give the same tensile properties, independent of volume fraction martensite (up to ~.4) due to strengthening of the ferrite by fine precipitates. This allows for the reproducibility of properties to be sustained over a wide range of two-phase annealing temperatures.

4) The strength of martensite, as a function of the amount of martensite formed, also influences the strength of the composite. At lower volume fractions of martensite, σ_m is higher due to increased carbon content.

5) In addition to the two-phase mixture rule, the size, shape, and distribution (connectivity) of the strong phase martensite influences the tensile properties of the composite. Large, globular, banded martensite particles produce higher strength but poorer ductility than do small, acicular, randomly dispersed martensite fibers.

6) The intermediate quench heat treatment, which produces small randomly dispersed martensite fibers, provides better combination of strength and ductility than those produced by the direct anneal heat treatment.

7) The fibrous martensite morphology produced by the intermediate quench heat treatment is due to both the partitioning effect of alloying elements on carbon diffusion and the presence of retained austenite in the martensite. If either of these factors are absent, a fibrous martensite morphology will not result. The formation of proeutectoid ferrite during the quench from the austenitization temperature of the intermediate quench heat treatment affects the distribution of martensite in the final composite product.

8) The initial morphology present prior to processing affects the distribution of martensite in the final morphology of the direct anneal process. In particular, a banded, textured initial morphology will result in a banded,textured DFM alloy.

9) Without thermomechanical treatment, the duplex steels studied in this report easily exceed specifications for commercial HSLA steels. The mechanical properties compare favorably with those of previously studied DFM steels.

ACKNOWLEDGEMENTS

The author extends his appreciation and gratitude to Professor Gareth Thomas for his support, encouragement and guidance throughout the course of this investigation. Discussions and criticisms of this investigation by Drs. J-Y Koo and B. V. N. Rao were instrumental in the understanding of the findings produced. Thanks are also due to Professors I. Finnie and J. W. Morris for reviewing this manuscript.

Technical assistance provided by the support staff of the Materials and Molecular Research Division of the Lawrence Berkeley Laboratories is gratefully acknowledged. Thanks are due in particular to Carolyn Gosnell, Lee Johnson, Gloria Pelatowski, Don Krieger, Rich Lindberg and Kathleen Wilkinson. The Republic Steel Company graciously supplied the alloys for this research. Dr. M. Raghavan of the Exxon Research Laboratories performed STEM studies on the Fe/C/Al alloy.

May Carolyn Gosnell pardon my clumsy ineptitude at the electron microscope, and may K. Wilkinson forgive my pestering impudence.

The author is greatly indebted to this parents and family for their patience, understanding and encouragement during this work. I congratulate my friends on enduring my irascible behavior during this research. A particular thanks to Monsieur R. E. Walker who helped in specimen preparation.

This research was supported by the U.S. Department of Energy.

REFERENCES

1. Carlo Parrani et. al., Micro Alloying 75, Symposium on High Strength, Low-Alloy Steels, Products and Process, p. 56 Washington D.C. (1975).

2. I. Tamura et. al., Trans. Iron Steel Inst. Japan 13, 283 (1973).

3. J. Y. Koo and G. Thomas, Mat. Sci. and Eng. 24, 187 (1976).

4. J. Y. Koo and G. Thomas, Met. Trans., 8a, 525 (1977).

5. J. Y. Koo, M.S. thesis, Univ. of Calif., Berkeley LBL-3587 (1975)

6. J. Y. Koo, Ph.D. thesis, Univ. of Calif., Berkeley LBL-6657 (1977).

7. R. G. Davies, Ford Research Report #SR-77-29 (1977).

8. R. G. Davies, Met. Trans. 9a, 671 (1978).

9. R. L. Cairns and J. A. Charles, JISI 205, 1044 (1967).

10. R. A. Grange, Met. Trans., 2, 65 (1971).

11. K. Nakoaka, K. Araki, and O. Uchida, Sosei Tokako 17, 190, p. 875 (1976).

12. K. Araki, S. Fukuneda and K. Ochida, Technical Research Publication, Nippon Kokan K. K. (1977).

13. G. E. Dieter, Mechanical Metallurgy, McGraw-Hill, p. 227 (1976).

14. E. Orowan, Nature, 149, 643 (1942).

15. G. C. Sih, E. P. Chen and S. H. Huang, Engr.-Fracture Mechanics 6, 343 (1974).

16. E. O. Hall, Proc. Phys. Soc., B64, 742 (1951).

17. W. J. Petch, Iron and Steel Inst. Journal, London, 174, 25 (1953).

18. G. Thomas, Battelle Conf. on Fundamental Aspects of Structural Alloy Design, LBL-4175 (1975).

19. P. Costello, M.S. thesis, Univ. of Calif., in printing (1979).

20. J. E. Hilliard and W. S. Owen, JISI, Nov. 1952, p. 268.

21. M. S. Bhat, Ph.D thesis, LBL #6046 (1977) p. 63.

22. Materials Handbook, Vol. 9, p. 410.

23. M. R. Plichta and H. I. Aaronson, Met. Trans. 5, 2611 (1974).

24. E. C. Bain, Alloying Elements in Steel ASM, (1940) p. 305.

25. M. J. Young, M.S. thesis, Univ. of Calif. Berkeley, LBL-6620 (1977), p. 10.

26. H. W. Paxton, Symposium on Transformations and Hardenability in Steels, Climax Molybdenum Company, p. 3 (1977).

27. R. W. Cahn, Recrystallization, Grain Growth and Textures, American Metals Society, Metals Park, pp. 109-116 (1966).

28. K. J. Ivine and F. B. Pickering, JISI, 201, 944 (1963).

29. P. G. Shewmon, Transformations in Metals McGraw-Hill, New York (1969).

30. Robert Clarke, M.S. thesis, University of Calif., Berkeley, LBL #1801 (1973).

31. G. Thomas and J-Y Koo, Aime Symposium on Duplex Steels, New Orleans, Feb. 1979, in press.

Table 1

Alloy Compositions (wt. pct.)

Nominal Composition	C	Si	Al	Mo	Mn	Fe
Fe/.07C/.94Mo	.070	.02	.027	.940	.15	bal
Fe/.075C/.6 Si/.94Mo	.075	.06	.020	.940	.15	bal
Fe/.06C/.93 Al	.060	.02	.930	-	.10	bal
Fe/.065C/.42 Si/.98 Al	.065	.42	.980	-	.11	bal

Table 2

HEAT TREATMENT TEMPERATURES

Alloy	100% Austenite	40% Austenite	20% Austenite
Fe|.07C|.94Mo	1050°C	870°C	820°C
Fe|.075C|.6Si|.94Mo	1050°C	910°C	850°C
Fe|.06C|.93Al	1080°C	1010°C	960°C
Fe|.065C|.42Si|.98Al	1350°C	1040°C	950°C

Table 3. Data Summary Sheet

	HEAT TREATMENT	% REDUCTION OF AREA	Yield ksi	Yield MPa	UTS ksi	UTS MPa	uniform %	total %
Fe 07C .94Mo	Intermediate quench 20% Martensite	49.4±1.9	58.86±1.59	405.8±11.0	94.33±0.99	650.4± 6.8	11.47±0.86	17.58±0.84
	Direct anneal 20% Martensite	45.0±1.9	61.77±0.59	425.9± 4.1	98.38±0.77	678.3± 5.3	10.05± 0.50	14.68±0.99
	Intermediate quench 40% Martensite	50.8±1.0	65.33±2.24	450.5±15.5	102.10±1.73	703.9±11.9	9.59±0.40	15.21±1.00
	Direct anneal 40% Martensite	42.0±1.9	66.90±2.27	461.3±15.7	105.04±1.44	724.2± 9.9	8.04±0.62	12.77±0.76
Fe .075C .6Si .94Mo	Intermediate quench 20% Martensite	58.5±0.7	57.58±0.84	397.0± 5.8	99.79±0.70	688.0± 4.8	14.64±0.93	22.41±0.87
	Direct anneal 20% Martensite	46.0±1.1	67.13±1.70	462.9±11.7	110.71±1.03	763.3± 7.1	10.71±0.52	15.39±0.77
	Intermediate quench 40% Martensite	62.5±0.6	70.39±2.12	485.3±14.6	111.78±1.54	770.7±10.6	12.05±0.63	20.86±0.72
	Direct anneal 40% Martensite	45.8±1.0	79.63±2.55	549.1±17.6	119.88±1.35	826.6± 9.3	9.22±0.41	15.23±0.85
Fe .06C .93Al	Intermediate quench 20% Martensite	71.8±1.8	73.16±1.09	504.4± 7.5	111.01±1.25	765.4± 8.6	11.76±0.88	21.83±0.53
	Direct anneal 20% Martensite	74.5±1.5	70.92±1.05	489.0± 7.2	104.32±1.94	719.3±13.4	10.64±0.47	20.68±0.74
	Intermediate quench 40% Martensite	74.3±0.9	74.20±0.97	511.6± 6.7	108.65±1.40	749.1± 9.6	11.14±0.89	21.81±1.35
	Direct anneal 40% Martensite	75.6±1.9	71.85±2.15	495.4±14.8	102.70±3.36	708.1±23.2	10.37±89	21.81±1.35
Fe .065C .42Si .98Al	Intermediate quench 20% Martensite	63.3±1.9	64.53±0.95	479.4± 6.6	108.66±1.84	749.19±12.7	11.92±0.68	21.84±1.12
	Direct anneal 20% Martensite	66.9±1.4	72.52±0.73	500.0± 5.0	111.86±1.62	771.3±11.2	11.96±0.75	20.88±0.56
	Intermediate quench 40% Martensite	68.6±1.2	80.66±2.07	556.1±14.3	115.10±2.0	793.6±13.8	11.18±1.12	21.18±0.88
	Direct anneal 40% Martensite	71.3±0.9	77.09±1.41	531.5± 9.7	112.76±1.84	777.5±12.67	11.19±1.36	20.87±1.78

Table 4

Microhardness Data: Ferrite in Directly Annealed Specimens

Composition	% Martensite	V_H	σ_α (Ksi)
Fe|.07C|.94Mo	20	177.0	82.0
	40	164.2	77.0
Fe|.075C|.6Si|.94Mo	20	176.6	82.0
	40	168.2	78.0
Fe|.06C|.93Al	20	198.4	91.0
	40	182.0	85.0
Fe|.065C|.42Si|.98Al	20	197.2	90.5
	40	188.6	87.0

Table 5

Martensite and Ferrite Computed Strengths

ALLOY	V_m(%)	σ_{uts} (Ksi) I.Q.	σ_{uts} (Ksi) D.A.	σ_m A1	V_m (Ksi) A2	V_m (Ksi) A3	σ_α (I.Q.Ksi) A1	σ_α (I.Q.Ksi) A2	σ_α (I.Q.Ksi) A3	σ_α (D.A.,Ksi) A1	σ_α (D.A.,Ksi) A2	σ_α (D.A.,Ksi) A3	σ_α * (Ksi)
Fe|.07C|.94Mo	20	94.3	98.4	128	62	49	-42	40	56	-37	46	62	82.0
	40	102.1	105.0	128	88	78	-43	24	40	-38	28	45	77.0
Fe|.075C|.6Si|.94Mo	20	99.8	110.7	128	62	49	-35	47	77	-22	61	77	82.0
	40	111.8	119.9	128	88	78	-27	40	56	-14	53	55	78.0
Fe|.06C|.93Al	20	111.0	104.3	128	62	49	-21	61	69	-30	53	59	91.0
	40	108.7	102.7	128	88	78	-32	35	51	-42	25	41	85.0
Fe|.065C|.42Si|.98Al	20	108.7	111.9	128	62	49	-24	58	75	-20	62	79	90.5
	40	115.1	112.8	128	88	78	-22	45	62	-25	41	58	87.0

*: from hardness measurements
I.Q.: intermediate quench
D.A.: direct anneal
A1: n=1 $\beta \sim 2140$ Ksi
A2: n=2 $\beta \sim 567$ Ksi
A3: n=3 $\beta \sim 365$ Ksi

Assumptions:

(a) at $V_m = .4\ C_m \sim 0.15$ wt. pct.

at $V_m = .2\ C_m \sim 0.30$ wt. pct.

(b) $\sigma_m = \beta(\%C)^{1/n}$ n = 1,2,3

(c) for a 100% martensitic 0.07%C steel

$\sigma_m = \sigma_{uts} \sim 150$ Ksi

(d) $\sigma_\alpha = 1-\frac{1}{V_m}\ [\sigma_{uts} - \sigma_m V_m]$

FIGURE CAPTIONS

1. Experimental heat treatments used in this study. Austenitizing and two-phase ($\alpha+\gamma$) annealing temperatures are specified in Table 2.

2. Cylindric test specimen used to determine two-phase ($\alpha+\gamma$) annealing temperatures for 20% and 40% martensite, as well as austenitizing temperatures.

3. Schematic drawing of an ASTM round tensile specimen cut from as-received, hot-rolled plates. Note that the specimen is cut transverse to the rolling direction.

4. Optical micrographs of the as-received, hot-rolled rolled steels: (a) Fe|.07C|.94Mo; (b) Fe|.075C|.6Si|.94Mo; (c) Fe|.06C|.93Al; (d) Fe|.065C|.42Si|.98Al

5. Optical micrographs of the ~100% martensitic structure present after the austenitization and subsequent quench of the intermediately quenched steels: (a) Fe|.07C|.94Mo; (b) Fe|.075C|.6Si|.94Mo; (c) Fe|.06C|.93Al; (d) Fe|.065C|.42Si|.98Al

6. Optical micrographs of the final products of the Fe|.07C|.94Mo alloy: (a) ~20% martensite, intermediate quench; (b) ~20% martensite, direct anneal; (c) ~40% martensite intermediate quench; (d) ~40% martensite, direct anneal.

7. Composite electron micrograph of a globular martensite particle found within a ~40% martensite, intermediately quenched Fe|.07C|.94Mo steel.

8. Electron micrographs of the ferrite within the Fe|C|Mo steels showing the presence of small spherical particles, which are presumed to be carbides: (a) from a ~20% martensite directly annealed steel; (b) from a ~40% directly annealed steel.

9. Martensite substructure in the Fe|C|Mo duplex steels, in which no retained austenite is found: (a) from a ~40% martensite, intermediate quench steel; (b) from a ~20% martensite, intermediate quench steel.

10. Adjacent martensite lath orientation in the Fe|C|Mo steels, in which no retained austenite was found. Twinning occurs on the $(\bar{2}11)$ plane across the lath boundary.

11. Martensite laths in the Fe|C|Mo steels showing the presence of carbides within the laths. Both figures are from a ~40% martensite, intermediate quench steel.

12. Optical micrographs of the final products of the Fe|.075C|.6Si|.94Mo alloy: (a) ~20% martensite, intermediate quench; (b) ~20% martensite, direct anneal; (c) ~40% martensite, intermediate quench; (d) ~40% martensite, direct anneal.

13. Composite electron micrograph of an acicular martensitic fiber found within a ~40% martensite, intermediately quenched Fe|.075C|.6Si|.94Mo steel.

14. Bright field/dark field electron micrograph pair illustrating the presence of thin films of retained austenite trapped between the martensitic laths of a ~40% martensite, directly annealed Fe|.075C|.6Si|.94Mo alloy.

15. A high magnification bright field/dark field pair of electron micrographs illustrating retained austenite in a ~20% martensite, direct anneal Fe|.075C|.6Si|.94Mo steel.

16. Small spherical carbides found within the ferrite phase of the Fe|.075C|.6Si|.94Mo steels: (a) from a ~20% martensite intermediate quench steel (low magnification); (b) from a ~40% martensite direct anneal steel (higher magnification).

17. Optical micrographs of the final products of the Fe|.06C|.93Al alloy: (a) ~20% martensite, intermediate quench; (b) ~20% martensite, direct anneal; (c) ~40% martensite, intermediately quench; (d) ~40% martensite, direct anneal.

18. Composite electron micrograph of a lath martensite fiber found in a ~20% martensite, intermediate quench Fe|.06C|.93Al steel.

19. Bright field/dark field electron micrograph pair illustrating retained austenite trapped as thin films between martensite laths of the Fe|.06C|.93Al, ~40% martensite, intermediate quench steel.

20. Bright field/dark field electron micrograph pair illustrating Widmanstatten cementite (Fe_3C) with martensite laths of the Fe|.06C|.93Al, ~20% martensite, directly annealed steel.

21. Particles within the ferrite phase of the Fe|.06C|.93Al steels: (a) a mixture of spheres and rods, (b) rods in higher magnification; (c) rods and spheres in higher magnification. These particles are found in the ferrite of all the Fe|C|Al Steels.

22. High magnification micrograph of rods within the ferrite of the Fe|C|Al steels. These particles are thought to be AlN.

23. Composition analysis trace for Al in a ~20% martensite, direct anneal steel. Results show an enrichment of Al in the ferrite.

24. Optical micrographs of the final products of the Fe|.065C|.42Si|.98Al alloy: (a) ~20% martensite, intermediate quench; (b) ~20% martensite, direct anneal; (c) ~40% martensite, intermediate quench; (d) ~40% martensite, direct anneal.

25. An energy dispersion analysis of x-rays in the Fe|C|Si|Al steel, ~40% martensite, intermediate quench. "Rivers" of ferrite are seen to be free of alloying element while composite "islands" are enriched.

26. Retained austenite in a ~40% martensite, intermediate quench Fe|C|Si|Al steel.

27. Composite electron micrograph of an acicular martensite fiber in a ~20% martensite, intermediately quenched Fe|.065C|.42Si|.98Al alloy.

28. An enlarged portion of Figure 27, illustrating twinned martensite laths and also spherical particles in the ferrite matrix.

29. Spherical particles within the ferrite phase of the Fe|C|Si|Al steels: (a) from a ~20% martensite, intermediate quench steel; (b) from a ~40% martensite, intermediate quench steel.

30. Spherical particles within the ferrite of a ~20% martensite, direct anneal Fe|.065C|.42Si|.98Al steel.

31. Representative fractographs of the failed tensile specimen: (a) from a Fe|C|Si|Mo, ~40% martensite intermediate quench specimen; (b) from a Fe|C|Al, ~20% martensite, direct anneal specimen.

32. Inclusions found within fractography specimens. Both (a) and (b) are from the Fe|C|Al alloy.

33. Aluminum particle within the fractograph of an Fe|C|Si|Al steel.

34. Strength vs. uniform elongation for the Fe|.07C|.94Mo steels.

35. Strength vs. total elongation for the Fe|.07C|.94Mo steels.

36. Strength vs. uniform elongation for the Fe|.075C|.6Si|.94Mo steels.

37. Strength vs. total elongation for the Fe|.075C|.6Si|.94Mo steels.

38. Strength vs. uniform elongation for the Fe|.06C|.93Al steels.

39. Strength vs. total elongation for the Fe|.06C|.93Al steels.

40. Strength vs. uniform elongation for the Fe|.065C|.42Si|.98Al steels.

41. Strength vs. total elongation for the Fe|.065C|.42Si|.98Al steels.

42. The Fe-rich portion of the Fe-C diagram and the same Fe-C diagram with a ferrite stabilizer added. Tie-lines for the 20 and 40 percent austenite volume fractions are shown.

43. Strength vs. total elongation for various alloys previously studied at the University of California, Berkeley. Each symbol of the same alloy reflects a different volume fraction of martensite.

44. Strength vs. volume fraction martensite. The banded regions are for the yield and tensile strengths of the alloys listed on Figure 43. Outlined data is for those alloys which do not follow the trend.

45. Elongation vs. volume fraction martensite. The banded regions are for the total and uniform elongations of the alloys listed on Figuer 43. Outlined data is for those alloys which do not follow the trend.

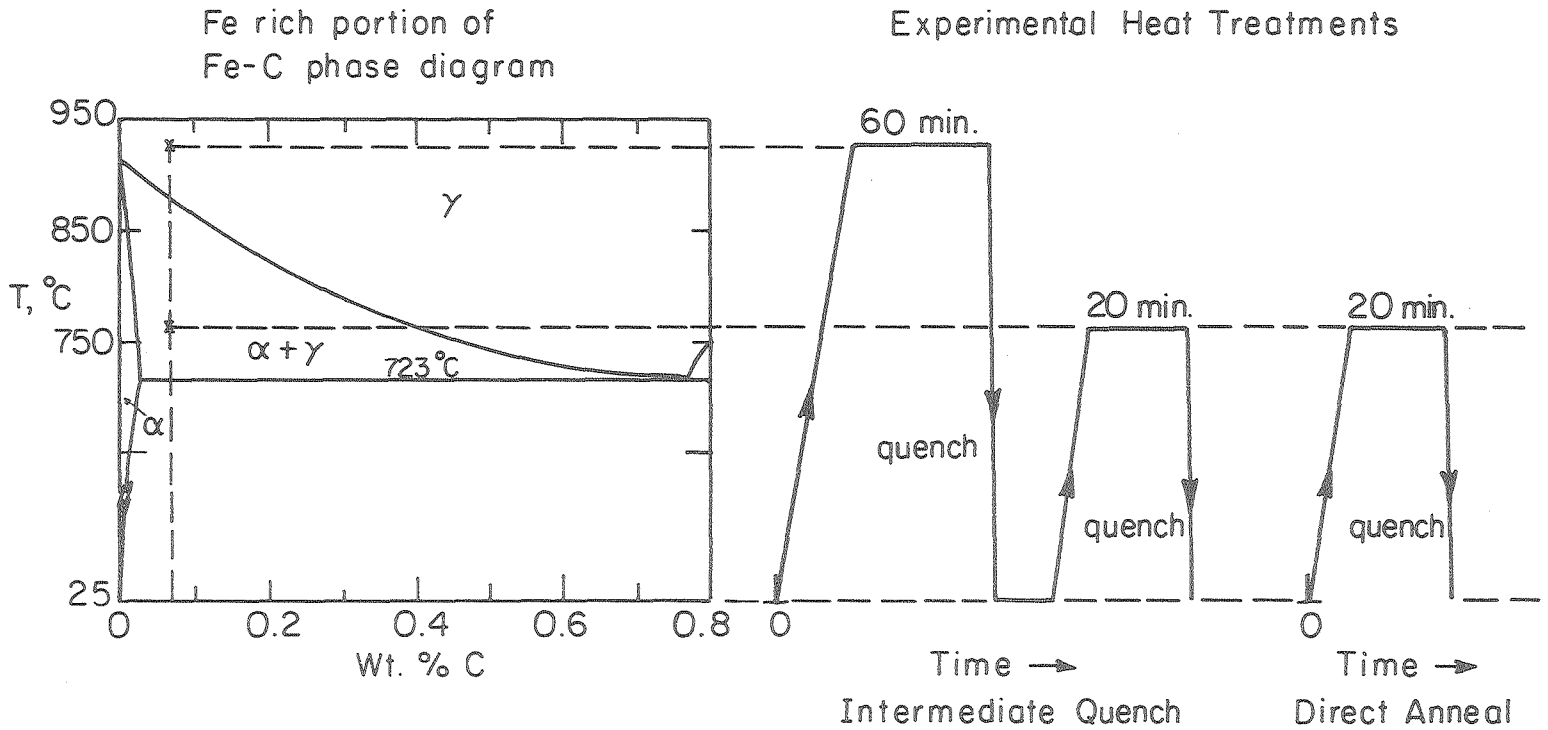

XBL 789-5833

Fig. 1

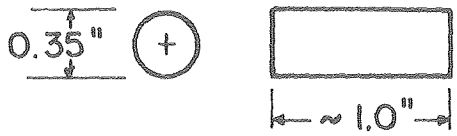

Fig. 2 Cylindrical Test "Pellets" for Heat Treatment

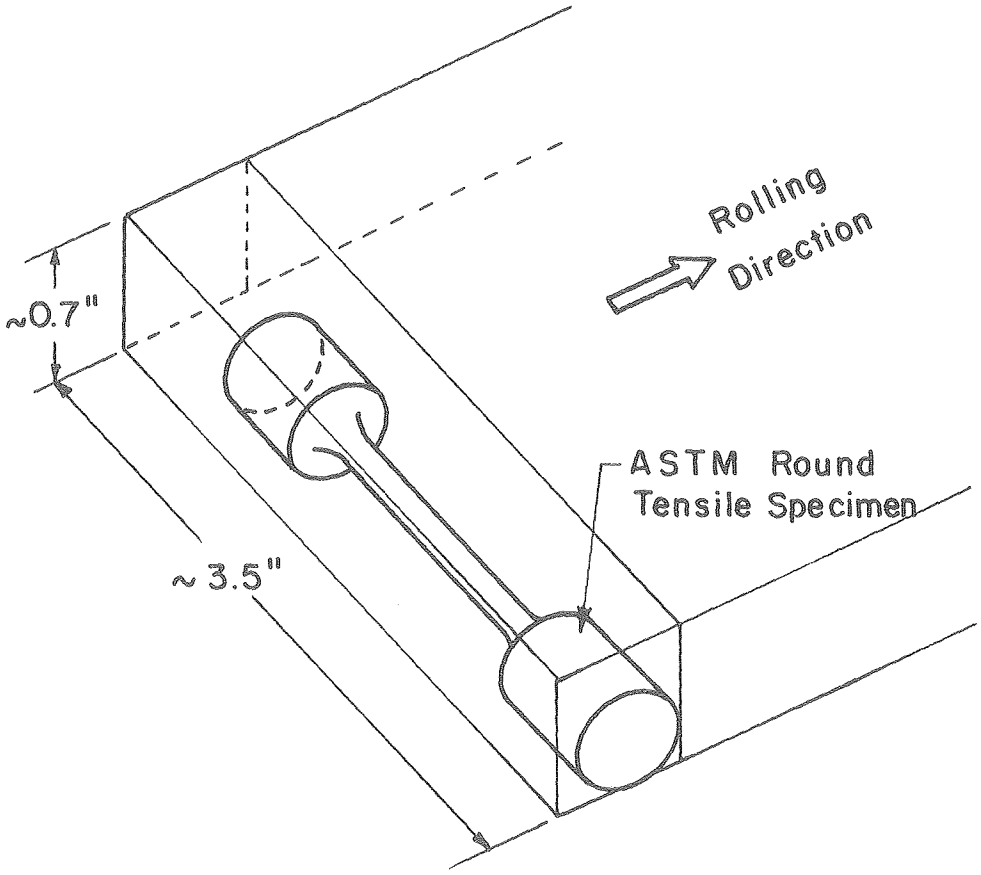

Fig. 3

XBL792-5684

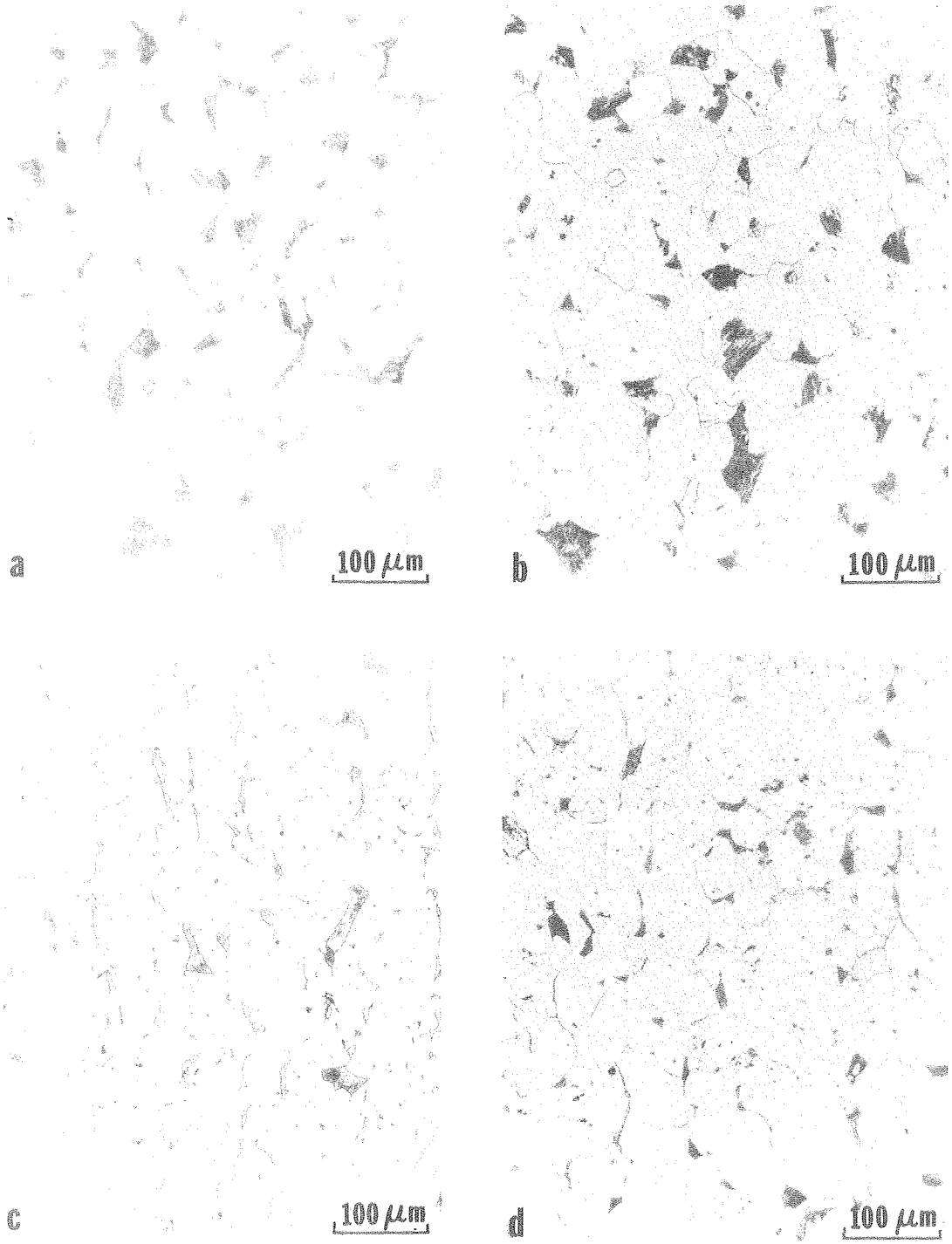

XBB 780 13107

Fig. 4

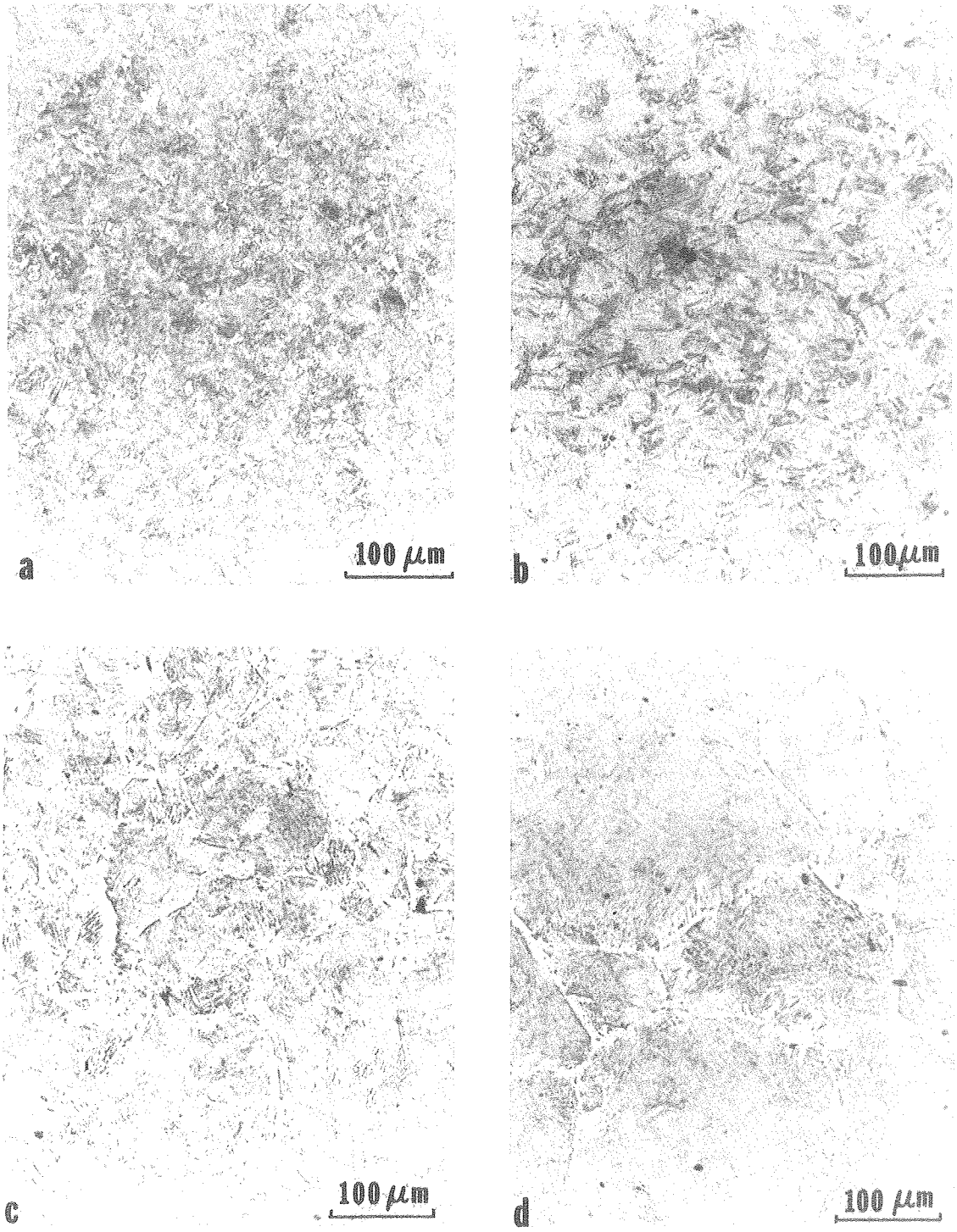

XBB 791 512

Fig. 5

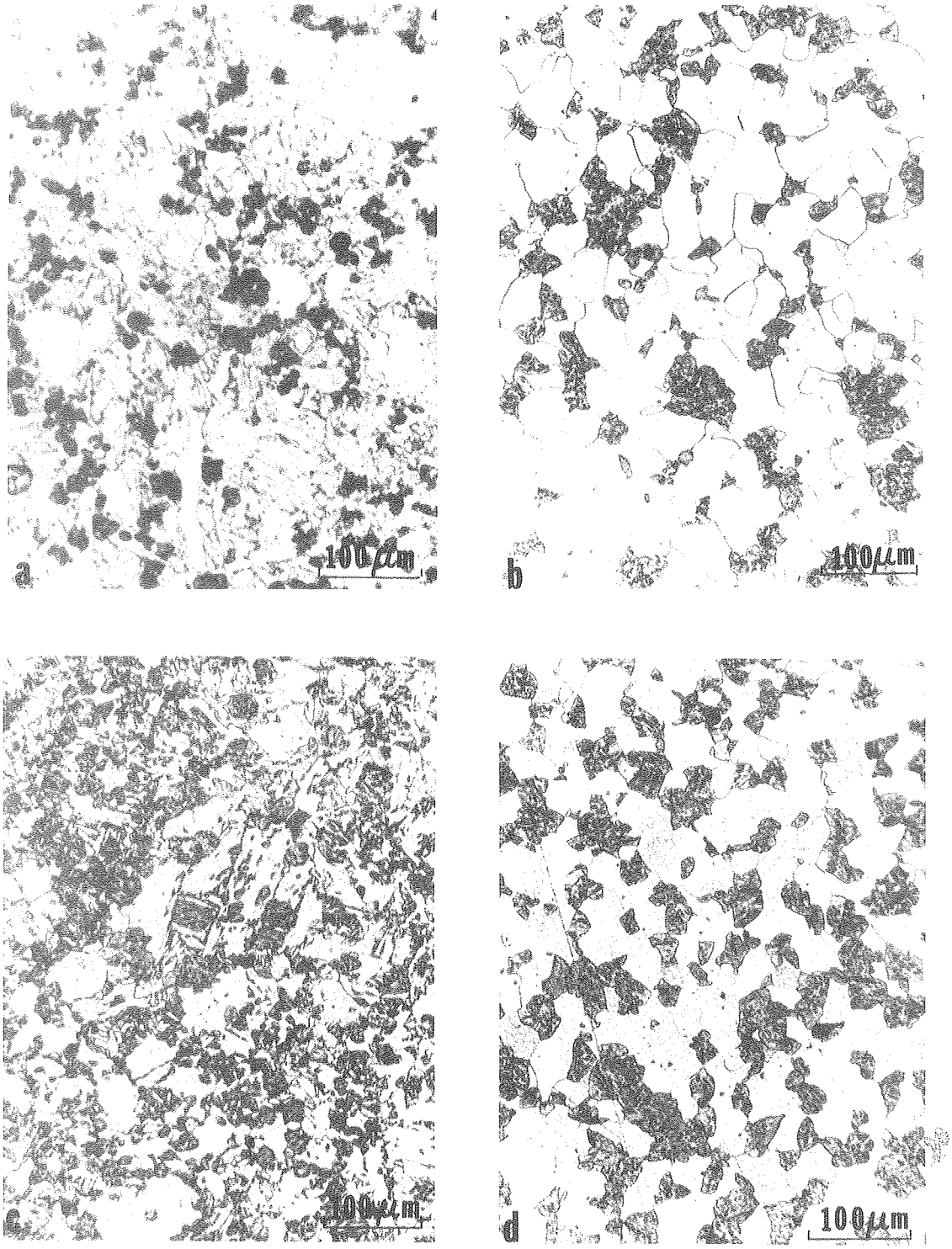

Fig. 6

XBB 789 10917

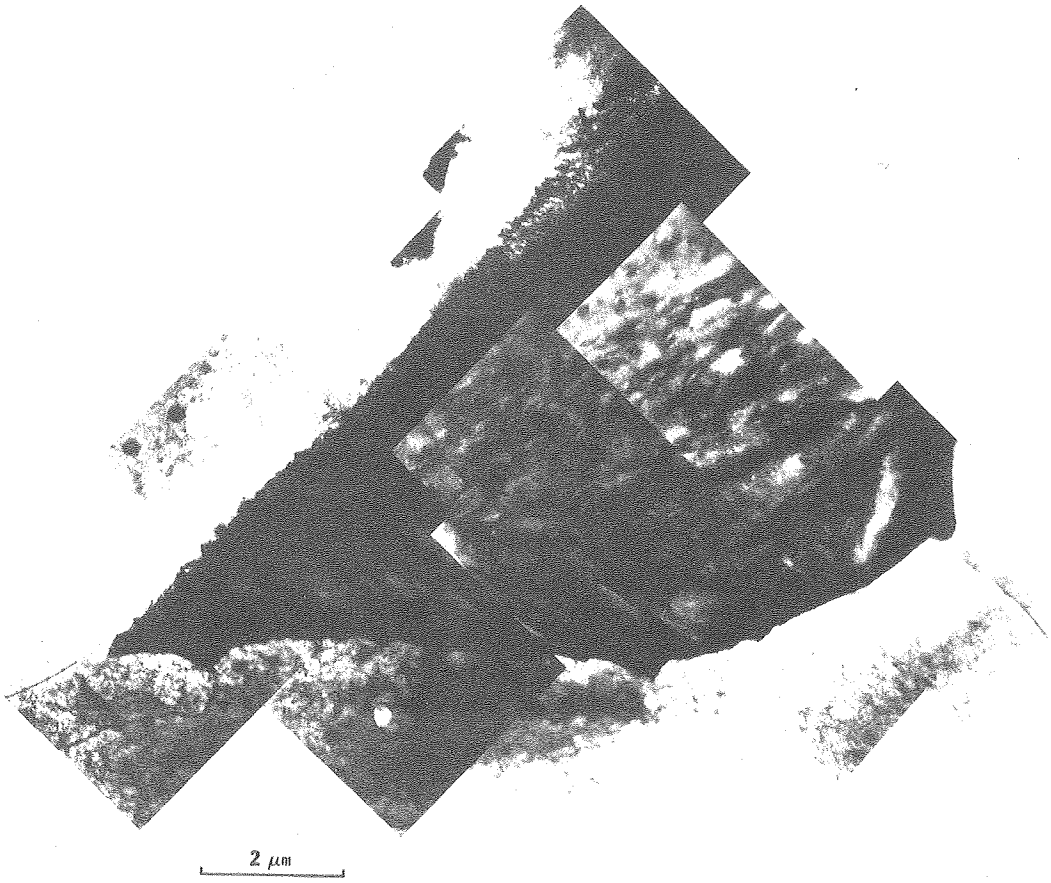

XBB 780 13297

Fig. 7

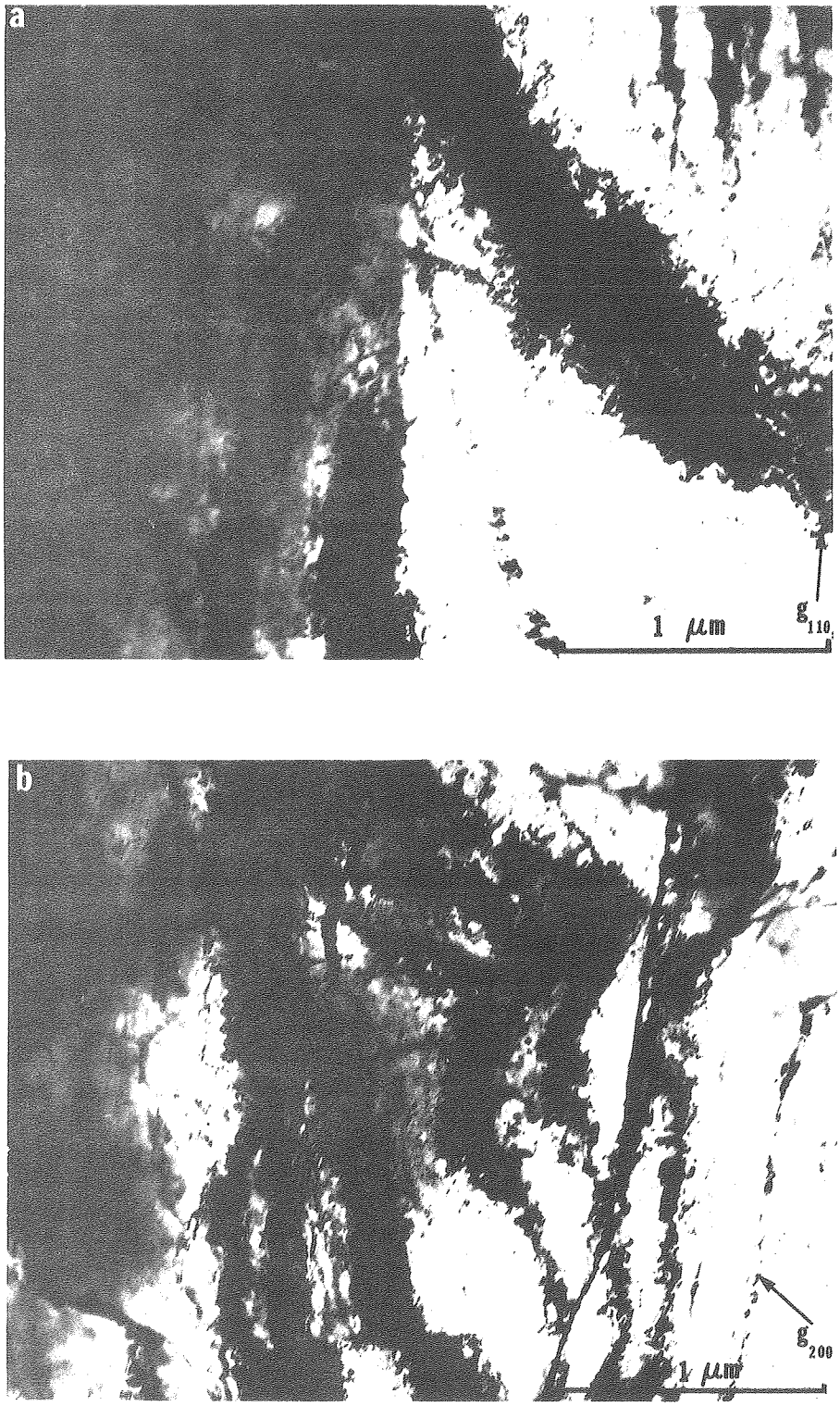

XBB 793 3317

Fig. 8

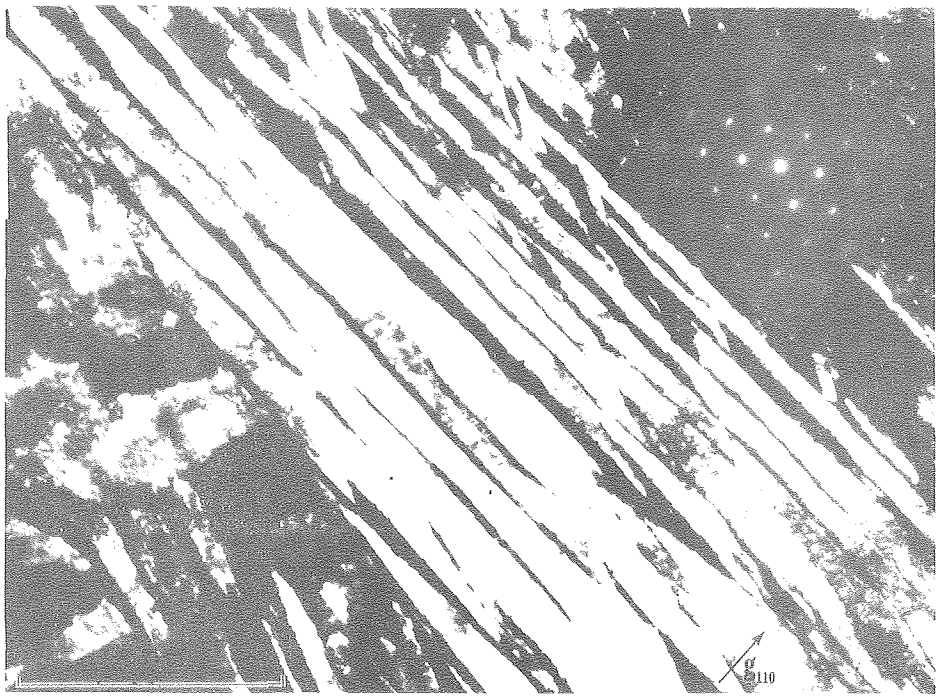

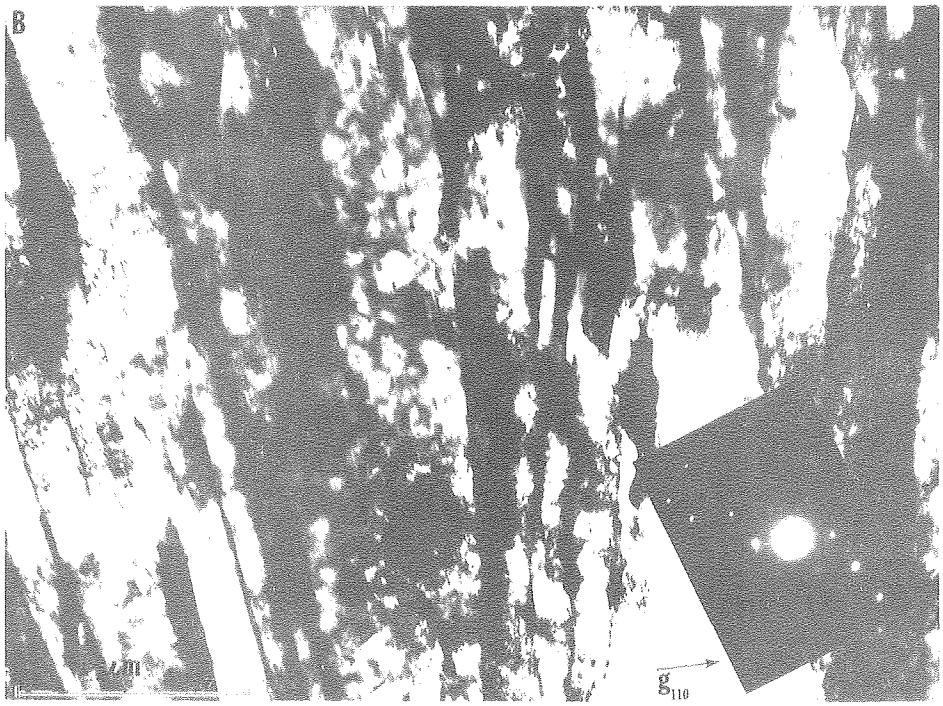

XBB 793 3328

Fig. 9

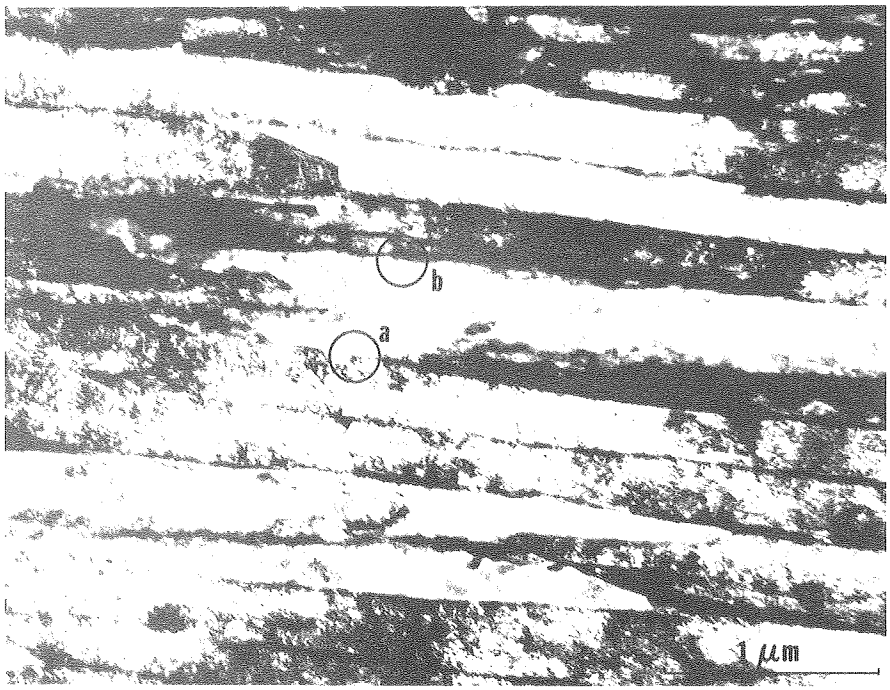

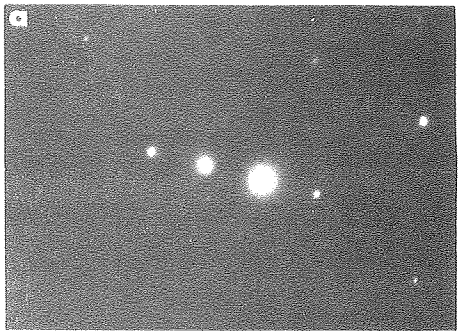

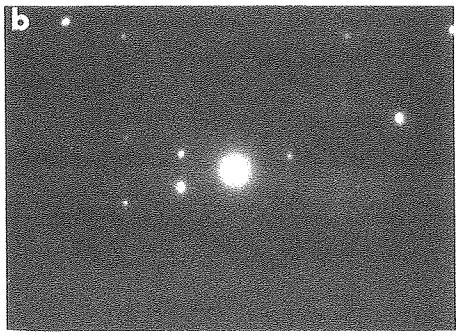

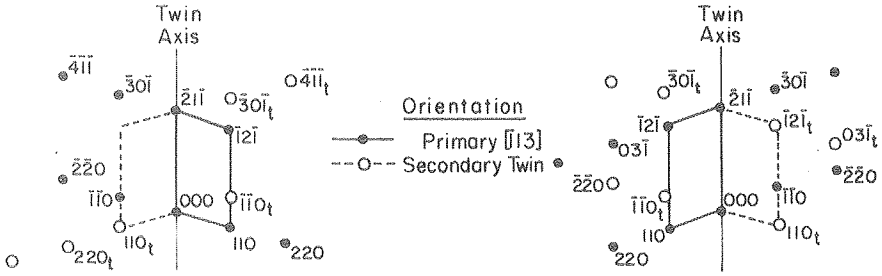

XBB 793 3339

Fig. 10

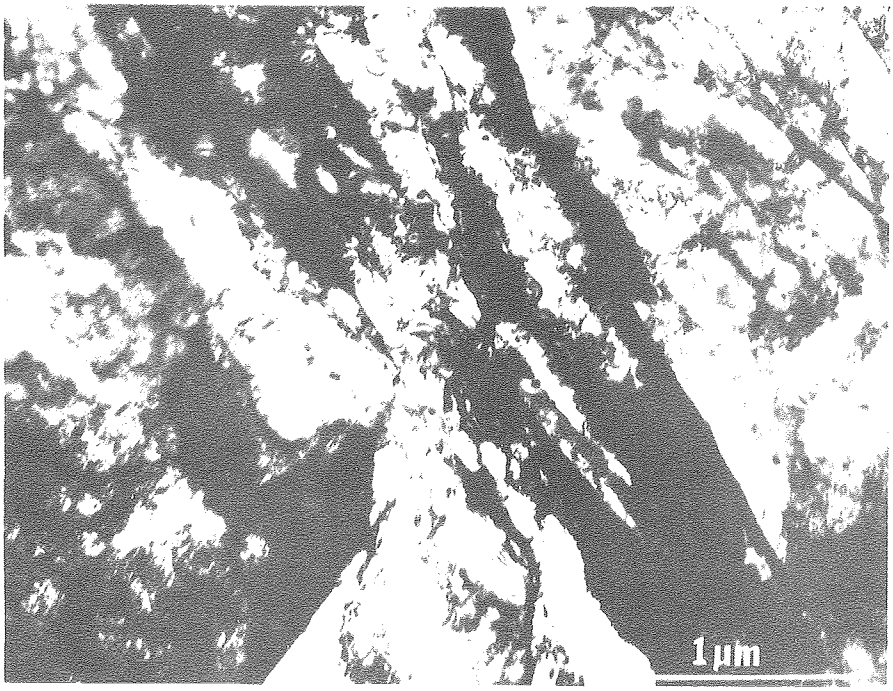

XBB 793 3325

Fig. 11

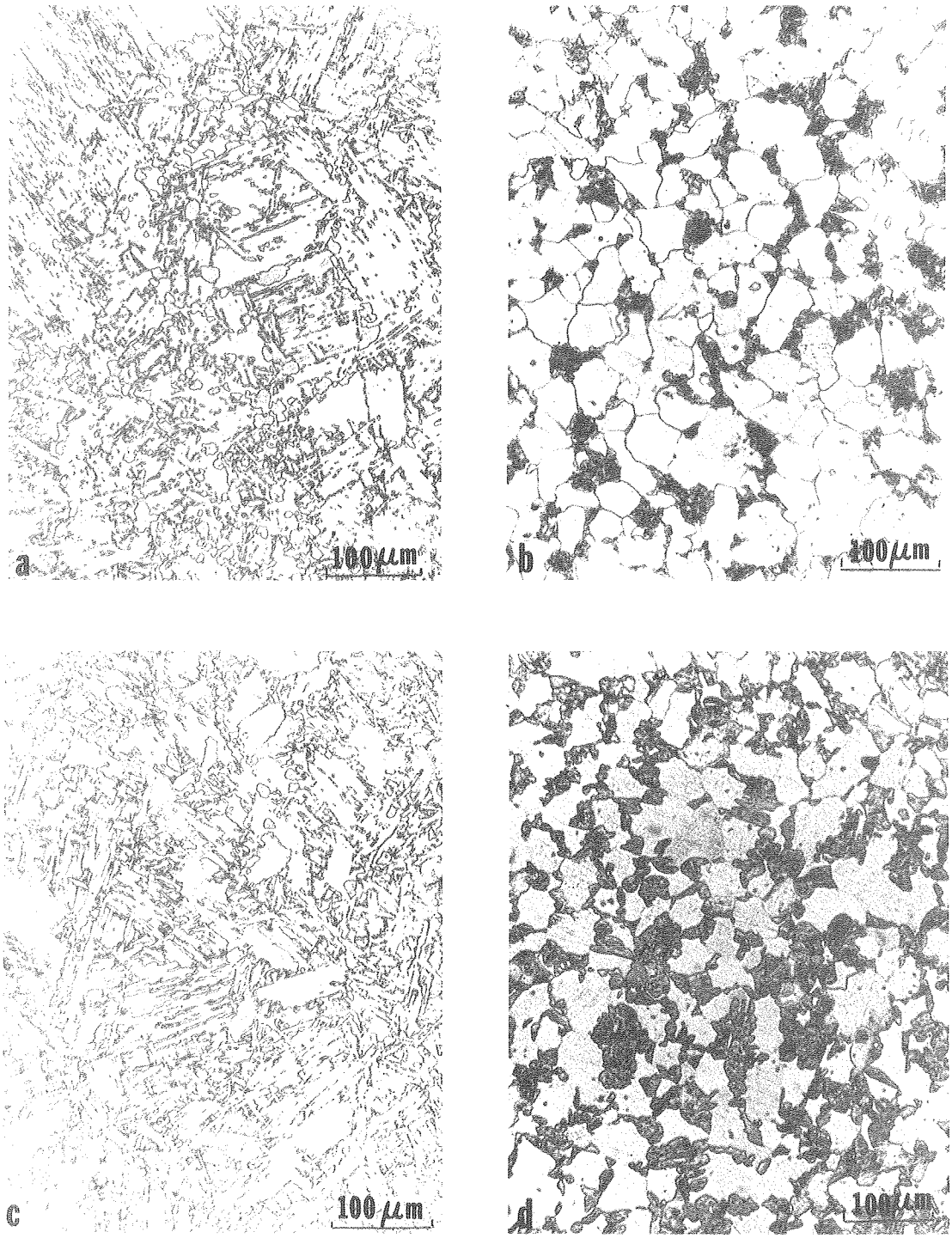

XBB 789 10918

Fig. 12

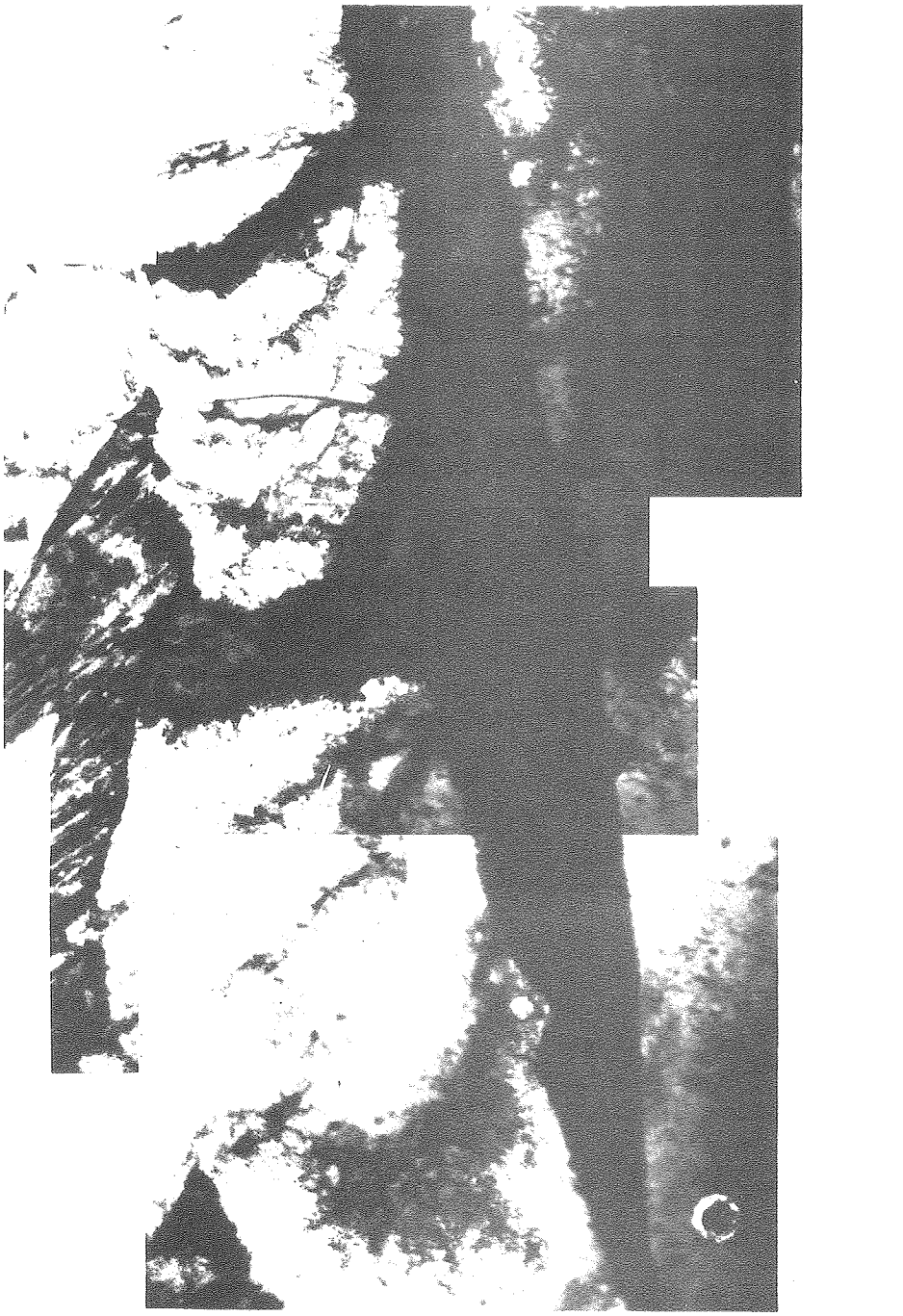

2 μm

XBB 793 3329

Fig. 13

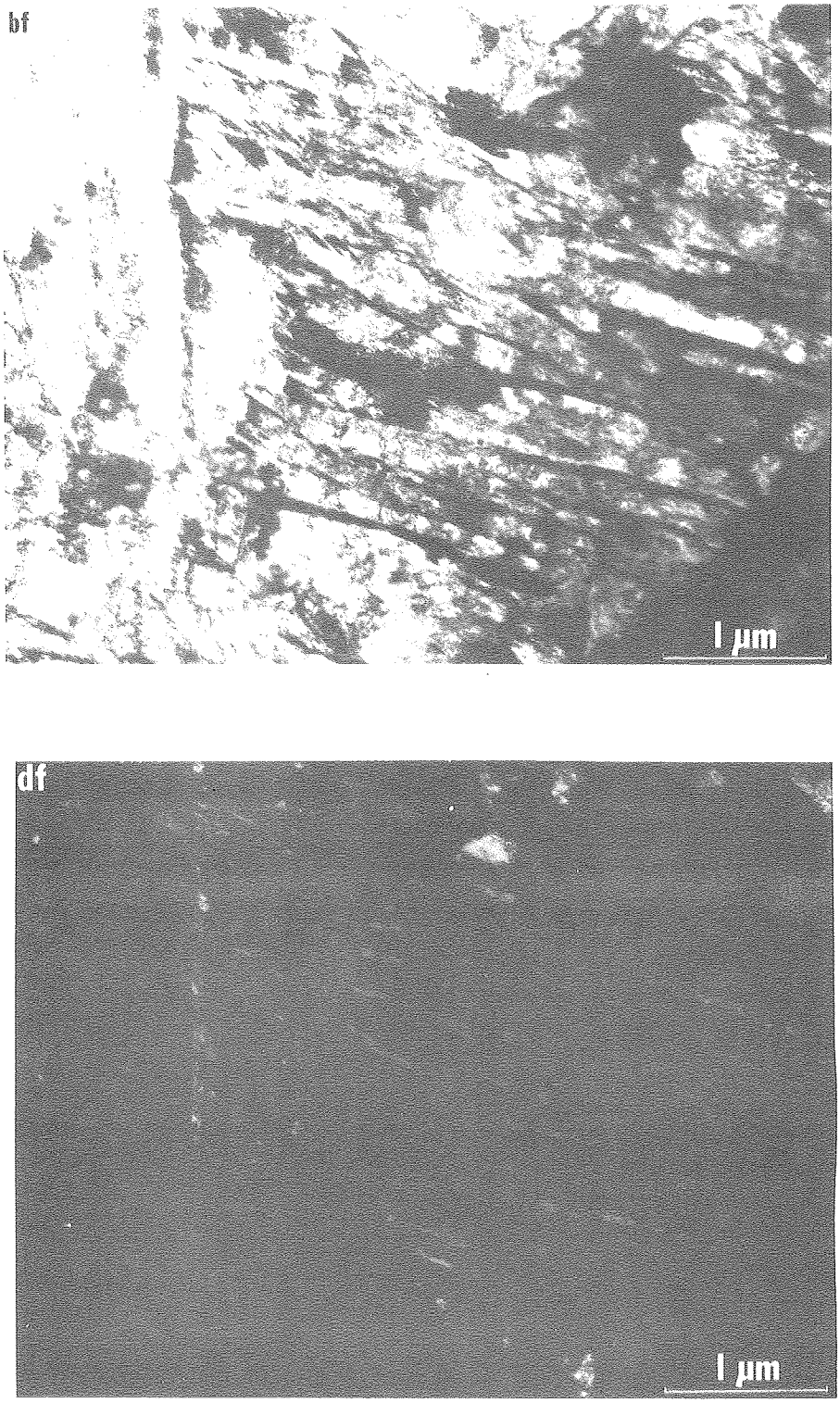

XBB 793 3319

Fig. 14

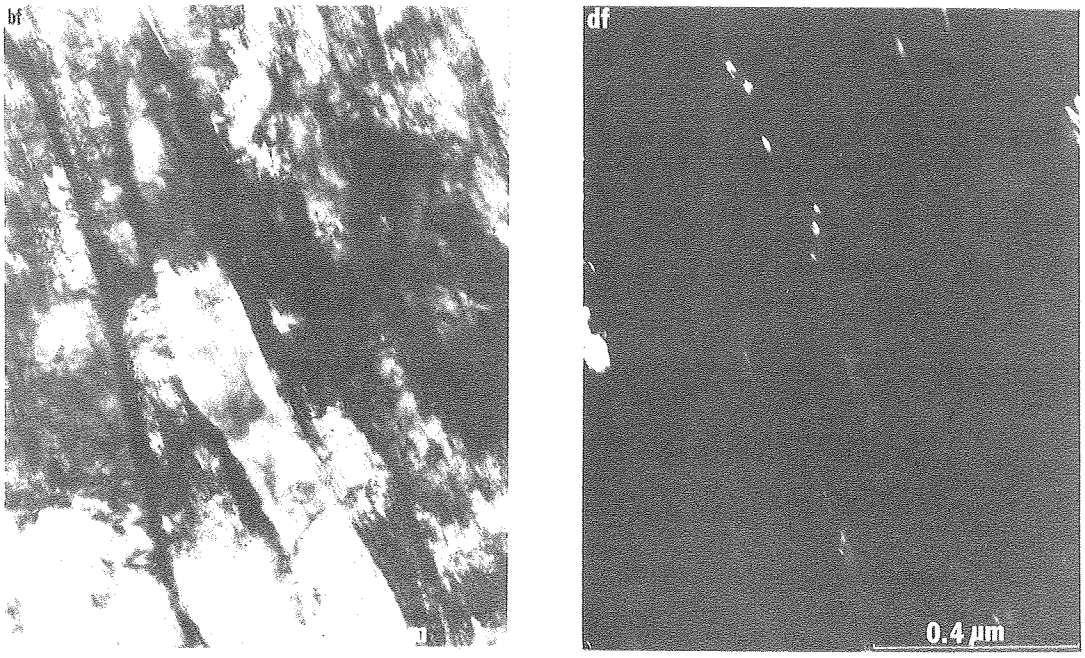

XBB 793 3320

Fig. 15

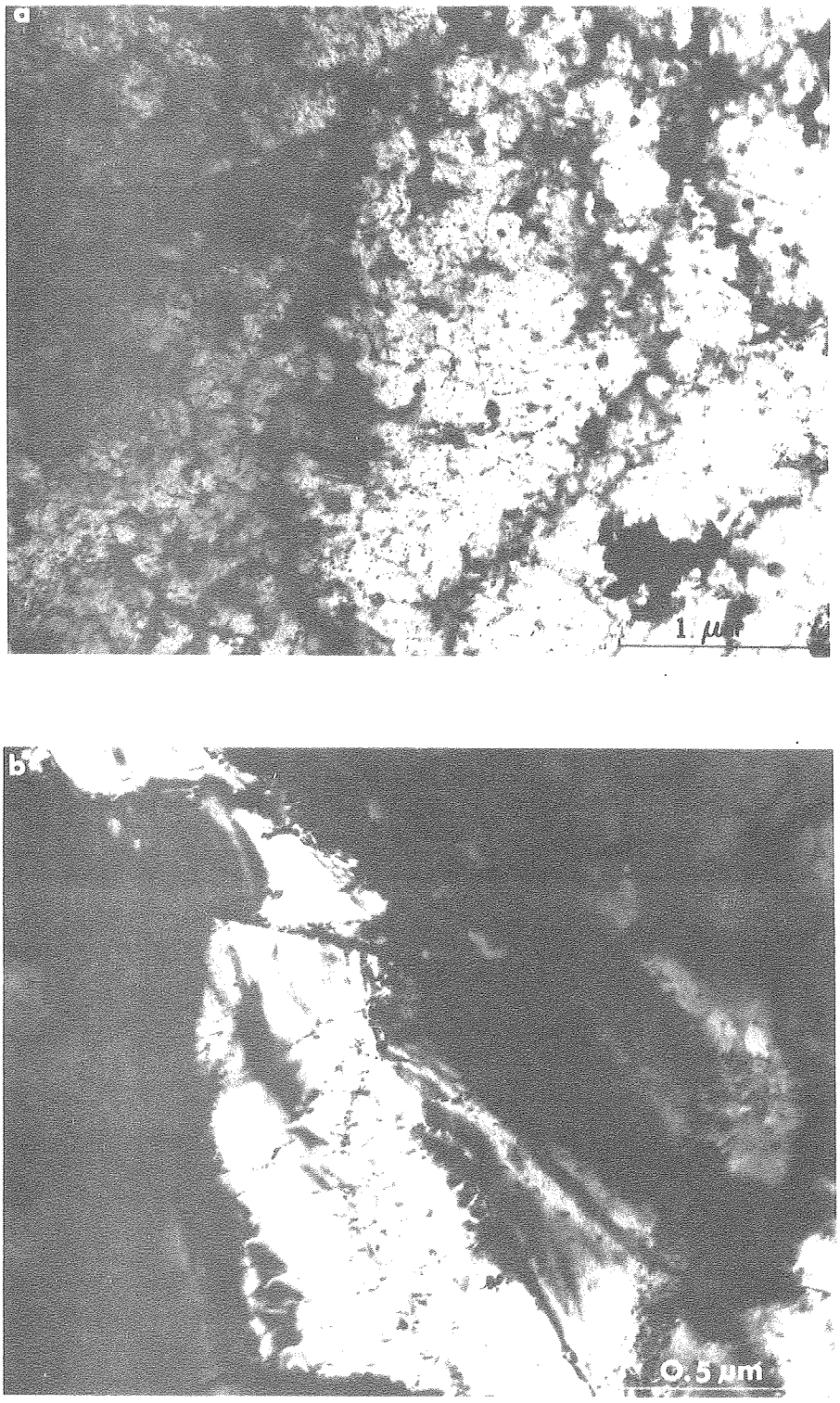

XBB 793 3318

Fig. 16

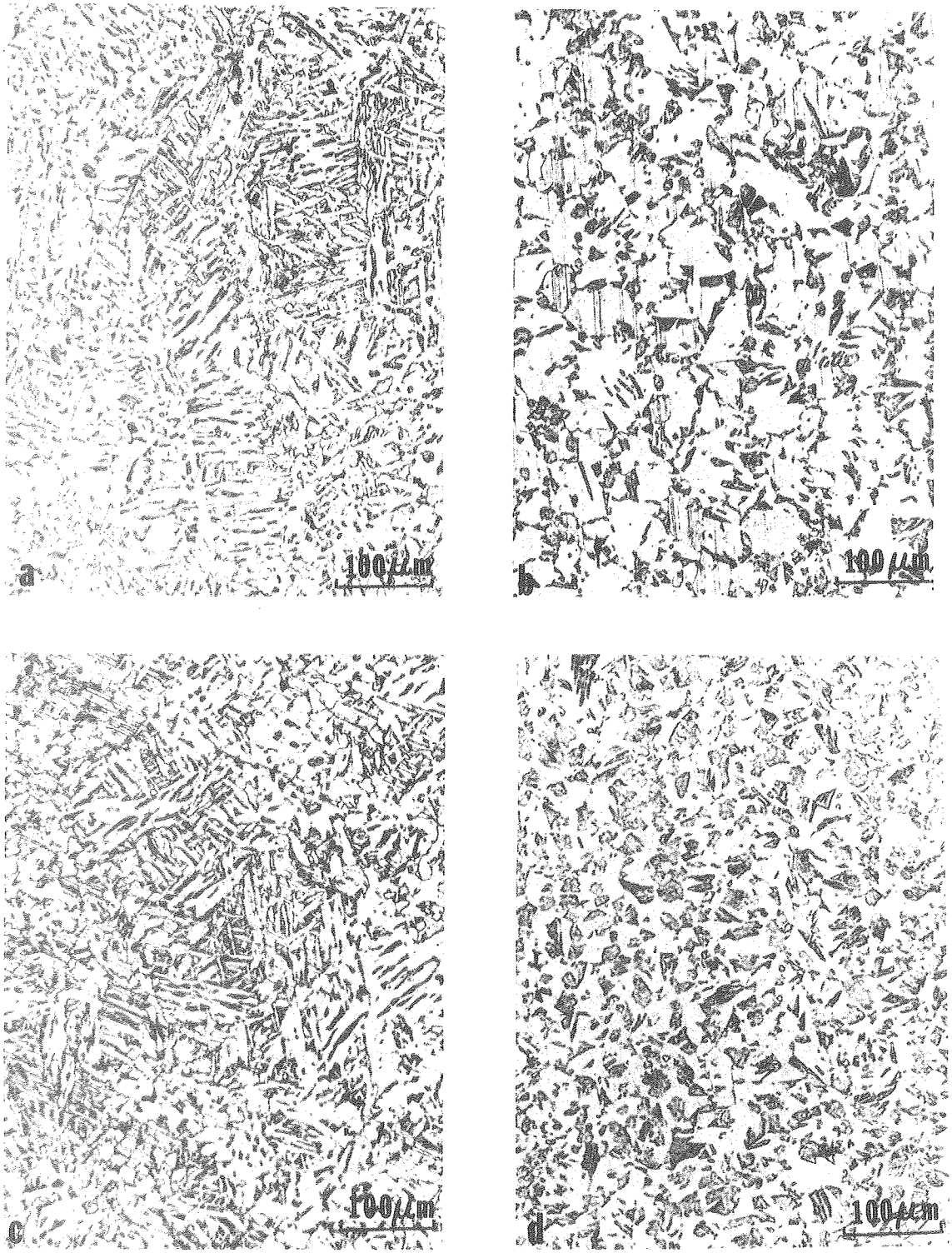

XBB 789 10919

Fig. 17

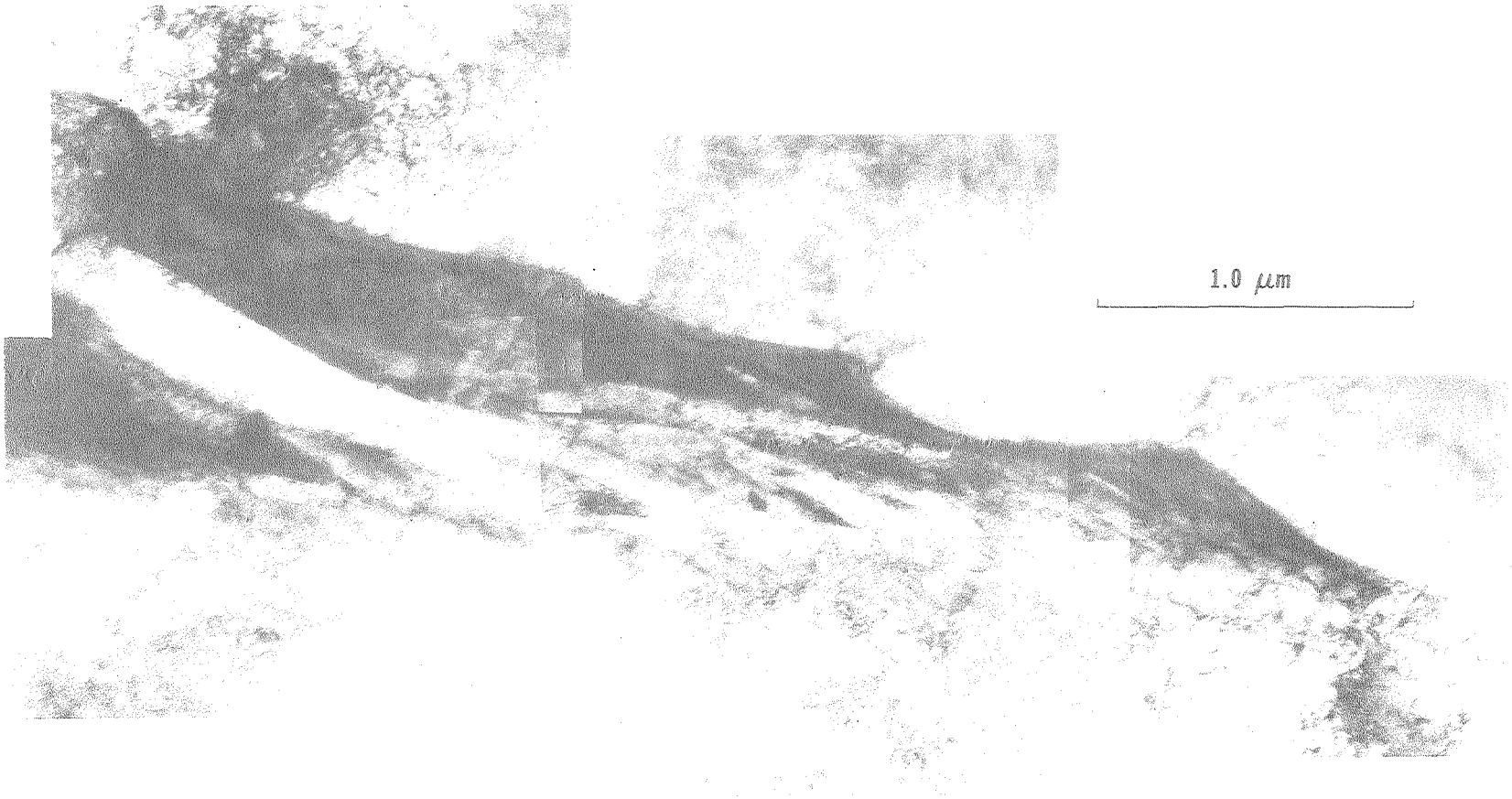

XBB 791 511

Fig. 18

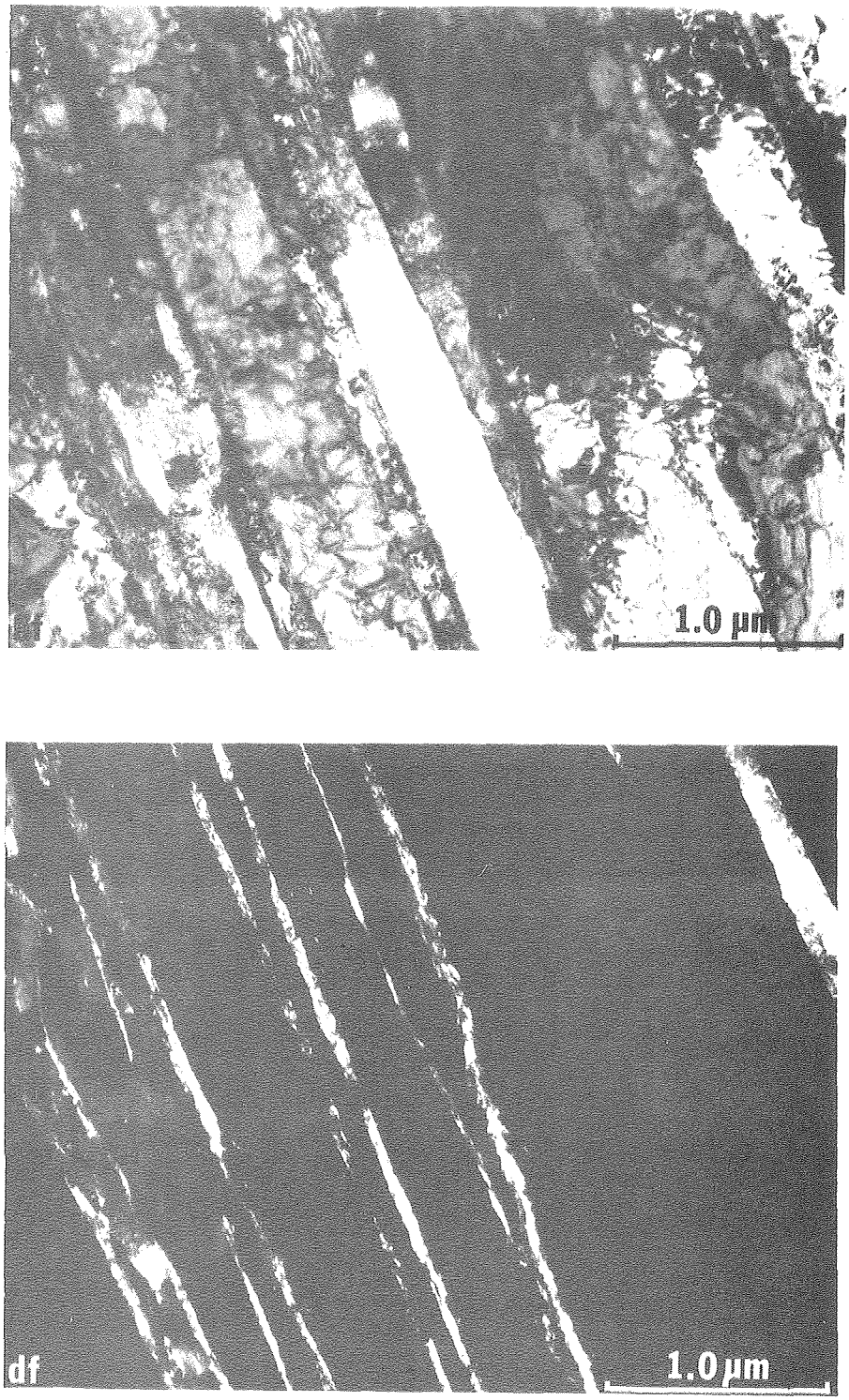

XBB 793 3327

Fig. 19

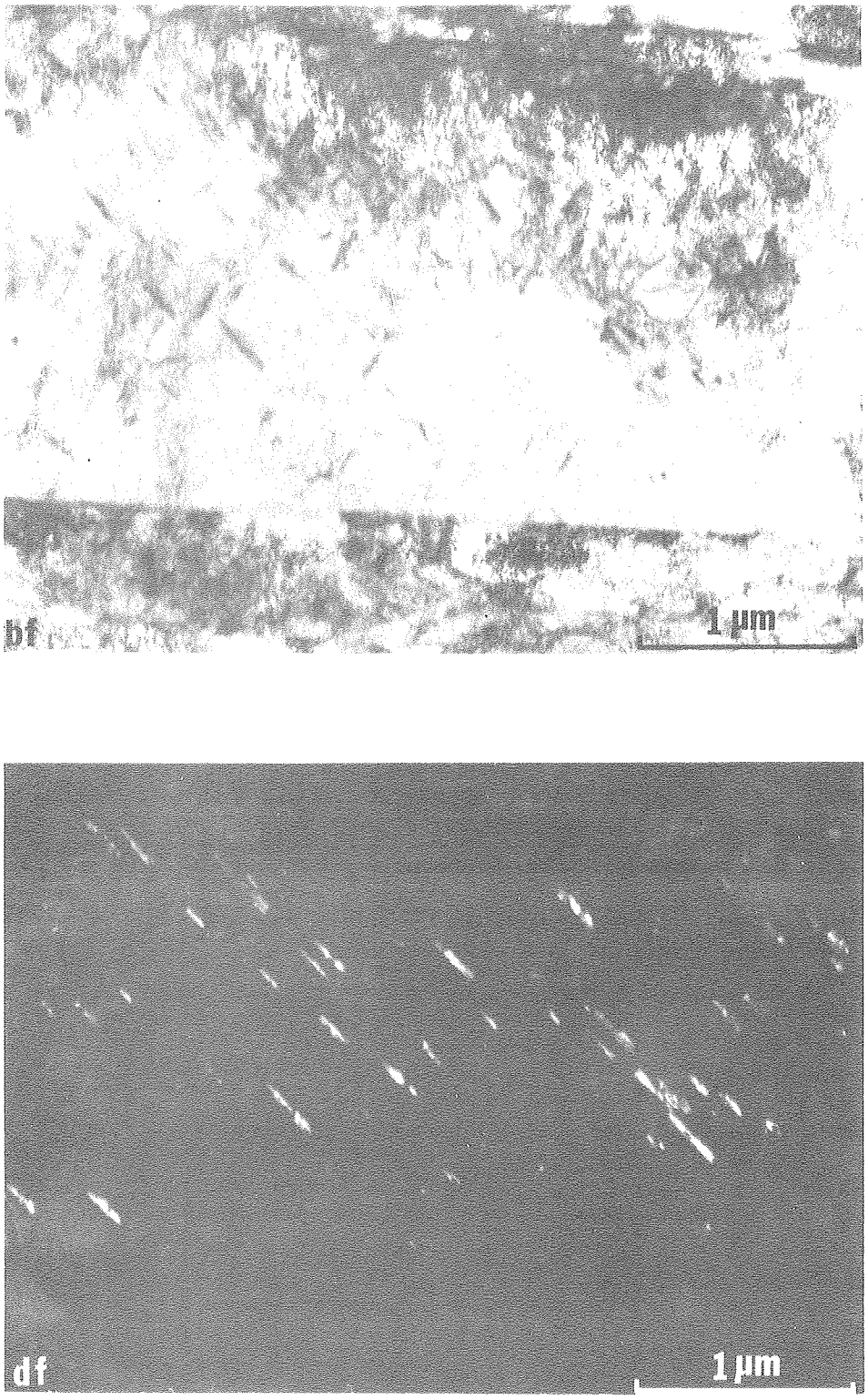

XBB 791 980

Fig. 20

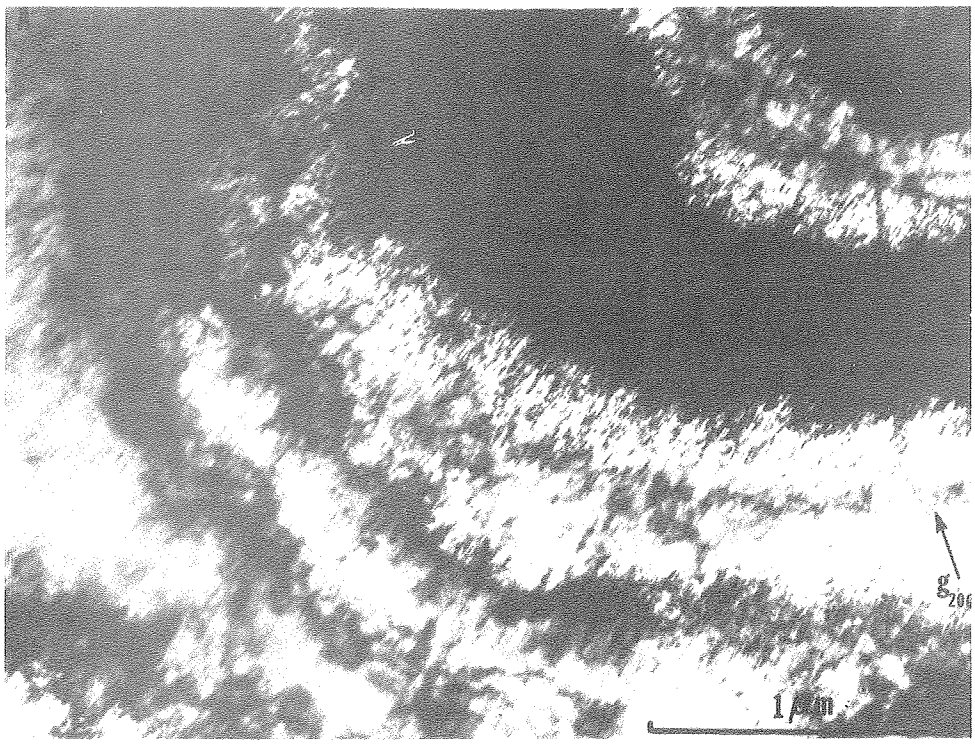

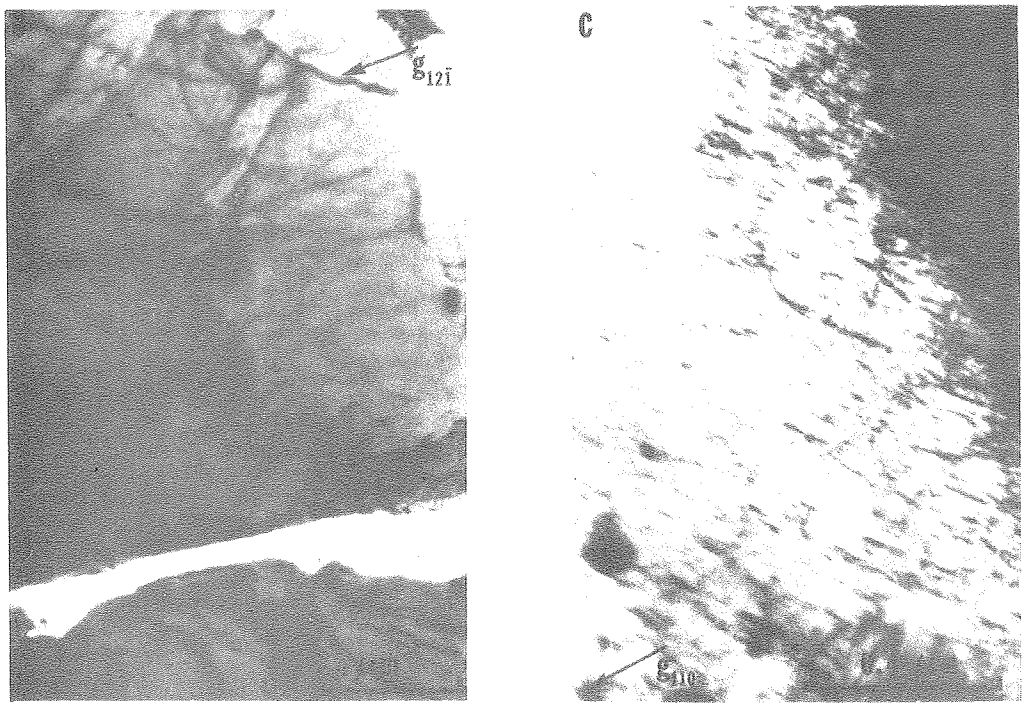

XBB 793 3333

Fig. 21

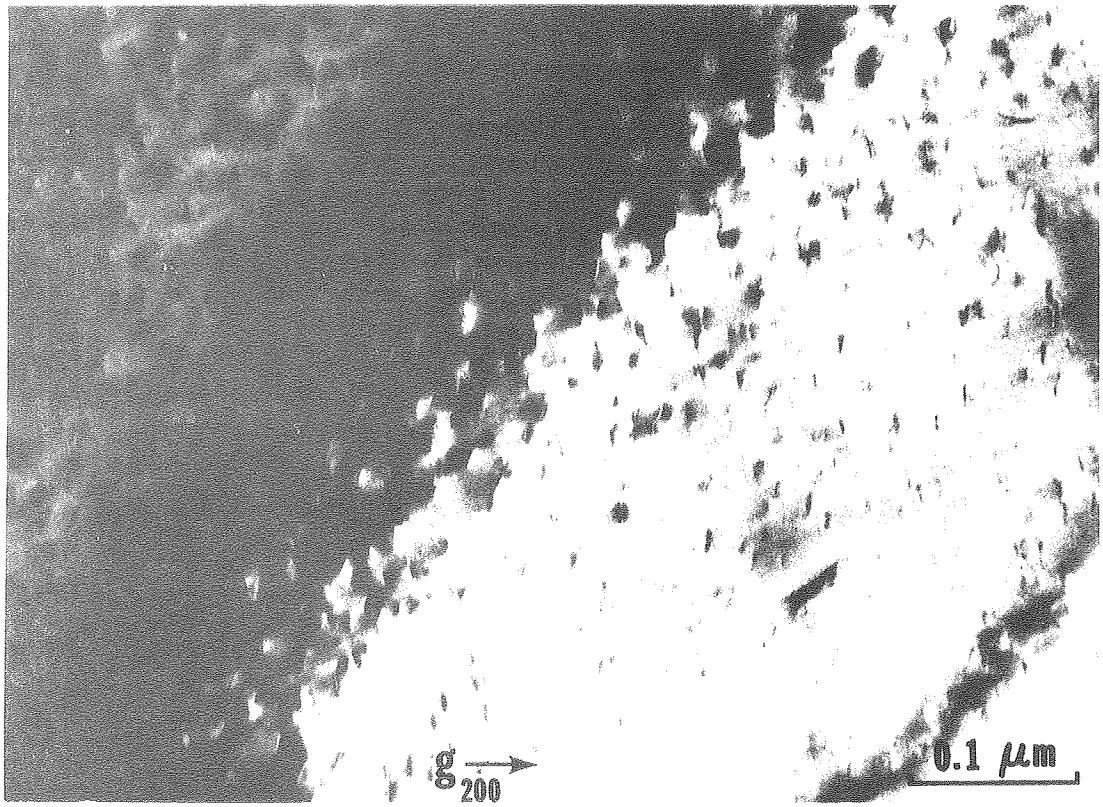

XBB 793 3332

Fig. 22

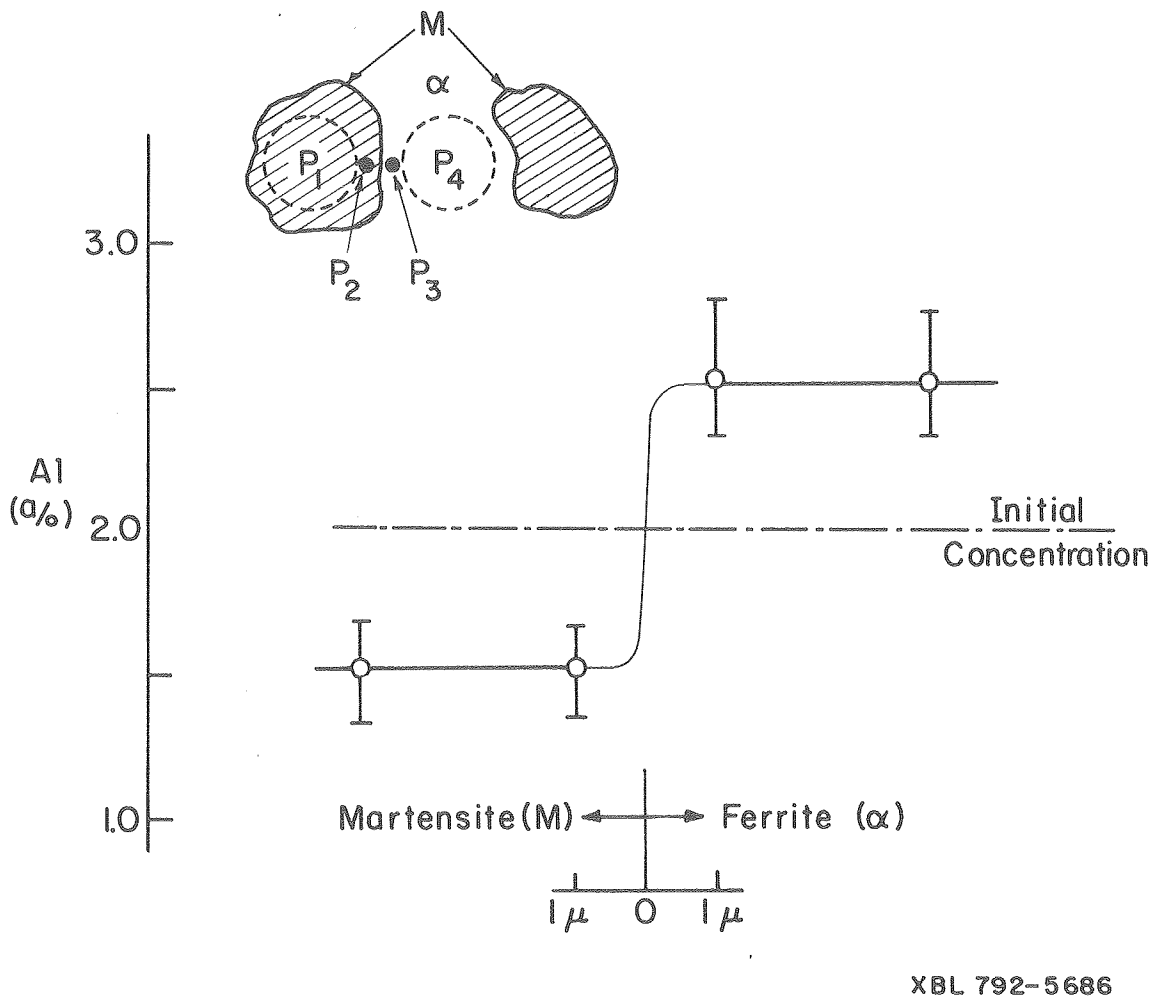
M
α
P1
P4
P2
P3
3.0
Al
(a/o)
2.0
1.0
Initial
Concentration
Martensite(M)
Ferrite (α)
1μ
0
1μ
XBL 792-5686

Fig. 23

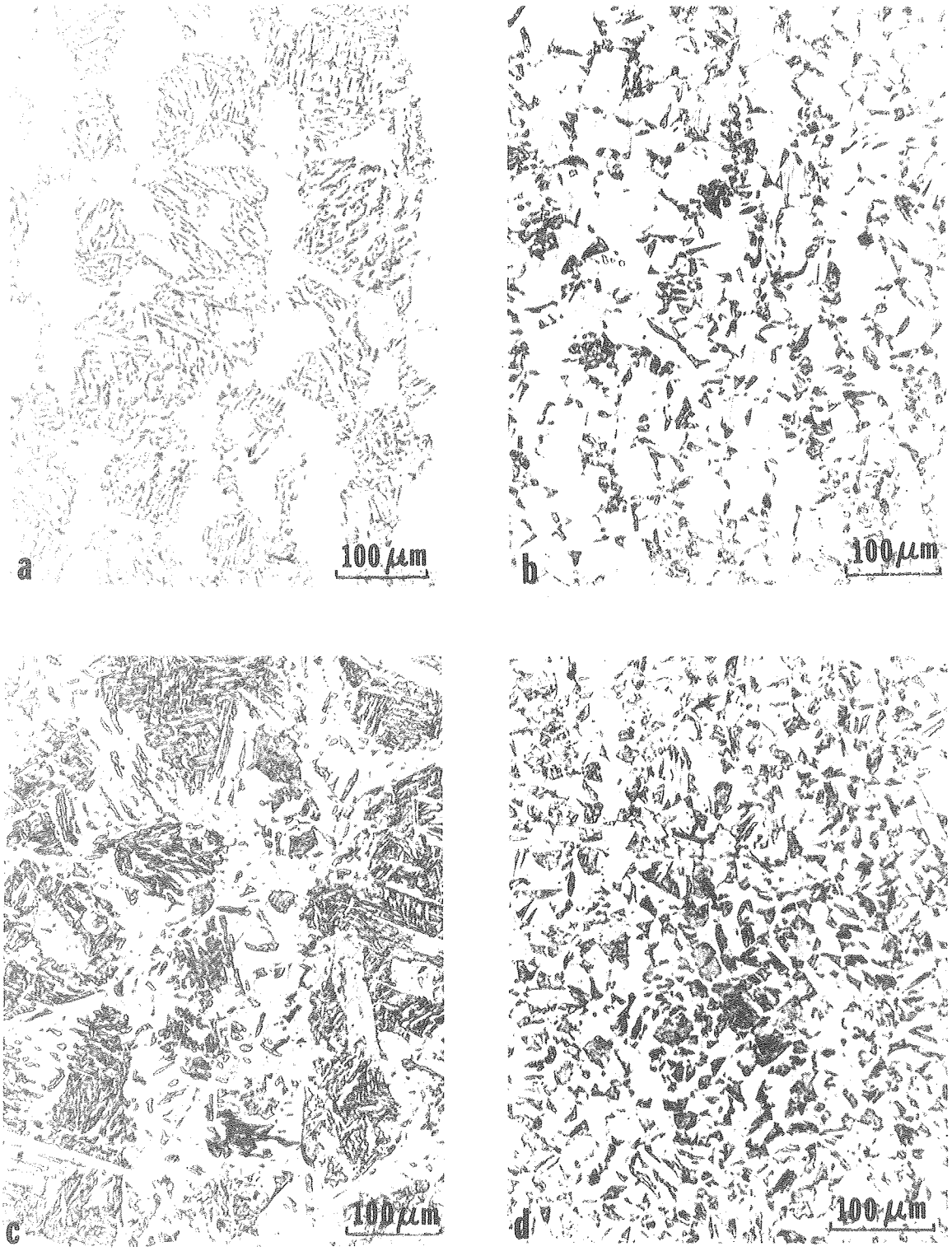

XBB 789 10920

Fig. 24

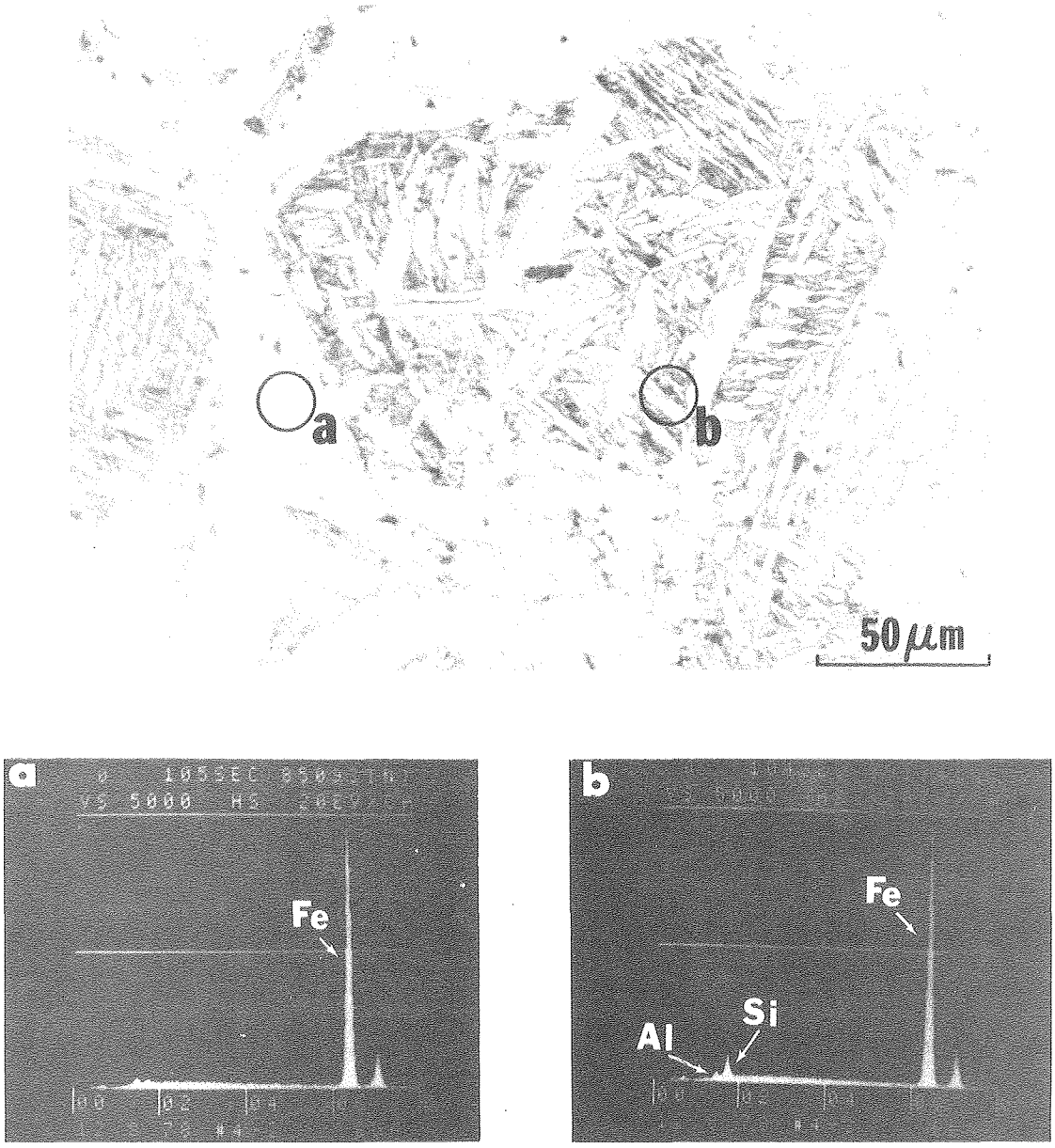

XBB 791 513

Fig. 25

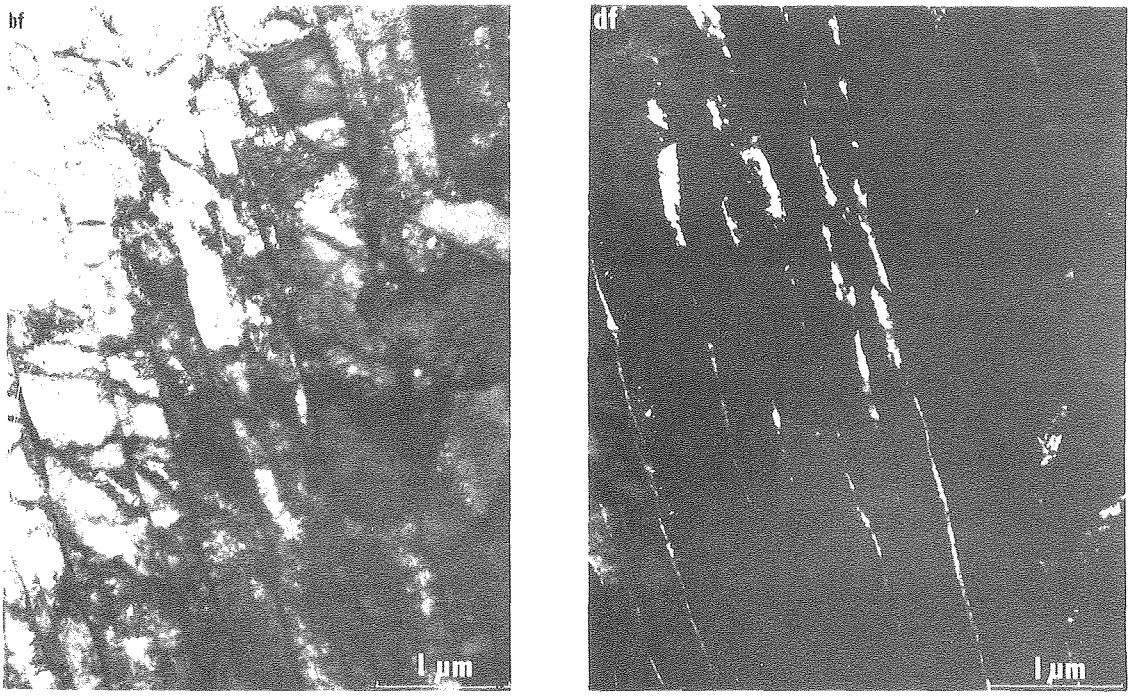

XBB 793 3331

Fig. 26

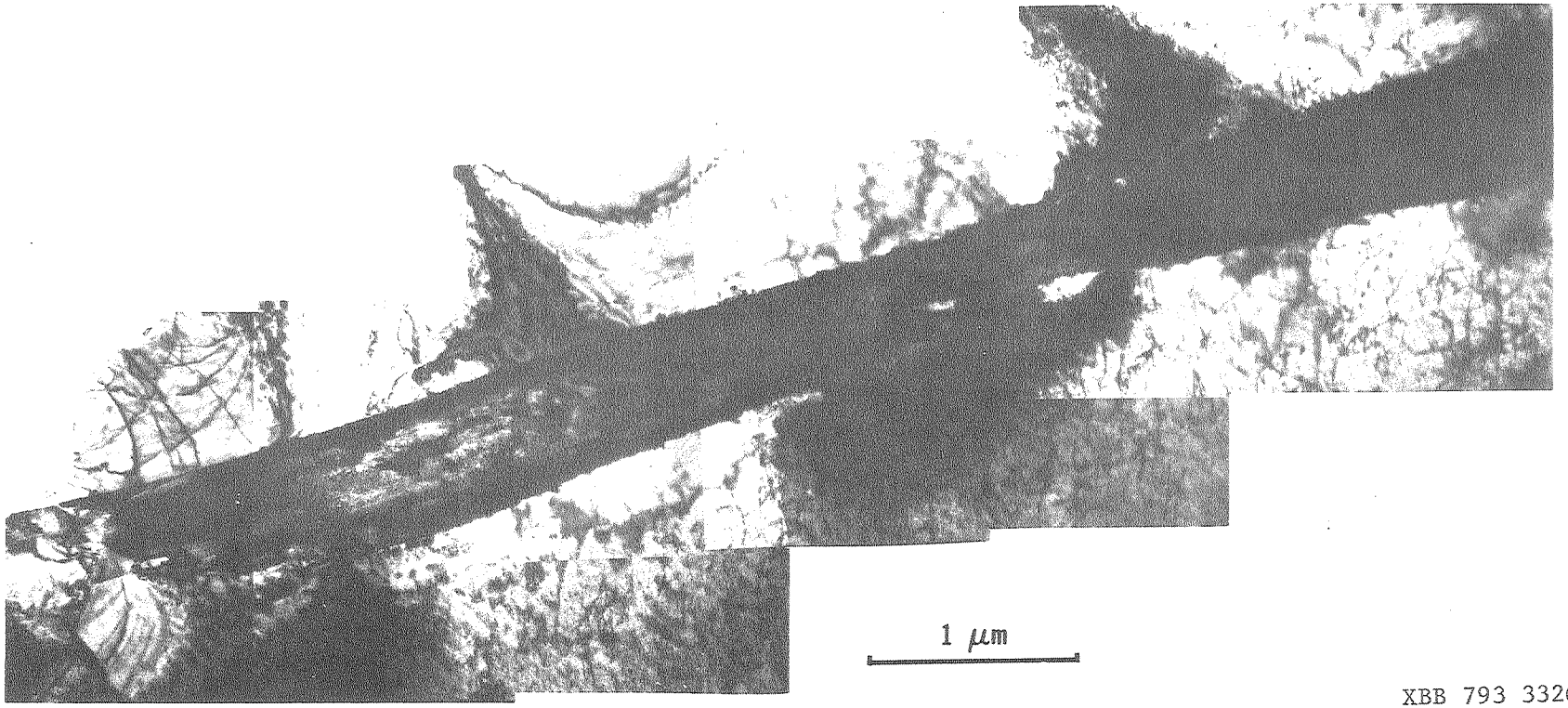

XBB 793 3326

Fig. 27

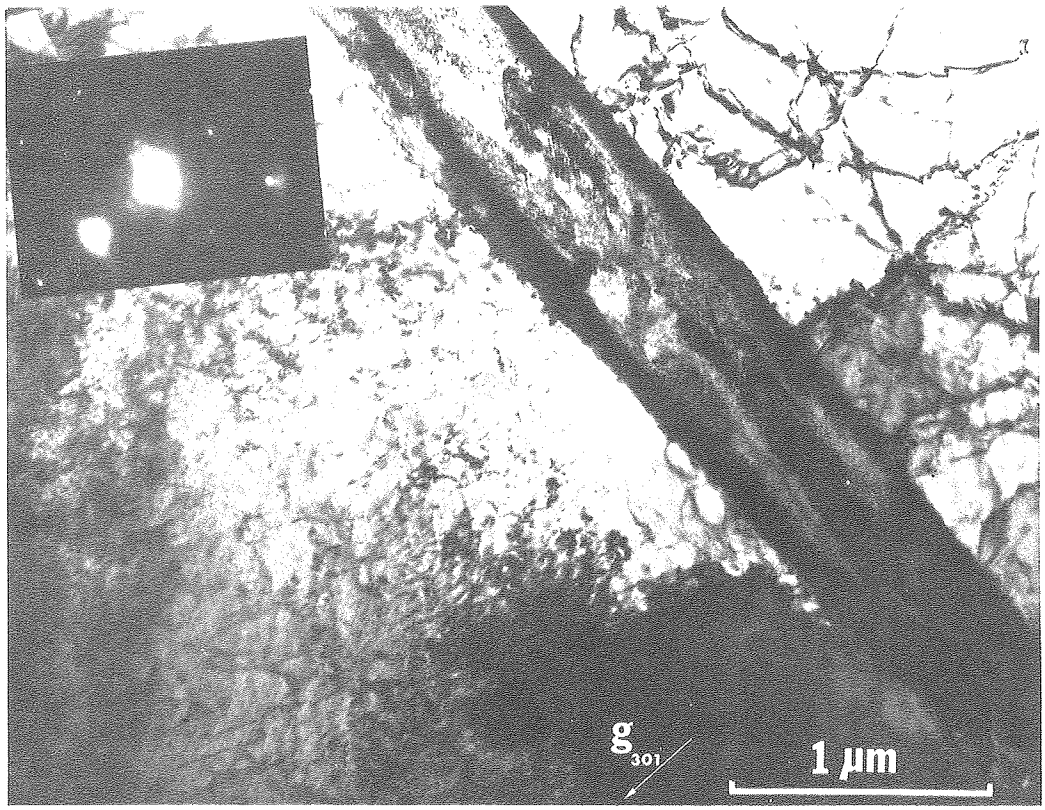

XBB 793 3324

Fig. 28

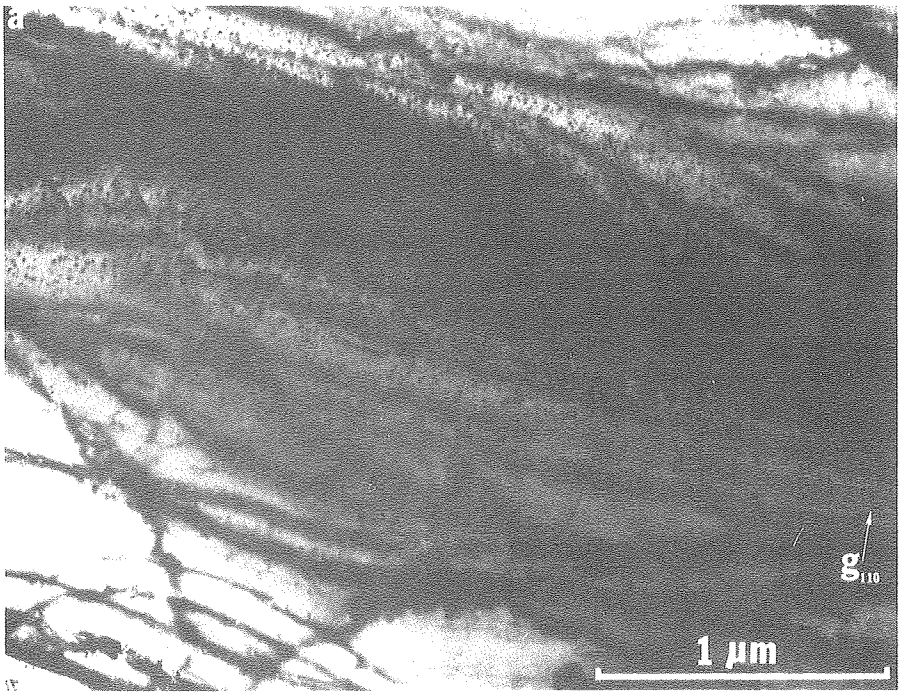

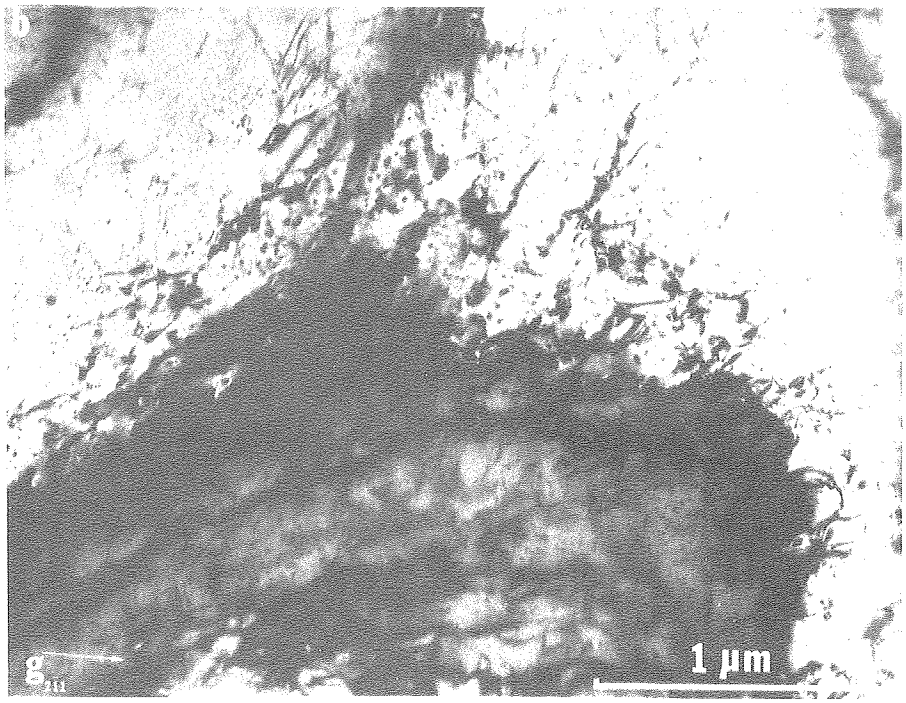

XBB 793 3334

Fig. 29

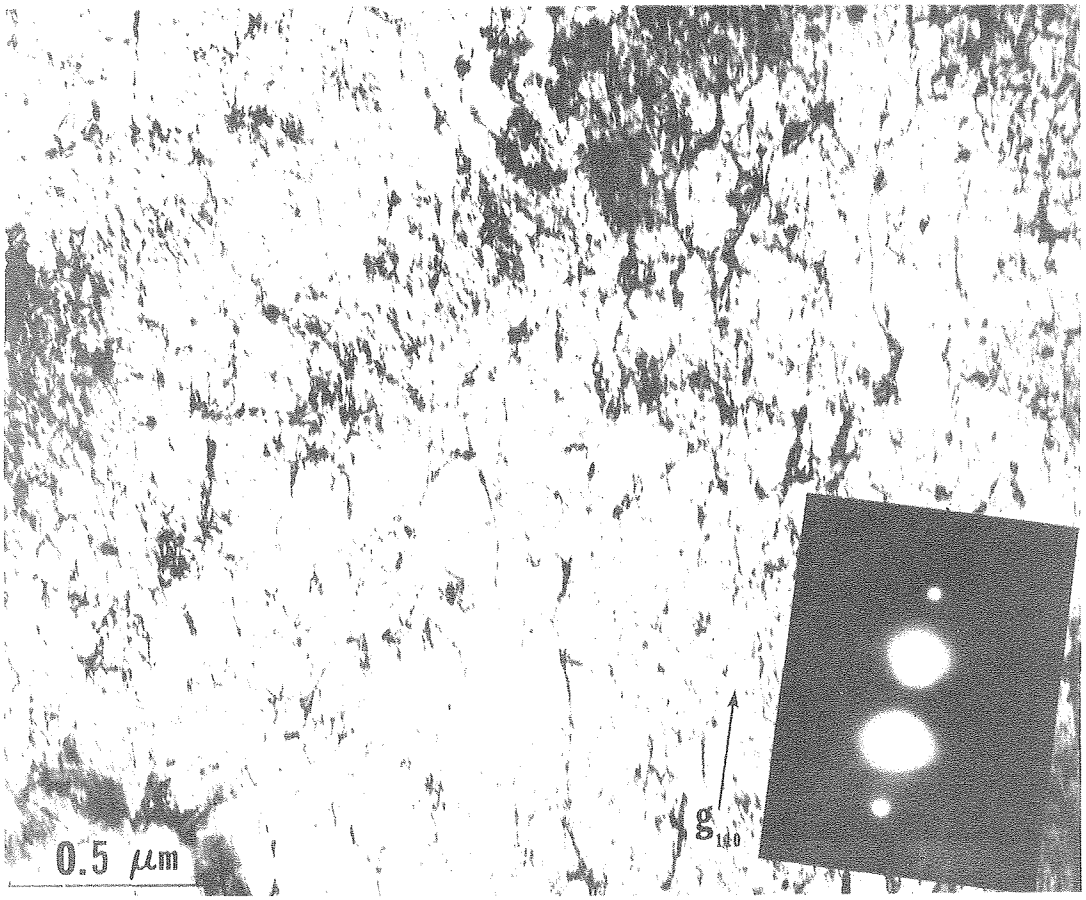

XBB 793 3322

Fig. 30

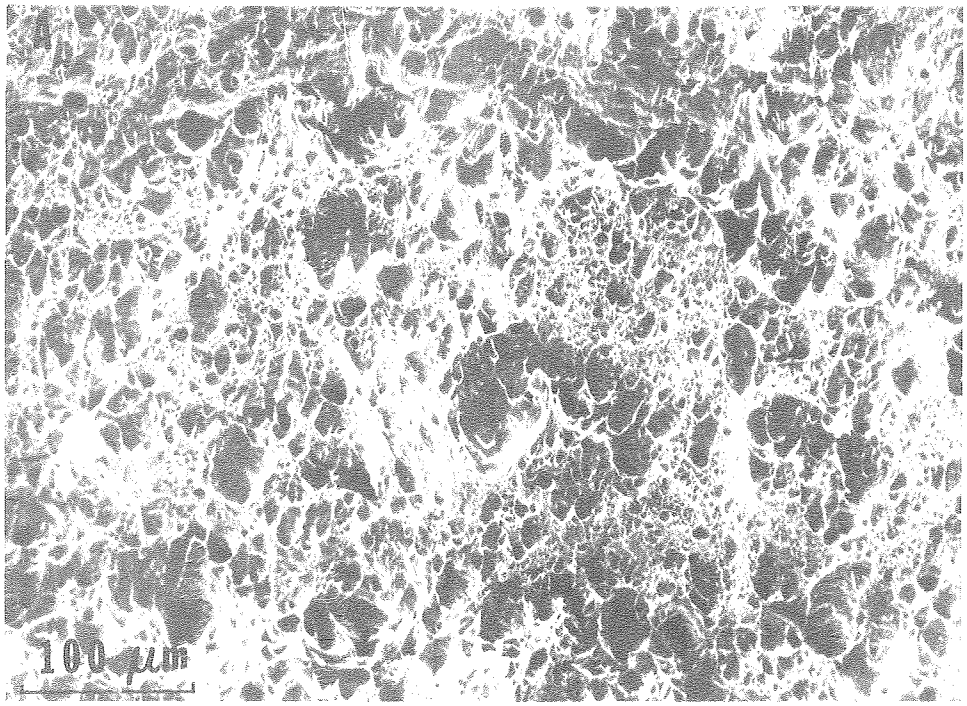

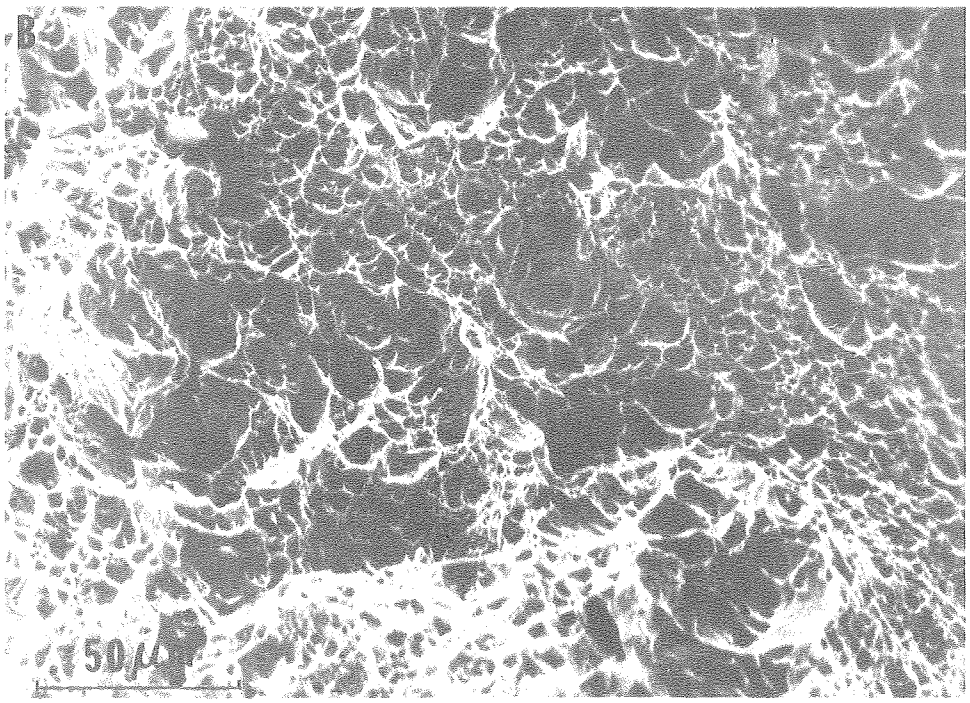

XBB 793 3323

Fig. 31

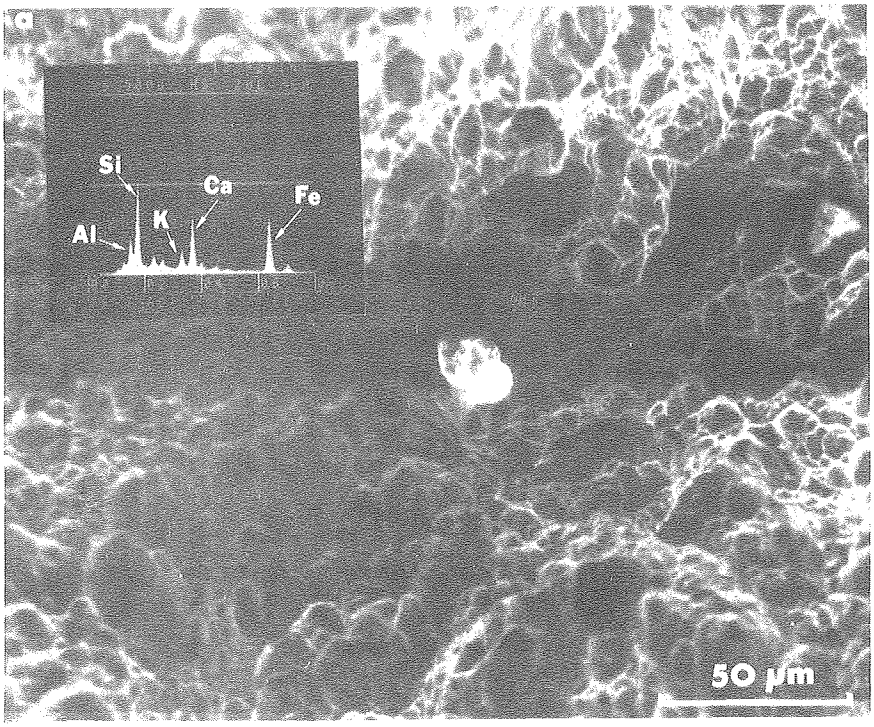

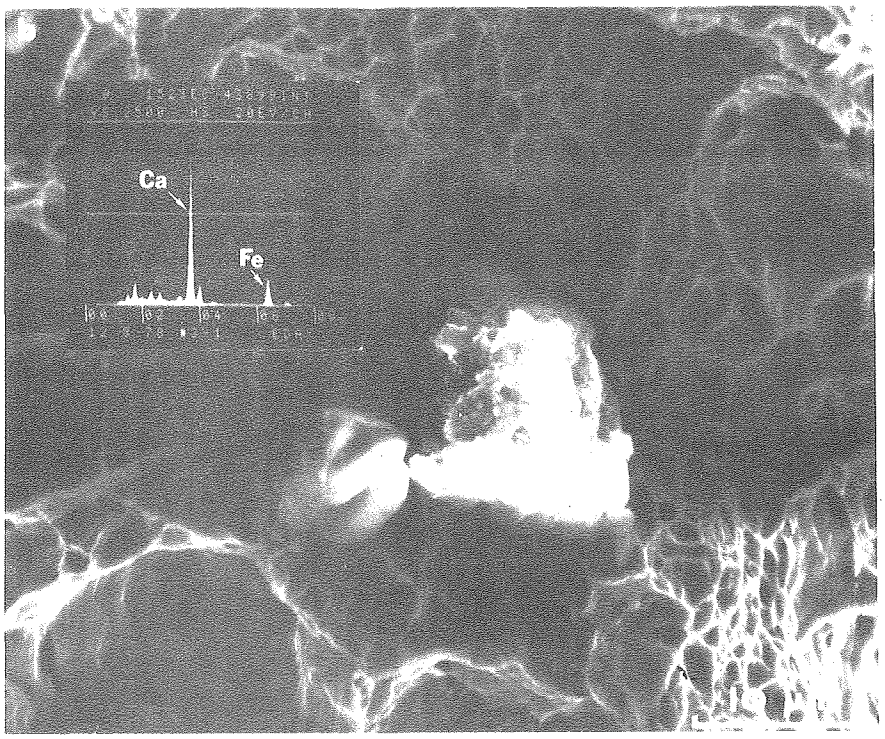

XBB 793 3330

Fig. 32

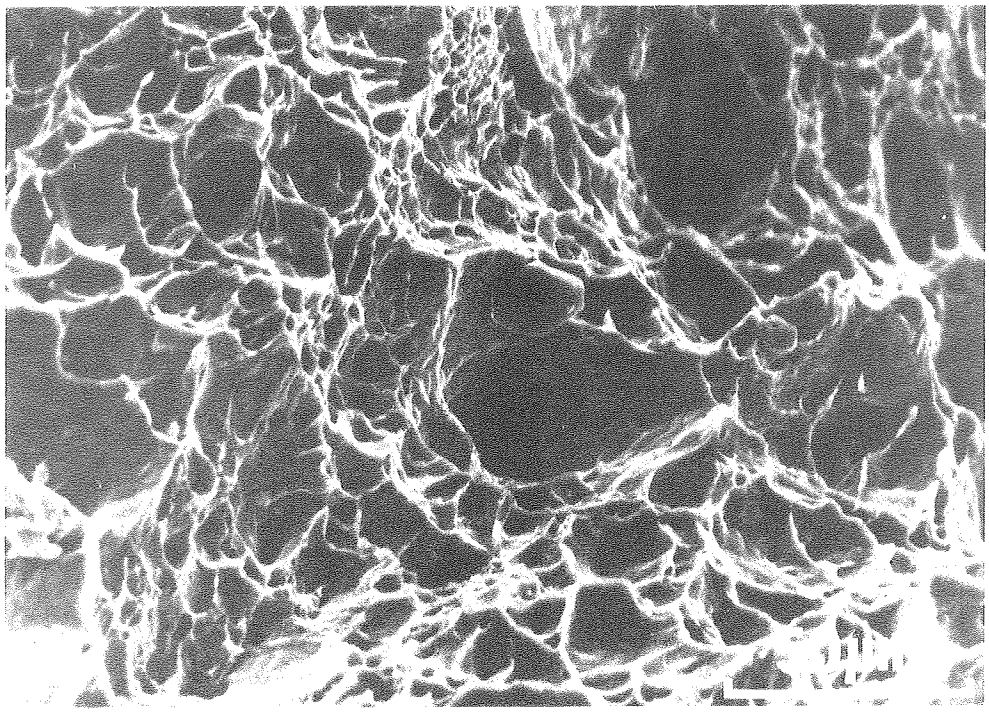

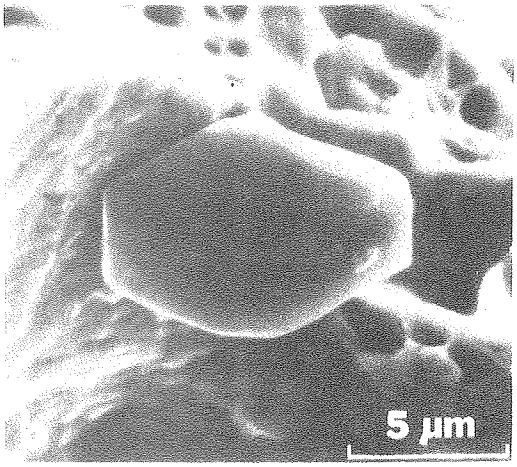

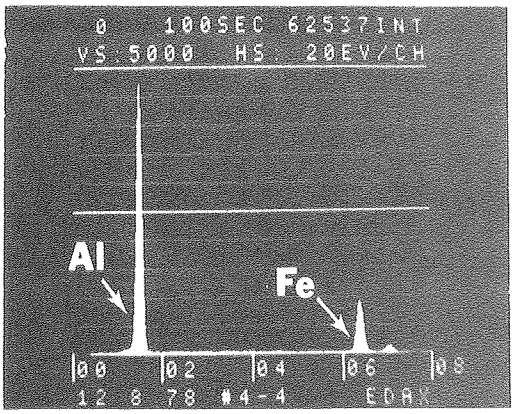

XBB 793 3321

Fig. 33

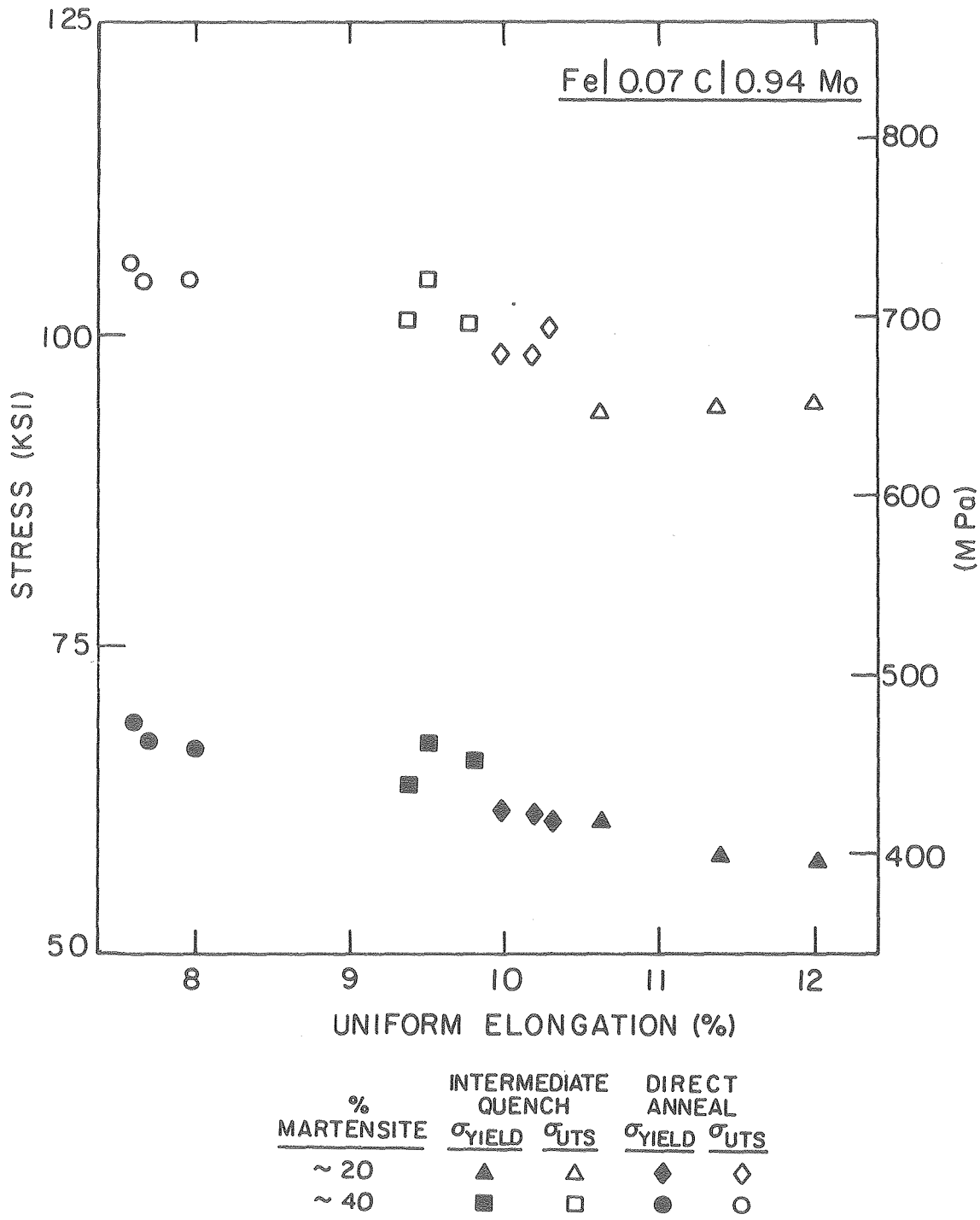
Fe | 0.07 C | 0.94 Mo
125
100
75
50
STRESS (KSI)
800
700
600
500
400
(MPa)
8
9
10
11
12
UNIFORM ELONGATION (%)
% MARTENSITE
INTERMEDIATE QUENCH
DIRECT ANNEAL
σYIELD
σUTS
σYIELD
σUTS
~ 20
~ 40
XBL 789-5826

Fig. 34

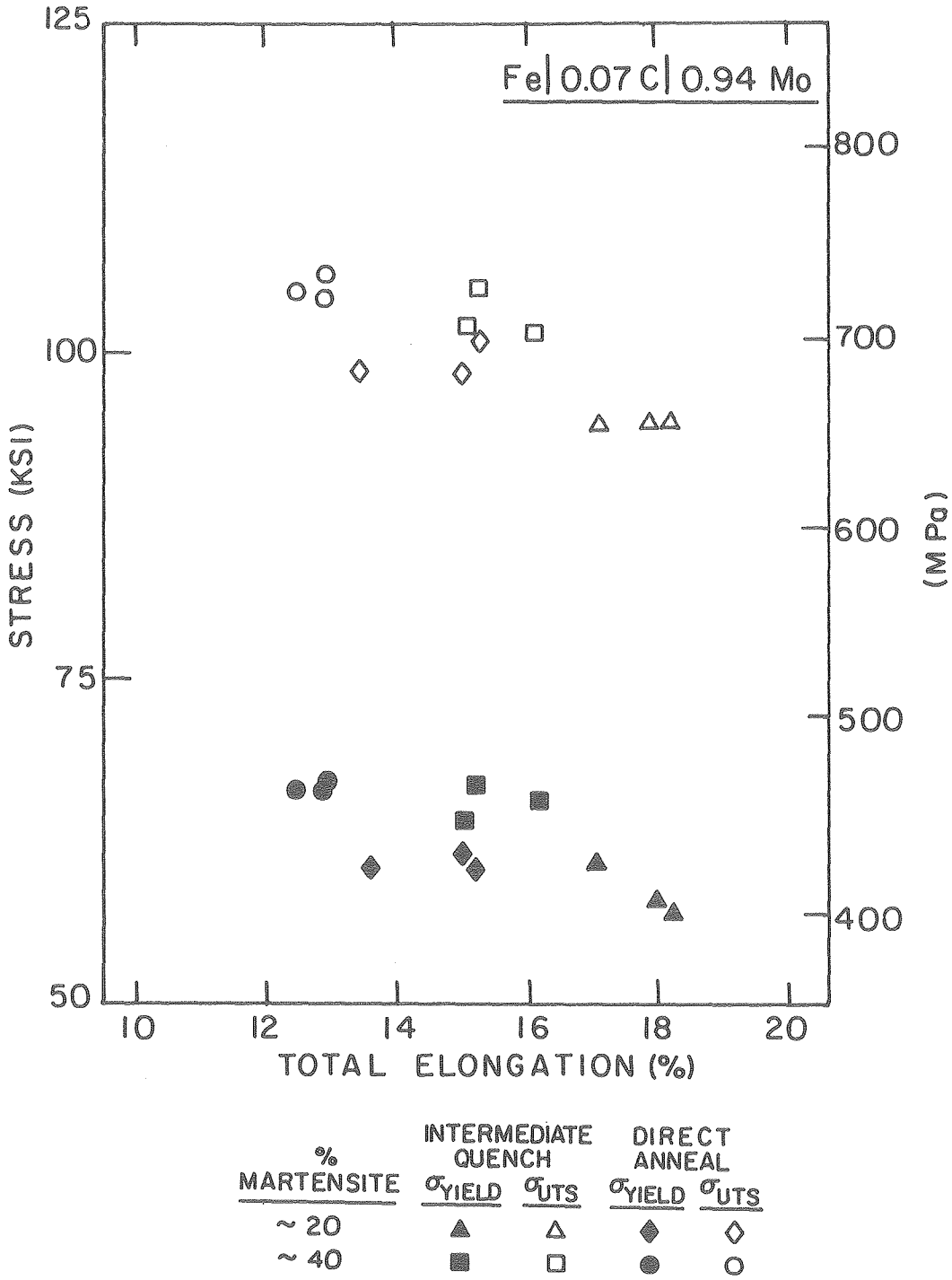

XBL 789-5830

Fig. 35

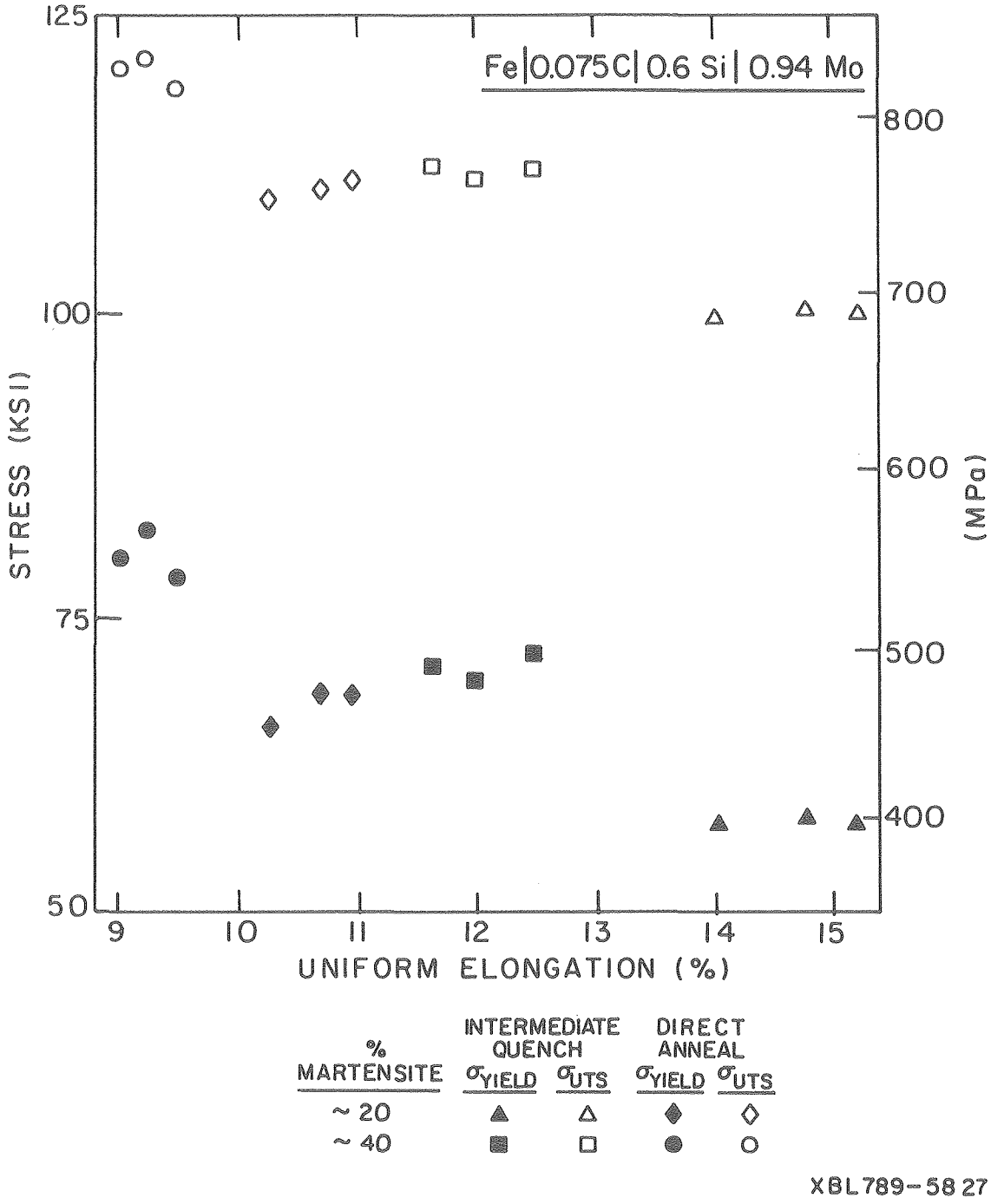
Fe|0.075C|0.6 Si|0.94 Mo
125
100
75
50
STRESS (KSI)
800
700
600
500
400
(MPa)
9
10
11
12
13
14
15
UNIFORM ELONGATION (%)
% MARTENSITE
INTERMEDIATE QUENCH
DIRECT ANNEAL
σYIELD
σUTS
σYIELD
σUTS
~ 20
~ 40
XBL789-5827

Fig. 36

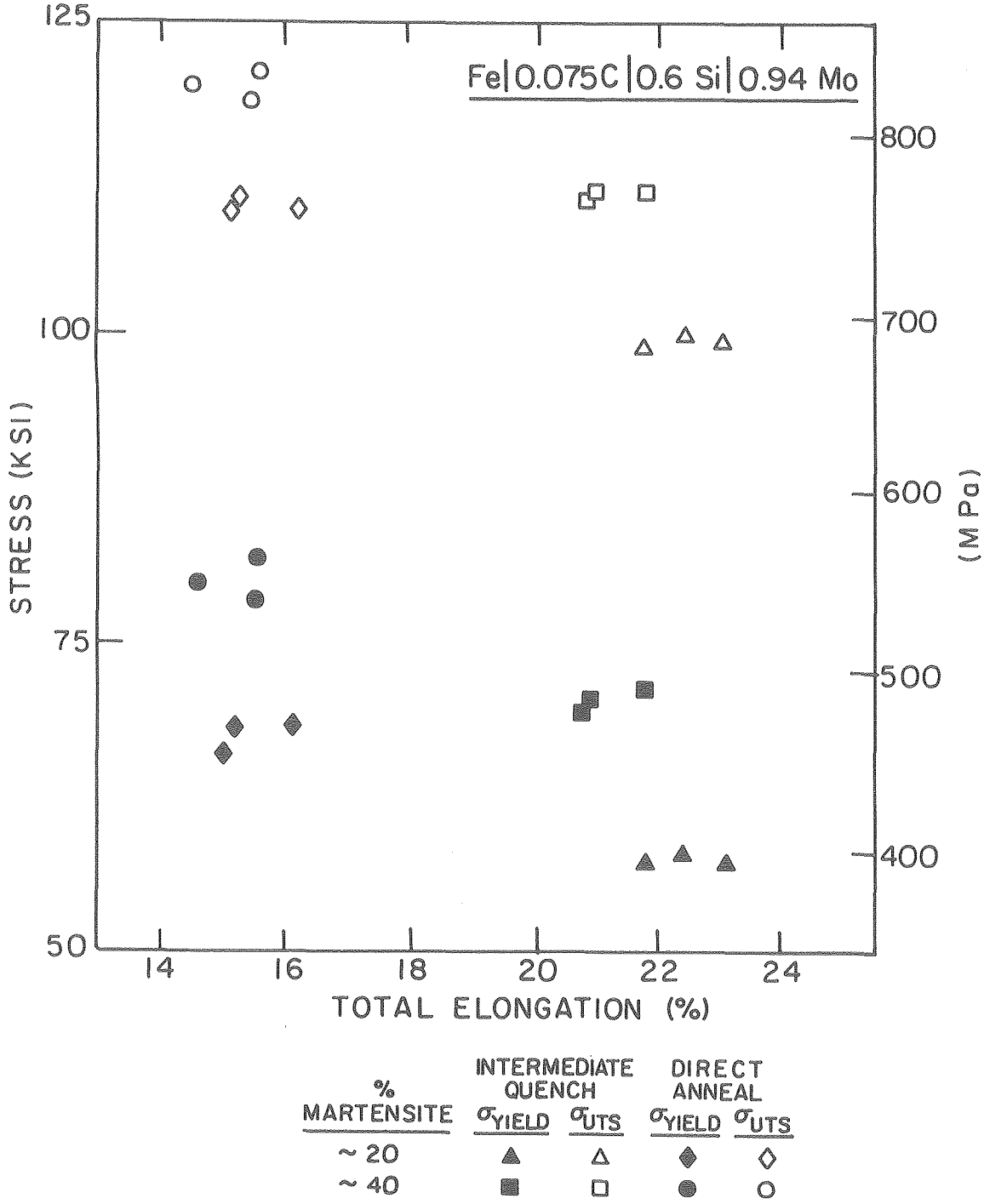

XBL 789-5831

Fig. 37

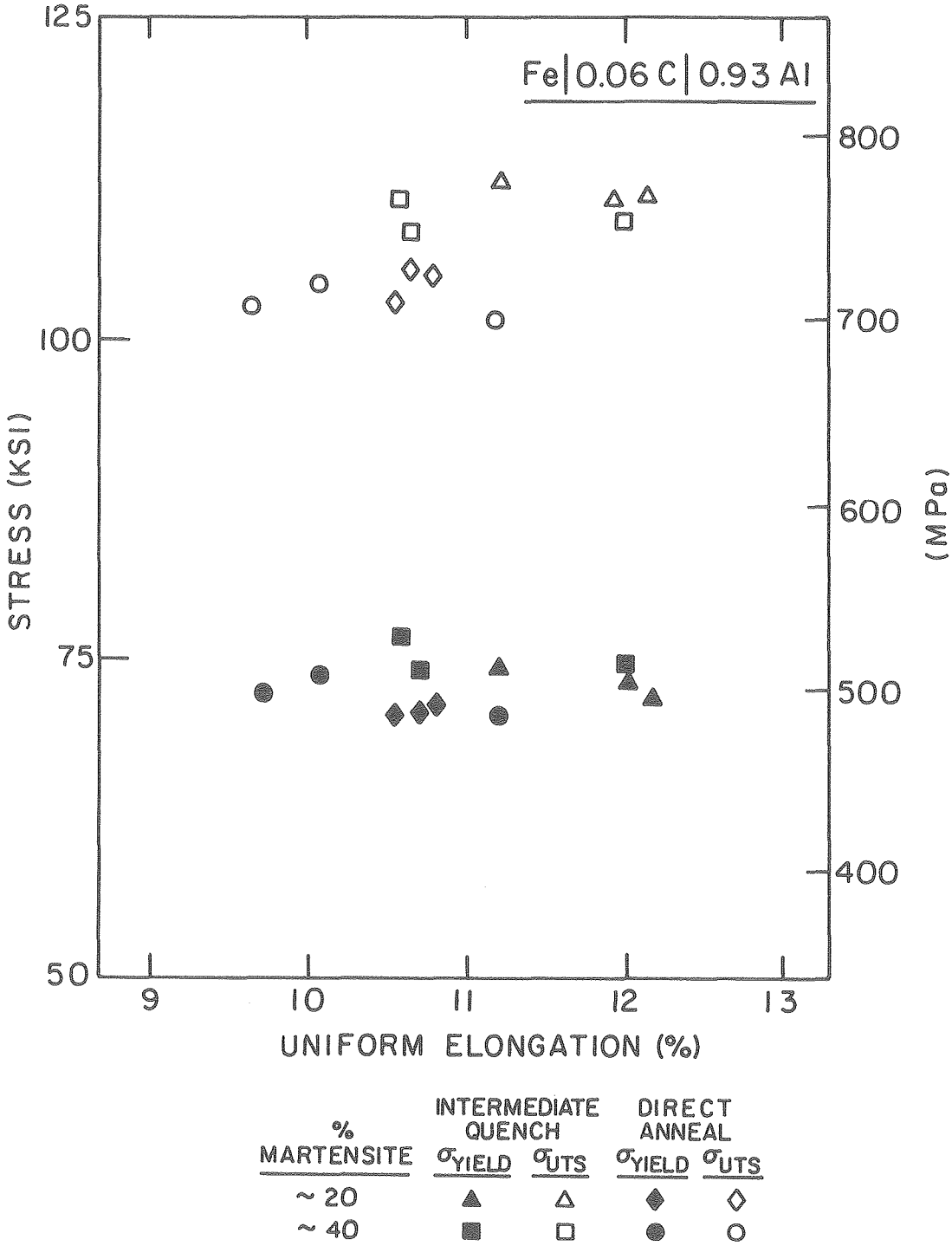

XBL 789-5824

Fig. 38

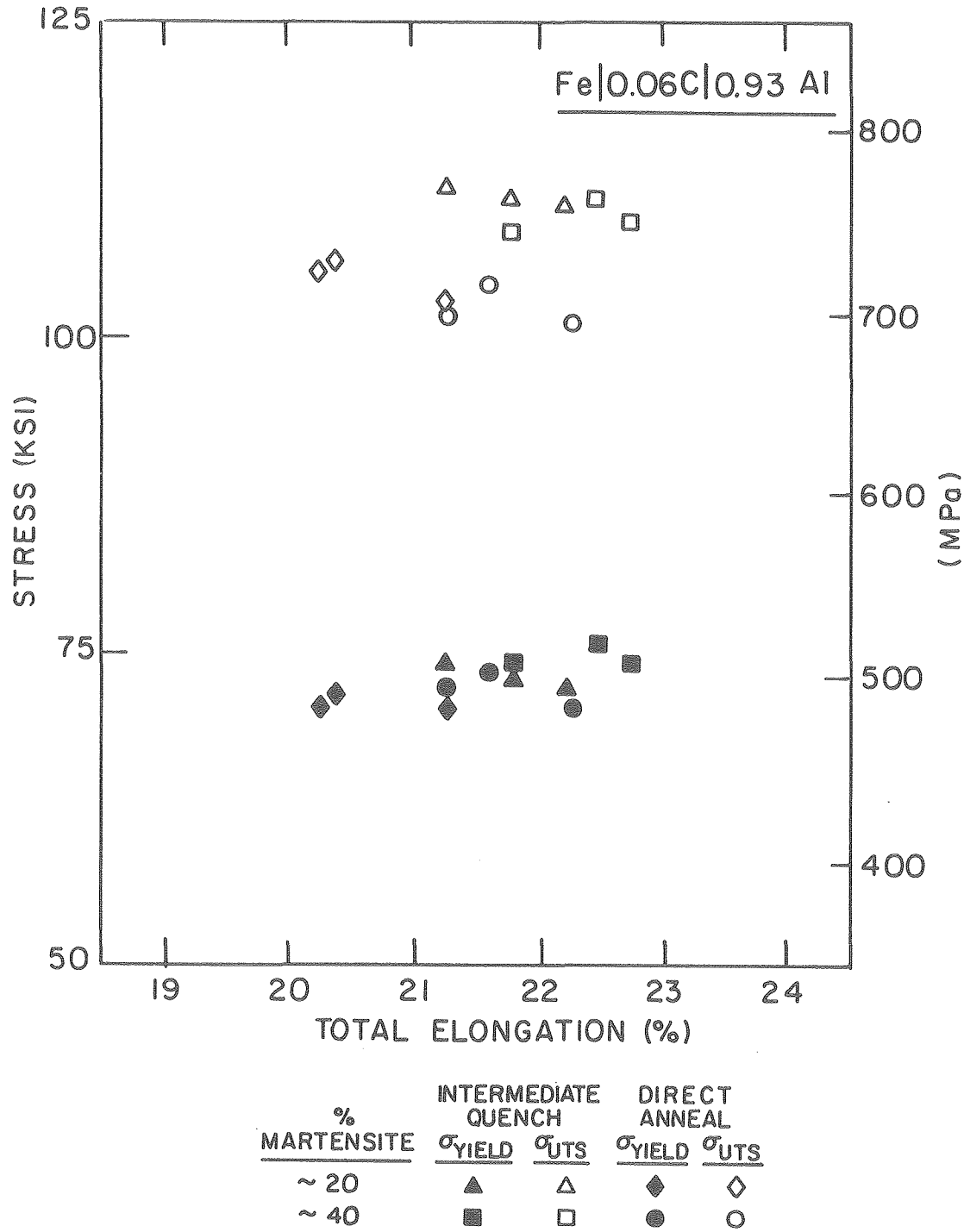

XBL 789-5828

Fig. 39

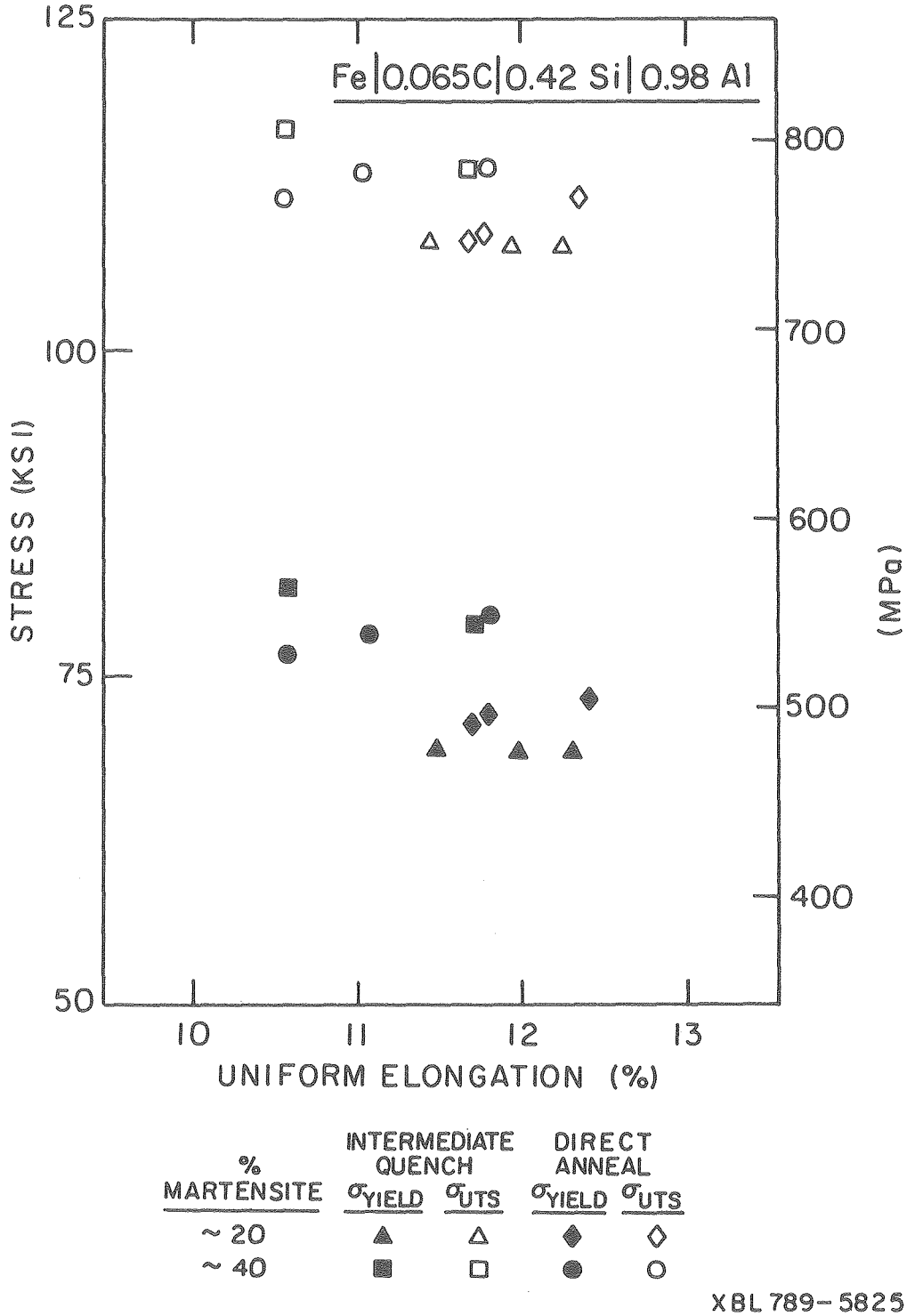
Fe|0.065C|0.42 Si|0.98 Al
125
100
75
50
STRESS (KSI)
800
700
600
500
400
(MPa)
10
11
12
13
UNIFORM ELONGATION (%)
% MARTENSITE
INTERMEDIATE QUENCH
DIRECT ANNEAL
σYIELD σUTS σYIELD σUTS
~ 20
~ 40
XBL 789-5825

Fig. 40

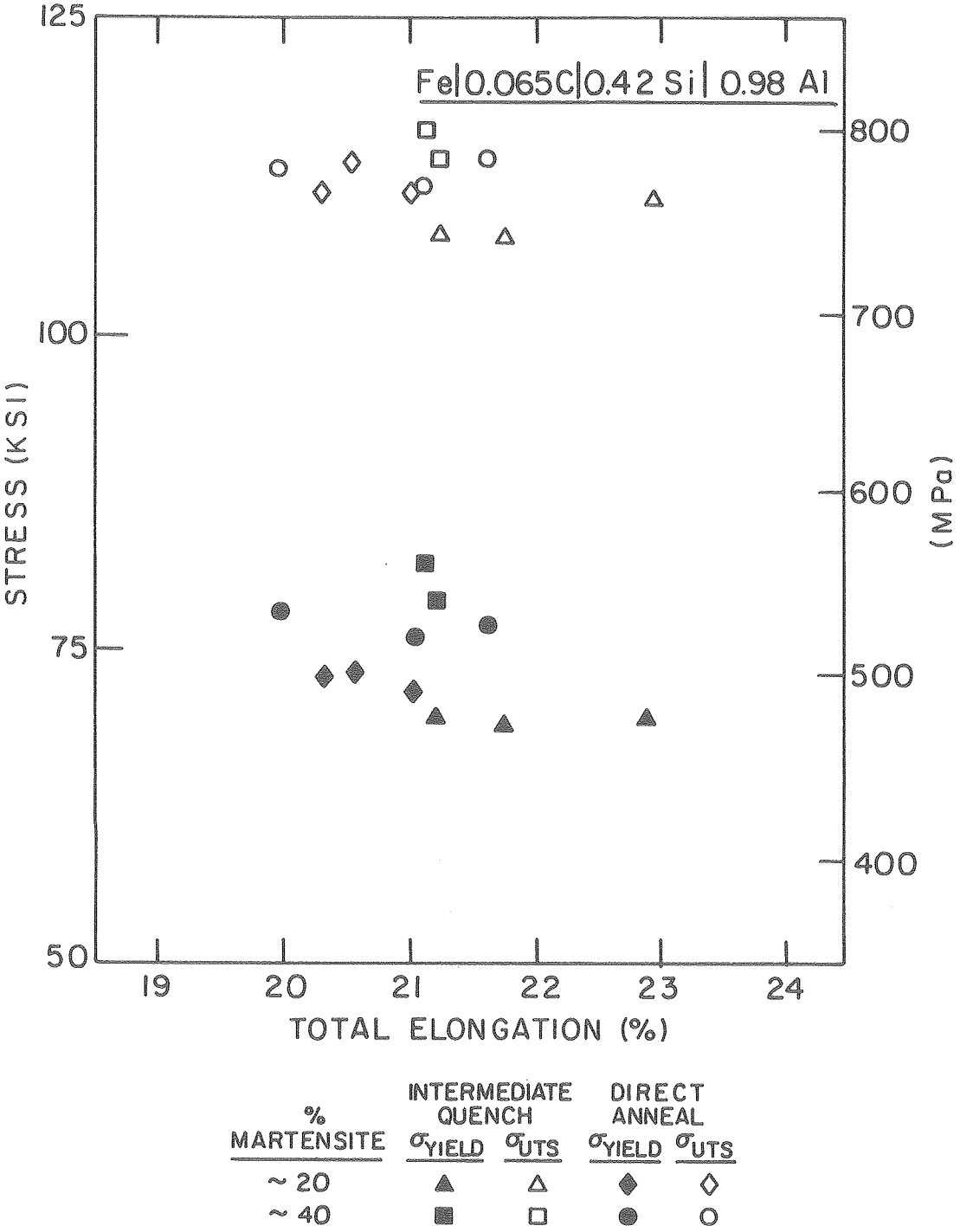

XBL 789-5829

Fig. 41

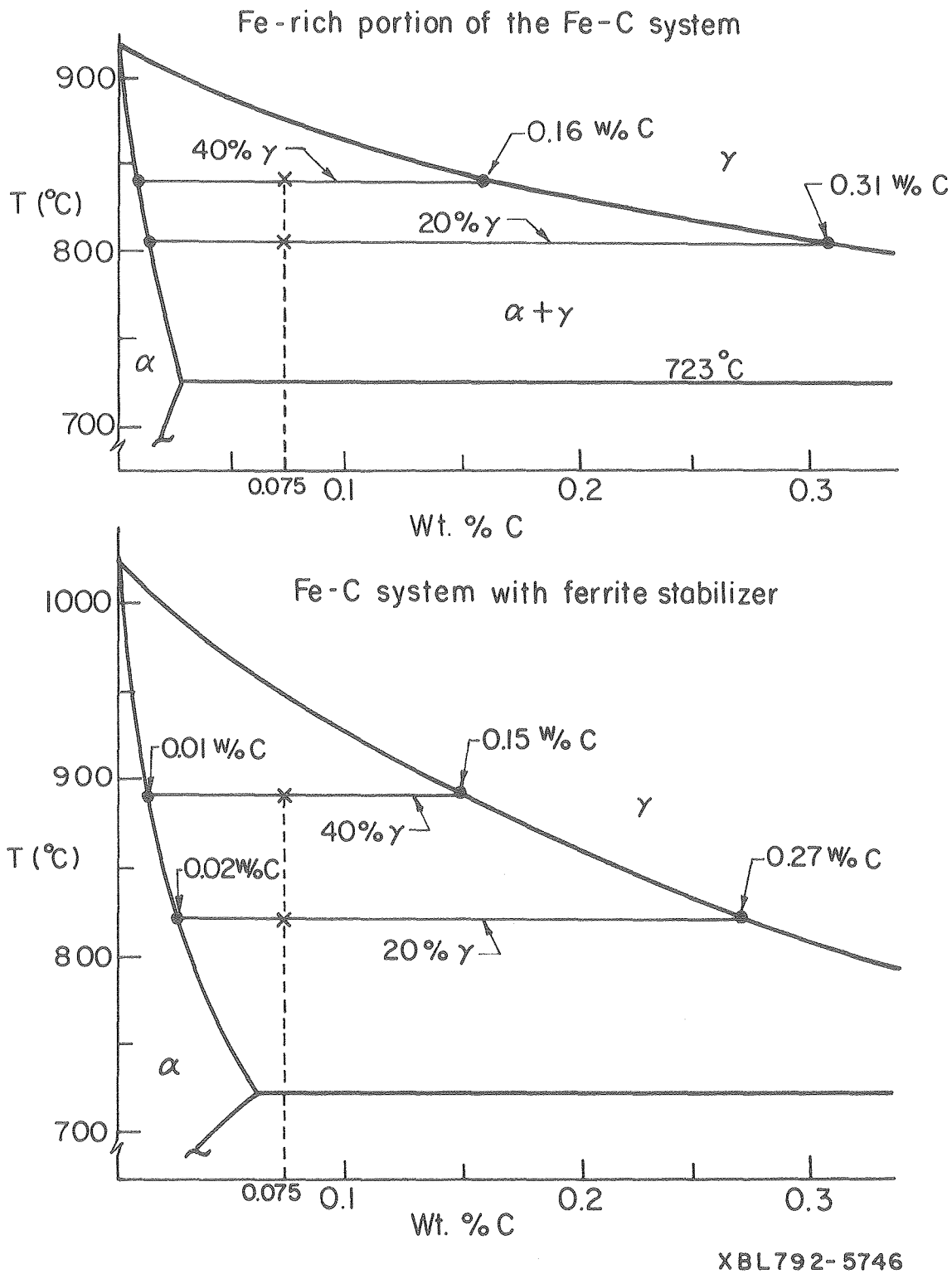
Fe-rich portion of the Fe-C system
900
800
700
T (°C)
40% γ
0.16 w/o C
γ
0.31 w/o C
20% γ
α + γ
α
723°C
0.075
0.1
0.2
0.3
Wt. % C
Fe-C system with ferrite stabilizer
1000
900
800
700
T (°C)
0.01 w/o C
0.15 w/o C
γ
40% γ
0.02 w/o C
0.27 w/o C
20% γ
α
0.075
0.1
0.2
0.3
Wt. % C
XBL792-5746

Fig. 42

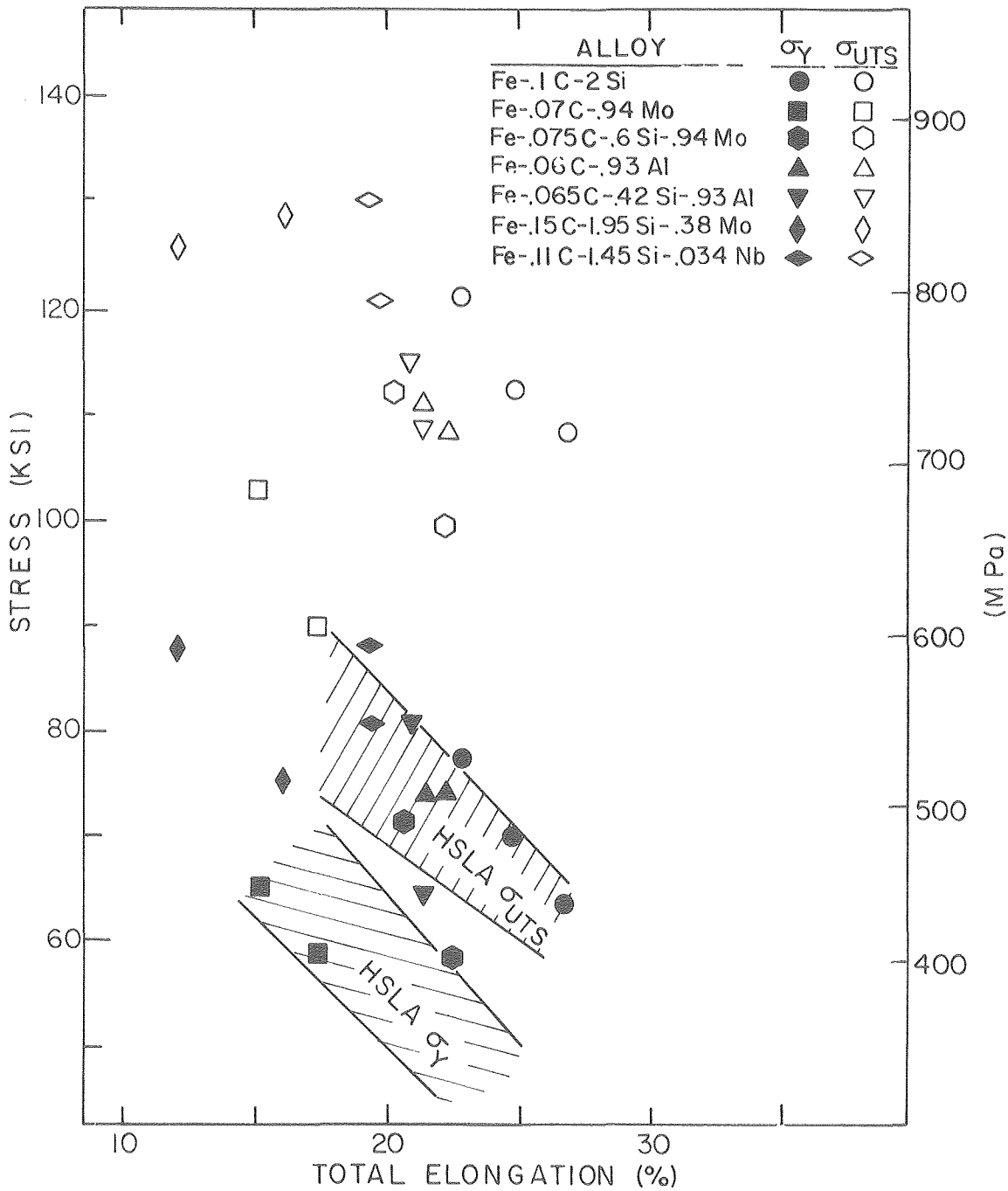

XBL7812-6281

Fig. 43

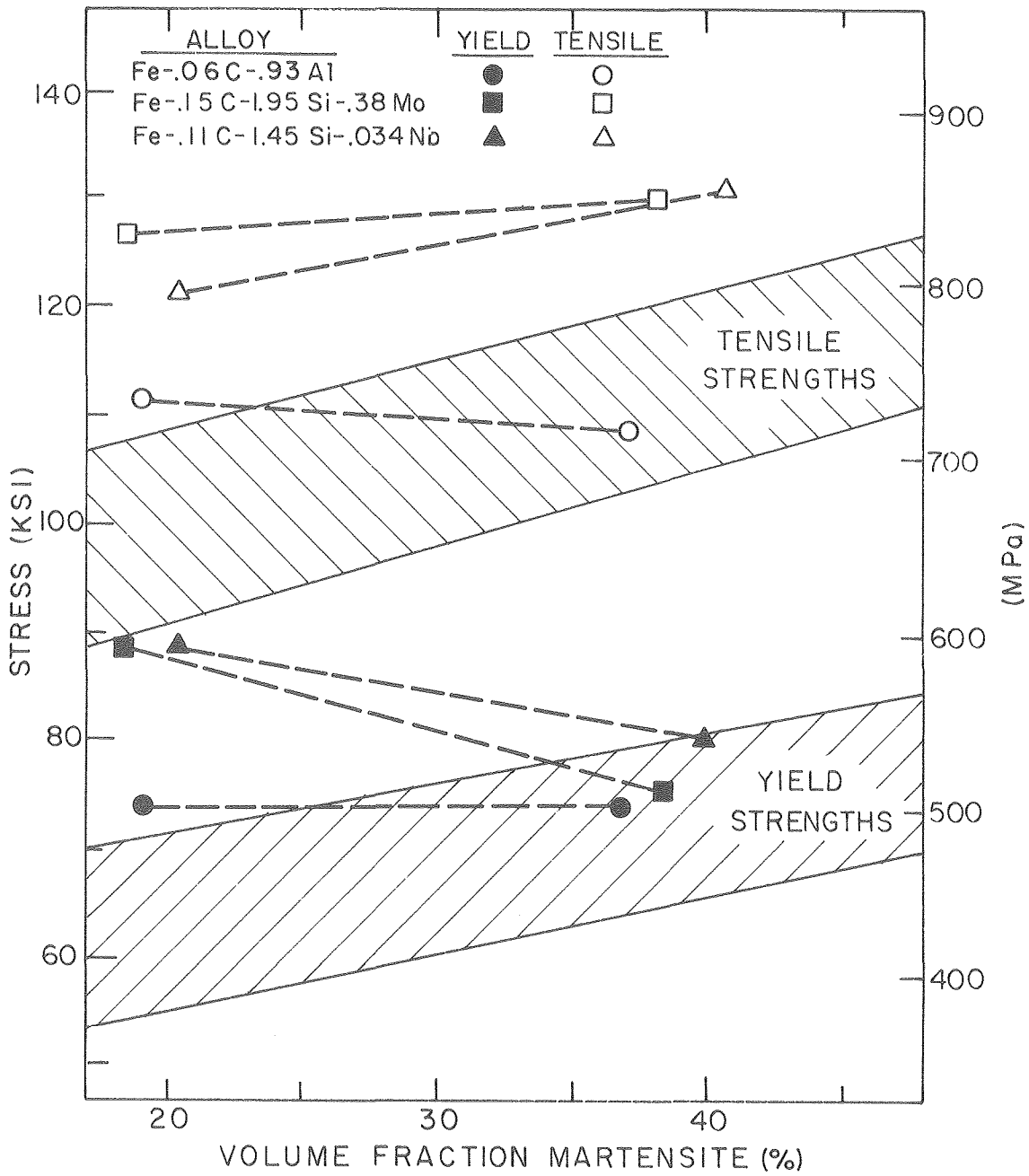

XBL 7812-6283

Fig. 44

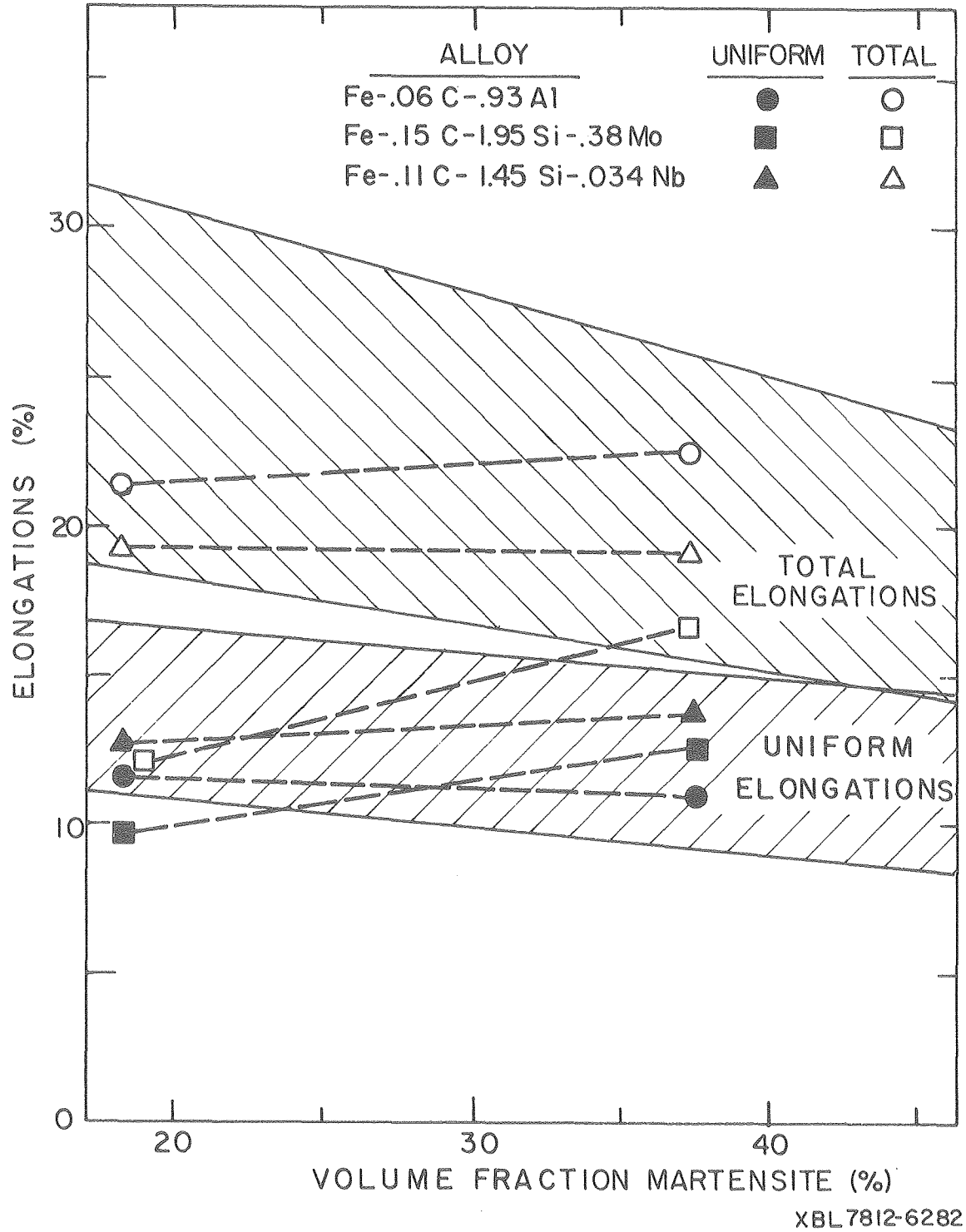

Fig. 45

U.S.GPO:1980-698-169/F-100

This report was done with support from the Department of Energy. Any conclusions or opinions expressed in this report represent solely those of the author(s) and not necessarily those of The Regents of the University of California, the Lawrence Berkeley Laboratory or the Department of Energy.

Reference to a company or product name does not imply approval or recommendation of the product by the University of California or the U.S. Department of Energy to the exclusion of others that may be suitable.

TECHNICAL INFORMATION DEPARTMENT
LAWRENCE BERKELEY LABORATORY
UNIVERSITY OF CALIFORNIA
BERKELEY, CALIFORNIA 94720